BERICHTE
aus dem
INSTITUT FÜR MEERESKUNDE
an der
CHRISTIAN-ALBRECHTS-UNIVERSITÄT KIEL

Nr. 315

The North Atlantic Oscillation: Variability and Interactions with the North Atlantic Ocean and Arctic Sea Ice

DOI 10.3289/IFM_BER 315

von

Thomas Jung

Kiel 2000

Kopien dieser Arbeit können bezogen werden:
Institut für Meereskunde an der Universität Kiel
Fachbereich Ozeanzirkulation und Klima
Düsternbrooker Weg 20
D-24105 Kiel, -FRG-

ISSN 0341-8561

Diese Arbeit wurde von der Mathematisch-
Naturwissenschaftlichen Fakultät der
Christian-Albrechts-Universität zu Kiel
als Dissertation angenommen.

Contents

Zusammenfassung

Die Nordatlantische Oszillation (NAO) ist der dominante Mode atmosphärischer Variabilität im Nordatlantik und beschreibt Änderungen in der Stärke der Westwinde in mittleren Breiten. In dieser Studie wird die Variabilität der NAO während der Wintersaison und ihre Wechselwirkung mit dem Nordatlantik sowie dem arktischen Meereis untersucht. Dazu werden Beobachtungsdaten und Modellsimulationen des atlantischen Ozeans, des arktische Meereises sowie des globalen gekoppelten Klimasystems analysiert.

Die NAO zeigt statistisch signifikante interdekadische Variabilität während des 20. Jahrhunderts. Variabilität der NAO auf anderen Zeitskalen ist konsistent mit Realisierungen von Zufallsprozessen ("Weißes Rauschen"). Die Wiederkehr von NAO-Anomalien von Winter zu Winter, in Zusammenhang mit fehlenden NAO-Anomalien während der anderen Jahreszeiten, ist primär auf interdekadische NAO-Variabilität während der Wintersaison zurückzuführen. Dieses Phänomen deutet auf das Vorhandensein eines externen Antriebs auf interdekadischen Zeitskalen hin, zumindest während des 20. Jahrhunderts.

Interdekadische Variabilität der NAO ist von ausgeprägten Anomalien der nordatlantischen Ozeanoberflächentemperatur (SST) begleitet. Obwohl diese Anomalien teilweise durch einen lokalen NAO-Antrieb erklärt werden können, so erfordert eine vollständige Erklärung der beobachteten SST-Anomalien vermutlich auch einen Beitrag von Änderungen der ozeanischen Zirkulation. Um diese Hypothese zu testen, wird die Integration eines atlantischen Zirkulationsmodells für den Zeitraum 1865–1997 analysiert. Das Modell wurde mit monatlichen Flüssen an der Ozeanoberfläche angetrieben, deren zeitliche Variabilität vollständig durch den beobachteten NAO Index beschrieben wird. Die beobachteten und modellierten interdekadischen SST-Anomalien zeigen eine gute Übereinstimmung. Die Analyse der Modellintegration deutet darauf hin, daß interdekadische SST-Variabilität im Nordatlantik während des 20. Jahrhunderts auf zwei Prozesse zurückzuführen ist: (i) ein instantaner lokaler Antrieb durch die NAO und (ii) eine verzögerte Reaktion der nordatlantischen thermohalinen Zirkulation sowie des subpolaren Wirbels auf den Wärmeflußantrieb durch die NAO. Die Ergebnisse eines zusätzliches Sensitivitätsexperimentes weisen darauf hin, daß die Impuls- und Frischwasserflußantriebe auf interdekadischen Zeitskalen eher eine untergeordnete Rolle spielen. Die Phasenbeziehung zwischen der NAO und ozeanischen Zirkulationschwankungen auf interdekadischen Zeitskalen liefert wenig Hinweis auf eine zweiseitige Kopplung zwischen Ozean und Atmosphäre. Daher ist die beobachtete interdekadische Variabilität der NAO während des 20. Jahrhunderts vermutlich auf einen anderen externen Antrieb zurückzuführen.

Die NAO und Schwankungen der nordatlantischen thermohalinen Zirkulation zeigen in einer Kontrollsimulation über 300 Jahre des globalen gekoppelten Zirkulationsmodells ECHAM4/OPYC3 keine signifikante Kohärenz auf interdekadischen Zeitskalen. Weiterhin zeigt die simulierte NAO wenig Hinweis auf das Vorhandensein von deterministischen Komponenten, so daß wenig Raum für eine erfolgreiche Vorhersage der modellierten NAO einige Jahre im voraus bleibt.

Die ausgeprägte Verstärkung der NAO während der letzten drei Jahrzehnte, die ein Segment interdekadischer Variabilität darstellt, ging mit einer Ostwärtsverschiebung der Zentren *interannualer* NAO-Variabilität Ende der Siebziger Jahre einher. Diese Ostwärtsverschiebung führte dazu, daß positive und negative NAO-Winter von verstärkten meridional Windanomalien im Bereich der Framstraße begleitet waren. Dadurch läßt sich die Zunahme der Kohärenz auf interannualen Zeitskalen zwischen der NAO und dem Eisexport

durch die Framstraße während der letzten beiden Dekaden erklären. Diese Verschiebung führte ferner zu einer beträchtlichen Veränderung des Einflusses der NAO (i) auf Lufttemperaturanomalien über dem europäischen und nordamerikanischen Kontinent sowie (ii) auf die Wechselwirkung zwischen Ozean und Atmosphäre. Die Analyse historischer Luftdruckdaten deutet darauf hin, daß die Lage der Zentren interannualer NAO-Variabilität während der letzten beiden Jahrzehnte eher ungewöhnlich ist.

Um die "Ungewöhnlichkeit" von Verschiebungen der NAO-Zentren abzuschätzen, wird eine Kontrollsimulation und eine Szenariosimulation für einen transienten Anstieg der Treibhausgaskonzentration des ECHAM4/OPYC3-Modells analysiert. Die Lage der NAO-Zentren ist in der Kontrollsimulation relativ stabil und ähnelt der beobachteten Lage der NAO vor den Siebziger Jahren. Damit läßt sich auch das Fehlen einer signifikanten Korrelation ($r = 0.0$) zwischen dem modellierten NAO Index und Eisexport durch die Framstraße erklären. Schließlich wird gezeigt, daß die modellierte Verschiebung der Aktionszentren der NAO unter erhöhten Treibhausgaskonzentrationen (um 2020), die zuerst von Ulbrich und Christoph beschrieben wurde, der beobachteten Verschiebung Ende der Siebziger Jahre ähnelt.

Abstract

The North Atlantic Oscillation (NAO) represents the dominant mode of atmospheric variability in the North Atlantic region and describes the strengthening and weakening of the mid-latitude westerlies. In this study, variability of the NAO during wintertime and its relationship to the North Atlantic ocean and Arctic sea ice is investigated. For this purpose, observational data are analyzed along with integrations of models for the Atlantic ocean, Arctic sea ice, and the coupled global climate system.

From a statistical point of view, the observed NAO index shows unusually high variance on interdecadal time scales during the 20th century. Variability on other time scales is consistent with realizations of random processes ("white noise"). Recurrence of wintertime NAO anomalies from winter-to-winter with missing signals during the inbetween non-winter seasons is primarily associated with interdecadal variability of the NAO. This recurrence indicates that low-frequency changes of the NAO during the 20th century were in part externally forced.

Interdecadal variability of the observed NAO is associated with pronounced North Atlantic sea surface temperature (SST) anomalies. Whereas parts of these SST anomalies can be explained by a local net surface heat flux forcing from the NAO, the remaining part may be explained by interdecadal changes of the oceanic circulation. In order to test this hypothesis, an integration of an ocean general circulation model for the period 1865–1997 is analyzed. The model has been forced by monthly surface fluxes whose variability is solely determined by the observed NAO index. The observed and modelled interdecadal SST variability is in good agreement. It is shown that modelled interdecadal SST anomalies in the North Atlantic region were generated by two processes: (i) An instantaneous local surface flux forcing by the NAO, along with (ii) a lagged response of the North Atlantic thermohaline circulation and of the subpolar gyre to the net surface heat flux forcing by the NAO. An additional sensitivity experiment reveals that interdecadal wind stress and freshwater flux variability was of minor importance. The phase-relationship between variability of the NAO and the North Atlantic ocean on interdecadal time scales is less indicative for a two-way coupling between atmosphere and ocean — thus, leaving space for other external mechanisms that may have forced interdecadal NAO variability during the 20th century.

No significant coherence between the NAO and the North Atlantic thermohaline circulation is found on interdecadal time scales in a century-scale control integration of the coupled general circulation model ECHAM4/OPYC3. Moreover, there is no strong statistical evidence for the presence of deterministic components in the modelled NAO index leaving the modelled NAO rather unpredictable several years in advance.

The pronounced increase of the NAO during the last three decades, which represents a segment of its interdecadal variability, was accompanied by an eastward shift of the NAO's centers of *interannual* variability around the late 1970s. This eastward shift was associated with increased anomalous meridional wind components near Fram Strait during high and low NAO winters and, hence, with increased coherence between the NAO and Arctic sea ice export through Fram Strait on interannual time scales. This shift was also accompanied by pronounced changes in the response of (i) near-surface temperature anomalies over the European and North American continent, and (ii) North Atlantic air-sea interaction to an interannual forcing by the NAO. The analysis of historical sea level pressure (SLP) data suggests that the recent location of the NAO's centers of interannual variability is rather

unusual.

In order to evaluate the unusualness of changes in the location of the NAO's centers of interannual variability, integrations of the coupled ECHAM4/OPYC3 model under present-day conditions and under increasing greenhouse gas concentrations are investigated. In the control integration the location of the NAO is relatively stable resembling that of the observed NAO before the late 1970s. This may explain the missing link between the NAO and Arctic sea ice export through Fram Strait ($r = 0.0$) in the control integration of this coupled model. Finally, it is shown that the eastward shift of the NAO in the scenario run (around 2020), first described by Ulbrich and Christoph, is similar to the observed shift around the late 1970s.

List of Figures

List of Tables

Abbreviations

AGCM	Atmosphere General Circulation Model
AR(1)	First-order Autoregressive Model
CCA	Canonical Correlation Analysis
CGCM	Coupled General Circulation Model
ECHAM4	Hamburg version of the ECMWF model
ECHAM4/OPYC3	see ECHAM4 and OPYC3
ECMWF	European Center for Medium Range Weather Forecasts
EOF	Empirical Orthogonal Function
GIN Seas	Greenland/Icelandic/Norwegian Seas
KISS	Kiel Sea Ice Simulation System
MHT	Meridional Heat Transport
MSSA	Multichannel Singular Spectrum Analysis
NAC	North Atlantic Current
NAO	North Atlantic Oscillation
NCAR	National Center for Atmospheric Research
NCEP	National Center for Environmental Prediction
NCEP/NCAR	see NCEP and NCAR
OGCM	Ocean General Circulation Model
OPYC3	Ocean and Isopycnal Coordinate
PC	Principal Component
PDF	Probability Density Function
SLP	Sea Level Pressure
SSA	Singular Spectrum Analysis
SST	Sea Surface Temperature
THC	Thermohaline Circulation

1 Introduction

Knowing the governing laws of nature is one thing. Understanding their manifestations is something quite different.

John D. Barrow

It is well-known that the earth's climate system shows variability over a broad range of frequencies. This can be inferred from Fig. 1.1 showing an idealized, schematic spectrum of atmospheric surface temperature from hours to 10^{10}-yrs. The physical mechanisms that are responsible for the generation of this spectral shape depend on the time scale under consideration. The spectral peak at 1-year period, for example, can be associated with the annual cycle of incoming solar radiation, whereas enhanced variability from 3- to 7-days can be associated with the turbulent nature of the atmospheric flow field (synoptic-scale variability).

Looking at the spectrum in Fig. 1.1 it may surprise that interannual to interdecadal climate variability — a relatively "quiescent" frequency-range — has attracted so much attention in recent years (e.g., CLIVAR, 1998). However, especially climate variability in this frequency-range has to be taken into account in order (i) to separate a possible anthropogenic climate change from natural climate variability (e.g., Houghton et al., 1996), and (ii) to assess the potential predictability of climate anomalies several years in advance.

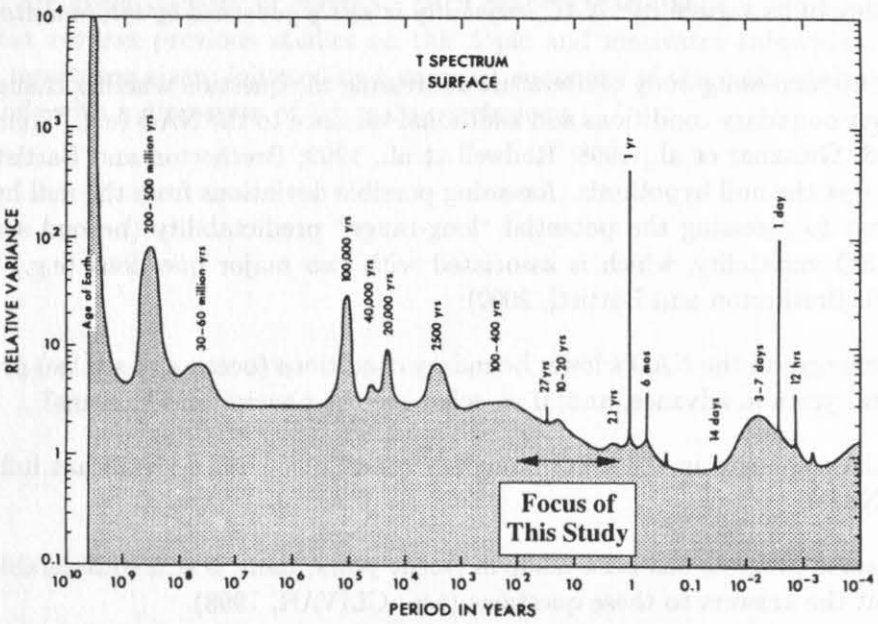

Figure 1.1: Schematic spectrum of atmospheric surface temperature between 10^{-4} and 10^{10} years adapted from Mitchell (1976) and Peixoto and Oort (1992). The horizontal arrow spans the time scales considered in this study.

The North Atlantic region is of particular interest when dealing with interannual to interdecadal climate variability. In this region three components of the climate system interact: Atmosphere, ocean, and sea ice[1]. Our current knowledge about the nature of these interactions (physics, direction and strength) depends on the components and time scales under consideration.

The North Atlantic Oscillation (NAO), which describes the strengthening and weakening of the mid-latitude westerly winds, is the dominant mode of atmospheric variability in the North Atlantic region[2] (e.g., Cayan, 1992b). It is well-known,

- that a dynamical coupling between the NAO and the North Atlantic ocean and/or sea ice is not essential for the basic characteristics of the NAO (e.g., Barnett, 1985; Limpasuvan and Hartmann, 1999),

- that the NAO has profound impacts (i) on regional climates over the neighbouring continents (e.g., Hurrell, 1995; Hurrell and van Loon, 1997), (ii) on North Atlantic sea surface temperatures (e.g., Cayan, 1992a,b, SST hereafter), and (iii) on the ice extent in the northern North Atlantic (e.g., Fang and Wallace, 1994), and

- that interdecadal changes of the NAO project onto Northern Hemisphere mean surface temperatures (e.g., Hurrell, 1996; Timmermann et al., 1998).

The strong impact of the NAO onto a variety of parameters in the North Atlantic region along with its projection onto Northern Hemisphere mean surface temperatures may explain the increasing scientific interest in the nature of interannual to interdecadal NAO variability (CLIVAR, 1998). The fact that the basic characteristics of the NAO do not depend on a coupling with the ocean and/or sea ice provides an appropriate null hypothesis for the nature of its variability: *NAO variability is solely governed by internal atmospheric dynamics.*

There is an increasing body of literature addressing the question whether changes in the NAO's lower boundary conditions add additional variance to the NAO (e.g., Timmermann et al., 1998; Grötzner et al., 1998; Rodwell et al., 1999; Bretherton and Battisti, 2000), that is, to test the null hypothesis. Assessing possible deviations from the null hypothesis is equivalent to assessing the potential "long-range" predictability (beyond seasons) of natural NAO variability, which is associated with two major questions (e.g., Grötzner et al., 1999; Bretherton and Battisti, 2000):

- Are changes in the NAO's lower boundary conditions (ocean and sea ice) predictable several years in advance, and, if so, what are the physical mechanisms?

- Do these changes in the lower boundary conditions exert a significant influence on the NAO?

Although some progress has been made in recent years, there is still considerable controversy about the answers to these questions (e.g., CLIVAR, 1998).

[1] In this study the North Atlantic climate system is treated as a closed system. A possible forcing from outside the North Atlantic region, however, cannot be excluded (e.g., Rajagopalan et al., 1998; Latif et al., 2000). Moreover, possible impacts from the biosphere are not considered.

[2] A recent study by Deser (2000) shows that the NAO represents even the dominant mode of atmospheric variability over the Northern Hemisphere.

It is the objective of this study to contribute to our understanding about the nature of interannual to interdecadal variability in the North Atlantic region. The focus is on the variability of the NAO and its interaction with the North Atlantic ocean and Arctic sea ice during wintertime.

This thesis is organized as follows: Chapter 2 is devoted to introduce statistical methods that are widely used throughout this study. In chapter 3 the basic characteristics of the observed NAO are discussed. Special emphasize is dedicated to possible deviations from the null hypothesis that NAO variability is solely governed by internal atmospheric dynamics. The results from this chapter form the basis for subsequent investigations. In chapter 4 the relationship between the NAO and the North Atlantic circulation on interdecadal time scales is investigated. This is done by analyzing observations and an Atlantic ocean general circulation model integration that was solely forced by NAO-related surface fluxes over the period 1865–1997. The focus is on those physical processes giving rise to the observed interdecadal variability in the North Atlantic region during the 20th century. In chapter 5 the characteristics of the NAO and its interactions with the North Atlantic ocean as simulated by the coupled general circulation model ECHAM4/OPYC3 are described. In chapter 6 the link between the NAO and Arctic sea ice export through Fram Strait is investigated. The results are based (i) on a realistic hindcast simulation using a dynamic-thermodynamic sea ice model that was forced with reanalyzed near-surface temperatures and winds over the last forty years, and (ii) on a century-scale integration of the ECHAM4/OPYC3 model under present-day climate conditions. Possible changes of this link under increasing greenhouse gas concentrations are also discussed on the basis of a scenario integration of the ECHAM4/OPYC3 model. The thesis concludes with a final discussion of the results and a short outlook.

I decided to write each chapter in such a manner that it can be read separately. Cross-references are given in cases of overlap. Each chapter starts with a short introductory section that reviews previous studies on this topic and motivates subsequent analyses. Then the results are given, followed by a compact summary of the main conlusions. Each chapter ends with a discussion of the main conclusions.

2 Methods

In this chapter statistical methods are introduced that were extensively used throughout this study. The statistical methods are not described in full detail. Rather, the focus is on the sketch, the advantages, and the disadvantages of each of the methods. A comprehensive list of references is given that allows further reading on methodological details and applications in different areas of climate research.

2.1 Uni- and Bivariate Methods

The analysis of uni- and bivariate time series is a common task in climate research. Separating deterministic components from the background noise for univariate time series leads to the concept of the "spectrum". Similarly, the concept of the "cross-spectrum" emerges when the characteristic covariation between two time series is studied in the spectral domain. The classical treatment of the spectrum and the cross-spectrum is not described in this section. Excellent introductions about these subjects are given, for example, by Jenkins and Watts (1968) and von Storch and Zwiers (1999). Here, two relatively new techniques for time series analysis are described, that is, Singular Spectrum Analysis and Wavelet analysis.

2.1.1 Singular Spectrum Analysis (SSA)

Singular Spectrum Analysis (SSA) is a technique to enhance the signal-to-noise ratio of univariate time series. SSA was introduced by Broomhead and King (1986) to visualize qualitative dynamics from experimental data. In this study, SSA is used to separate deterministic components like (nonlinear) trends and modulated oscillations from the background noise.

SSA is based on the idea of sliding a window down a time series and looking for recurrent "patterns in time". Thus, SSA is closely related to ordinary empirical orthogonal function (EOF) analysis, which became a standard tool in climate research[3]. Unlike classical methods, SSA uses data-adaptive basis functions, which are the eigenvectors of the time series' lag-covariance matrix, rather than fixed sines and cosines. By doing so, even non-sinusoidal oscillations can be captured by a single pair of eigenmodes, rather than by many overtones as required for fixed basis functions. The main problem in SSA is to separate between signal and noise eigenmodes (see below). Once the signal modes have been identified, the time series' signal-to-noise ratio can be enhanced by reconstructing only the signal part of the time series. Throughout the remainder of this section the basic SSA algorithm is introduced; then, Monte Carlo SSA is described, which is a method to make inference about the eigenmodes; and finally an example is given. More detailed introductions to SSA are given, for example, by Vautard (1995), Ghil and Yiou (1996), Ghil and Taricco (1997), and von Storch and Zwiers (1999).

The SSA formalism is based on three steps: (i) Embedding the time series x_t, with $t = 1, \ldots N$, in a vector space of dimension M; (ii) computing the $M \times M$ lag-covariance matrix $\mathbf{C}_D$; and (iii) diagonalizing the lag-covariance matrix[4] $\mathbf{C}_D$.

[3] EOF analysis is described in section 2.2.3.

[4] In contrast to ordinary EOF analysis the eigenvectors obtained by SSA are the same if the lag-correlation matrix is diagonalized instead of the lag-covariance matrix (e.g., von Storch and Zwiers, 1999).

First, for a given M a new vector series (trajectory) $\mathbf{y}_{t'} = (x_{t'}, x_{t'+1}, \ldots, x_{t'+M-1})^T$ is formed, which represents $t' = 1, \ldots, N'$ ($N' = N - M + 1$) views on the time series through the window of length M. $\mathbf{y}_{t'}$ is called the trajectory matrix $\mathbf{Y}$. In practice the choice of the embedding dimension M is subjective, since commonly the dimension of the underlying dynamical system is not known *a priori*. A practical guideline for the choice of M was proposed by Vautard et al. (1992), who suggest that SSA is typically successful at analyzing periods in the range ($M/5$, M). Nevertheless, it is important to test whether the results are sensitive against changes in M.

Next, the $M \times M$ lag-covariance matrix $\mathbf{C}_D$ has to be calculated. Two different methods are available: The Broomhead and King (1986) (BK) algorithm and the Vautard and Ghil (1989) (VG) algorithm. Here, the BK algorithm is used, that is,

$$\mathbf{C}_D = \eta \mathbf{Y}^T \mathbf{Y}, \qquad \text{where} \qquad \eta = 1/N'. \tag{2.1}$$

In the VG algorithm, $\mathbf{C}_D$ has Toeplitz matrix structure. As dicussed by Allen and Smith (1996) $\mathbf{C}_D$ is subject to more variance but less bias if the BK algorithm is used instead of the VK algorithm.

Finally, $\mathbf{C}_D$ diagonalized:

$$\mathbf{\Lambda}_D = \mathbf{E}_D^T \mathbf{C}_D \mathbf{E}_D, \tag{2.2}$$

where $\mathbf{\Lambda}_D$ is a $M \times M$ matrix containing the eigenvalues in decreasing order on the principal diagonal ($\lambda_1 \geq \lambda_2 \geq \ldots \geq \lambda_M$) and $\mathbf{E}_D$ is a $M \times M$ matrix having the eigenvectors $\mathbf{e}_k$, with $k = 1, \ldots, M$, as its columns. Throughout the manuscript the k-th eigenvector $\mathbf{e}_k$ is called k-th temporal EOF (T-EOF). Note, that $\mathbf{e}_k$ represents a "typical" trajectory. The eigenvalue λ_k gives the variance of the time series in the direction of $\mathbf{e}_k$. SSA bears its name, because the eigenvalues and eigenvectors are alternatively given by Singular Value Decomposition (SVD) of the time series' trajectory matrix $\mathbf{Y}$ (Broomhead and King, 1986).

Similar to ordinary EOF analysis, SSA yields *temporal* principal components (T-PCs) by projecting the trajectories onto the T-EOFs, that is,

$$\alpha_{t'k} = \sum_{j=1}^{M} x_{t'+j} e_{kj}, \qquad t' = 1, \ldots, N'. \tag{2.3}$$

Therefore, the $\alpha_{t'k}$ (T-PCs) represent filtered versions of the orignal time series; the objectively determined filter-weights are given by the T-EOFs ($\mathbf{e}_k$). Since generally T-EOFs are not symmetric, T-PCs do not contain informations about the phase.

The part of the time series that is associated with the k-th mode can be reconstructed using

$$r_{tk} = \frac{1}{M_t} \sum_{j=1}^{M} \alpha_{t-j,k} e_{kj}, \tag{2.4}$$

where r_{tk} is the k-th reconstructed component (T-RC, hereafter) and M_t is a normalization factor, which is M for the central part of the time series and has slightly different values near its endpoints (Vautard et al., 1992). The sum of r_{tk} over all eigenmodes gives back the original time series, that is, $x_t = \sum_k^M r_{tk}$. Notice, that once signal modes (K) have been determined, the signal-to-noise ratio of the original time series can be enhanced by

reconstructing for a subset $\mathcal{K}$:

$$r_{t\mathcal{K}} = \frac{1}{M_t} \sum_{k \in \mathcal{K}} \sum_{j=1}^{M} \alpha_{t-j,k} e_{kj}. \tag{2.5}$$

$r_{t\mathcal{K}}$ is an objectively filtered time series that (i) is of length N, (ii) contains informations about the phase, and (iii) represents the signal part of the original time series. A reconstruction of 2- and 4-yrs components of the Southern Oscillation index is given by Ghil and Yiou (1996).

The main problem in SSA is to separate between signal and noise eigenmodes. Monte Carlo SSA (MC-SSA) is a straitforward and efficient method to make inference. An excellent introduction is given by Allen and Smith (1996). Here, we give a short description of the sketch of the method.

In MC-SSA, first, one assumes a noise model or *null hypothesis*. In this study, first-order autoregressive models (AR(1) noise) are used. Then, the model parameters are estimated from the time series x_t. Here, we use the less biased method proposed by Allen and Smith (1996). Finally, in order to assess the significance of the eigenmodes, an ensemble of realizations of the null hypothesis is generated. For each realization the lag-covariance matrix $\mathbf{C}_R$ is calculated and projected onto the eigenvector basis $\mathbf{E}_D$ of the original time series x_t:

$$\mathbf{\Lambda}_R \equiv \mathbf{E}_D^T \mathbf{C}_R \mathbf{E}_D. \tag{2.6}$$

The elements on the principal diagonal of the matrix $\mathbf{\Lambda}_R$ represent the contribution of the noise in the direction of the data eigenvectors. Following Allen and Smith (1996), MC-SSA consists in asking, for each T-EOF, "*does the data contain significantly more (or significantly less) variance in the direction in state space defined by this EOF than we would expect if the null hypothesis is true?*" In order to answer this question, the distribution of the eigenvalues on the principal diagonal of $\mathbf{\Lambda}_R$ under the null hypothesis is estimated from the ensemble. Then, the unusualness of the data eigenvalues under the null hypothesis is assessed.

As pointed out by Allen and Smith the variance compression problem, that is, high-ranked (low-ranked) eigenvalues are overestimated (underestimated), changes the probability of type-1 errors by an unquantifiable amount if Eqn. 2.6 is used. To operate as close as possible at the nominal confidence level, we follow Allen and Smith in projecting, both, the data and the realizations of the null hypothesis onto the T-EOFs of the null hypothesis. These are obtained by diagonalizing the expected lag-covariance matrix of the null hypothesis[5] $\mathbf{C}_N$:

$$\mathbf{\Lambda}_N \equiv \mathbf{E}_N^T \mathbf{C}_N \mathbf{E}_N. \tag{2.7}$$

Then, the data and the realizations of the null hypothesis are projected onto the T-EOFs of the null hypothesis $\mathbf{E}_N$:

$$\mathbf{\Lambda}'_D \equiv \mathbf{E}_N^T \mathbf{C}_D \mathbf{E}_N \tag{2.8}$$

$$\mathbf{\Lambda}'_R \equiv \mathbf{E}_N^T \mathbf{C}_R \mathbf{E}_N. \tag{2.9}$$

The primes indicate that the T-EOFs of the null hypothesis have been used. In this study, inference about the significance of eigenmodes is made using Eqns. 2.8 and 2.9.

[5]For AR(1) noise $\mathbf{C}_N$ can easily be determined from the estimated process parameters (e.g., von Storch and Zwiers, 1999).

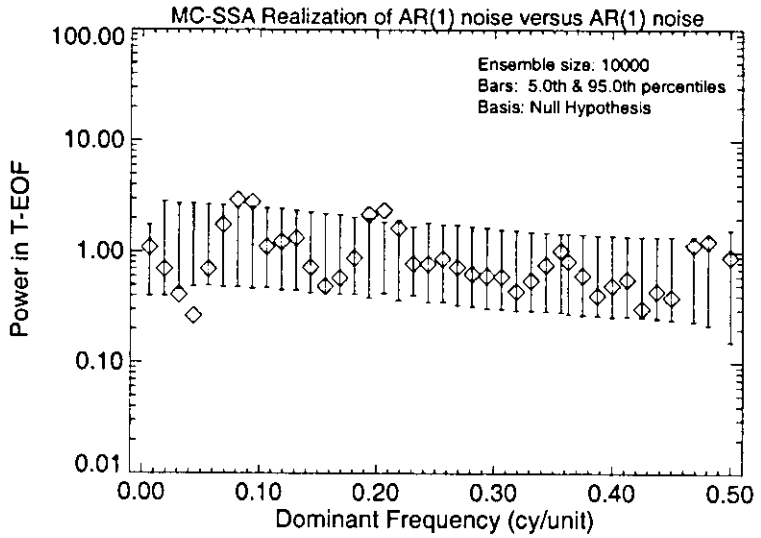

Figure 2.1: Test of a realization of AR(1) noise (see text for details) against AR(1) noise by means of Monte Carlo SSA. *Diamonds* denote the projection of the lag-covariance matrix of the data $\mathbf{C}_D$ upon the T-EOFs of the null hypothesis $\mathbf{E}_N$ (Eqn. 2.8), plotted against dominant frequency (obtained by reduced Fourier transform of T-EOFs). Each vertical bar contains 90% of the eigenvalues (5th and 95th percentile) out of 10000 realizations of the null hypothesis (Eqn. 2.9). A window length M of forty years was used.

The MC-SSA formalism becomes somewhat more elaborate, if a time series consists of one or more signals along with noise. Once a signal mode has been identified, the null hypothesis becomes more specific (so-called *composite null hypothesis*), that is, the time series represents a segment of the (previously identified) signal(s) that is superimposed on the noise. This process continues until there is no reasonable statistical evidence against the respective composite null hypothesis. Mathematical details are given by Allen and Smith (1996).

To illustrate MC-SSA, subsequently an example is given. A realization of AR(1) noise of length $N = 133$ is tested against the AR(1) noise null hypothesis. A memory parameter of $a_1 = 0.2$ was choosen (weakly red noise). The driving noise is Gaussian having unit variance. We decided to illustrate MC-SSA for a realization of AR(1) noise without a signal superimposed, in order to highlight the problems in interpreting the resulting spectra. Examples for the application of MC-SSA in the presence of signals are described elsewhere (e.g. Allen and Smith, 1996; Ghil and Yiou, 1996).

The MC-SSA eigenspectrum for the realization of AR(1) noise, tested against AR(1) noise, is depicted in Fig. 2.1. Instead of using rank-order, eigenvalues are plotted versus the dominant frequency of the respective T-EOFs, which was estimated using reduced Fourier transform (e.g., Plaut and Vautard, 1994). Four excursions above the *local* 95th percentile (confidence level) are evident, two at about 5 units and two at about 11 units[6]. At the first glance it may appear counterintuitive that four excursions above the local 95th percentile occur although the null hypothesis is true; and the reader might speculate that

[6]Notice, that the units are arbitrary. One may think, for example, of years.

a rather unusual realization of AR(1) noise was chosen. In order to test how unusual four excursions above the local 95th percentile are, a second run through the ensemble was performed counting the number of excursions for each ensemble member. The evaluation of the second run[7] reveals that four or more excursions above the 95th percentile out of forty possible have a probability of about 18% to occur if the null hypothesis is true. Thus, without any *a priori* expectations about the outcome at specific frequencies, the actual confidence would be 82% rather than 95% as suggested by the local confidence levels. This second run through the ensemble represents a *global* test, which is an important component when making inference in cases where no *a priori* expectations are available. Further examples about problems with local versus global significance descisions are given, for instance, by Livezey and Chen (1983) and Allen and Smith (1996).

2.1.2 Wavelet Analysis

There is some debate to what degree non-stationarities of a time series x_t may influence the results obtained by SSA. Note, that the lag-covariance matrix is estimated from the *whole* time series; that is, *local* properties of x_t are not considered independently. The continous wavelet transform provides a natural framework to deal with non-stationarities. It allows to investigate *local* power as a function of *time* and (equivalent) *period*, that is, in the two-dimensional time-frequency domain. An increasing body of literature deals with the application of wavelet analysis in geophysics (e.g., Wang and Wang, 1996; Lau and Weng, 1995; Kumar and Foufoula-Georgiou, 1997; Baliunas et al., 1997; Torrence and Compo, 1998; Higuchi et al., 1999). A practical guide to wavelet analysis is provided by Torrence and Compo (1998) (TC98, hereafter).

The continous wavelet transform is defined as the convolution of x_t with so-called wavelets ψ:

$$W_{ba} = \sum_{t=1}^{N} x_t \psi^*(\frac{t-b}{a}) \quad a > 0, \quad t = 1, \ldots, N. \tag{2.10}$$

The *scale* is denoted by a, which is equal to the period of the oscillation apart from a constant factor, b (displacement) describes *time*, and * indicates the complex conjugate. Here we use so-called Morlet wavelets, which are essentially sinusoidals (period depends upon a) modulated by a Gaussian function. Note, that this modulation allows to *localize* signals in time. Since Morlet wavelets are complex, W_{ba} is complex too, and *local wavelet power* becomes $|W_{ba}|^2$. In order to compare different wavelet power spectra it is convenient to normalize $|W_{ba}|^2$ by the variance of x_n (TC98).

According to Heisenberg's uncertainty principle neighboured estimates of $|W_{ba}|^2$ are not independent. This dependency in the direction of b is described by the *cone of influence*, which is defined as $\sqrt{2}a$ for Morlet wavelets (one-sided). Properties of x_t from outside the cone of influence contribute less than a factor e^{-2} to $|W_{ba}|^2$ (TC98). Eqn. 2.10 implies that zeros enter the convolution at the beginning and end of the time series. Therefore, the estimates of $|W_{ba}|^2$ are negatively biased within the cone of influence; the bias which depends on b and a. Notice, that side effects are negligible outside the cone of influence.

In order to test local wavelet power against the null hypothesis of AR(1) noise, the χ^2-test proposed by TC98 is used in this study. As for ordinary spectral estimates, averaging over scale and time, respectively, enhances the number of degrees of freedom (see TC98,

[7] Alternatively, we could have made use of the binomial distribution (Allen and Smith, 1996).

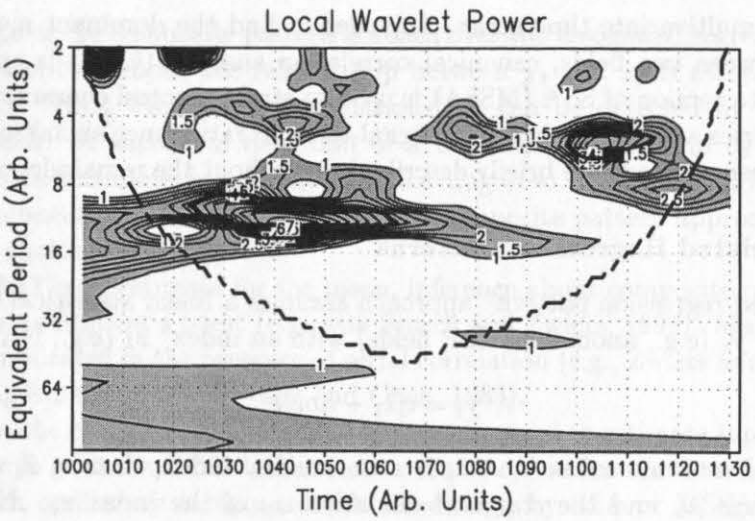

Figure 2.2: Normalized (by variance) local wavelet power for a realization of AR(1) noise (see text for details). Power exceeding 1.0 stands above the background noise (shaded). Contour interval is 0.5 for local wavelet power exceeding 1.0. The cone of influence (bold-dashed), within which side effects become important, and local wavelet power exceeding the local 95% confidence level (bold-solid) are also shown. Power estimates are smoothed in time (average over 5 time units).

for details). In order to illustrate problems with the interpretation of the test results, local wavelet power for the same realization of AR(1) noise as described in the previous section was estimated (Fig. 2.2). Recall that this realization is a segment of random variability. It becomes evident that locally significant excursions above the local 95% confidence level at about 5 and 11 time units (compare Fig. 2.1 for MC-SSA) are due to powerful spike-like events in the random series. This example shows that (as for MC-SSA) *local* excursions of local wavelet power above the 95% confidence level are difficult to interpret as long as there are no *a priori* expectations for specific times and frequencies. Since local wavelet power estimates are not independent (see above), an assessment of the global significance would require additional Monte Carlo experiments.

The concept of wavelet analysis can simply be extended to diagnose the connection between two time series x_t and y_t, that is, to wavelet cross-spectral analysis. Given the two time series with their wavelet transforms W^x_{ba} and W^y_{ba}, the wavelet cross-spectrum is defined by $W^{xy}_{ba} = W^x_{ba} W^{y*}_{ba}$. As for ordinary cross-spectral analysis, the wavelet co-spectrum $Re\{W^{xy}_{ba}\}$ and the wavelet quad-spectrum $Im\{W^{xy}_{ba}\}$ along with derived quantities are easily available. A more detailed treatment is given by TC98.

2.2 Multivariate Methods

A frequently faced question in climate research is how a time series ("index") is related to larger-scale features as decribed by fields. The methods of "associated regression patters" and "composite patterns" are used in this study to address this question. Empirical orthogonal function (EOF) analysis is applied to find dominant spatial modes of variability within fields. EOF analysis is also applied as a filter to reduced the spatial degrees

of freedom of multivariate time series. In order to find the dominant modes of coupled variability between two fields, canonical correlation analysis (CCA) is applied. Finally, the multivariate version of SSA (MSSA) is used to study spectral characteristics of multivariate time series and to enhance their signal-to-noise ratio, once signal modes have been identified. These methods are briefly described throughout the remainder of this chapter.

2.2.1 Associated Regression Patterns

The "associated regression pattern" approach assumes a linear statistical model to relate a vector series $\mathbf{y}_t$ (e.g., anomalous SLP fields) with an index[8] x_t (e.g., NAO index):

$$\mathbf{y}_t = \mathbf{q}\tilde{x}_t + noise, \tag{2.11}$$

where $\mathbf{y}_t$ represents anomalies, and $\tilde{x}_t$ is a *normalized* index, that is, $\tilde{x}_t = (x_t - \mu_x)/\sigma_x$ with the average μ_x and the standard deviation σ_x of the index x_t. Notice, that the normalization of x_t ensures that the *associated regression pattern* $\mathbf{q}$ has the same units as $\mathbf{y}_t$. Eqn. 2.11 can be read as follows: If $\tilde{x}_t = \beta$ then, on average, the pattern $\beta \cdot \mathbf{q}$ is observed. Here, $\beta = 1$ is used so that $\mathbf{q}$ refers to one standard deviation of x_t.

In practice the pattern $\mathbf{q}$ has to be estimated from the data. This is done by minimizing the mean squared error. It can easily be shown that this leads to (e.g., von Storch and Zwiers, 1999)

$$q_i = \frac{1}{N-1}\sum_{t=1}^{N} \tilde{x}_t y_{it}, \qquad i = 1, \ldots, L, \tag{2.12}$$

where L gives the number of components (grid points) of $\mathbf{y}_t$. Thus, associated regression patterns are estimated from the covariance between the normalized index x_t and anomalies of $\mathbf{y}_t$ at each grid point. If $\mathbf{y}_t$ at each grid point is normalized prior to the analysis, then Eqn. 2.12 gives the "associated correlation pattern".

Having in mind that $\mathbf{q}$ represents a set of regression slopes (or correlation coefficients) the significance can be easily assessed for each grid point using standard tests (e.g. von Storch and Zwiers, 1999). This becomes a more elaborate task, however, if serial correlation is present and/or no *a priori* expectation about the outcome is available (fishing experiment); in the latter case a *global* test has to be applied (Livezey and Chen, 1983).

2.2.2 Composite Patterns

In contrast to the "associated regression pattern" approach, the "composite pattern" approach is non-parametric, that is, no statistical model is assumed.

The relationship between the index x_t and the vector series $\mathbf{y}_t$ is established by estimating the "typical" pattern $\mathbf{y}_\mathcal{K}$ for a subset $\mathcal{K}$ that is keyed to the index x_t:

$$\mathbf{y}_\mathcal{K} = \frac{1}{K}\sum_{t\in\mathcal{K}} \mathbf{y}_t, \tag{2.13}$$

where K is the number of events meeting the criterion that is used to form $\mathcal{K}$. $\mathbf{y}_\mathcal{K}$ is called the *composite pattern*. Typically, all events with $x_t \geq \sigma_x$ or $x_t \leq \sigma_x$ are used to define the subset $\mathcal{K}$.

[8] Here, the "associated regression" approach is discussed for one index. A description of the method for more than one index is given by von Storch and Zwiers (1999).

An advantage of the composite pattern aproach over the associated regression approach is that no assumption about the relationship between $\mathbf{y}_t$ and x_t is associated with the former method. Thus, even nonlinear relationships can be detected by the composite pattern approach. A successful detection of a nonlinear relationship by means of the composite pattern technique is presented by Hoerling et al. (1997) for El Niño, La Niña, and their teleconnections. A disadvantage of the composite pattern approach arises from the subjective choice of the subset $\mathcal{K}$.

Since Eqn. 2.13 is an estimate for the mean, inference about composite patterns can be made by applying Student's t-test (e.g., von Storch and Zwiers, 1999). Making inference, however, is complicated in the presence of serial correlation (e.g., Zwiers and Storch, 1995) and for "fishing experiments" (Livezey and Chen, 1983).

In this study, the composite pattern approach is also used to estimate typical evolutions through one cycle of an oscillation, that is, to estimate *phase composites*. If, for instance, x_t represents an oscillatory component (obtained, e.g., by SSA or MSSA), then x_t can be complexified by taking its temporal derivative as imaginary part. Thus, for each time step the amplitude and phase for x_t can be determined. Then, Eqn. 2.13 can be applied for each phase sector and a prescribed amplitude (threshold). The "phase composite" technique was applied to study, for example, the Madden-Julian Oscillation (von Storch et al., 1988), North Atlantic intraseasonal atmospheric variability (Plaut and Vautard, 1994), and quasi-oscillatory characteristics of North Atlantic SST anomalies (Moron et al., 1998).

2.2.3 EOF Analysis

Empiricial orthogonal function (EOF) analysis is a technique to study the variability of a vector series $\mathbf{x}_t$. $\mathbf{x}_t$ can be written in matrix form as $\mathbf{X}$ (with temporal anomalies in its columns). Since EOF analysis is well-known and widely used, only its essentials are discussed along with potential pitfalls. A detailed introduction is given, for instance, by von Storch (1995) and von Storch and Zwiers (1999).

The first EOF $\mathbf{e}^1$ of $\mathbf{X}$ is the pattern (with $\|\mathbf{e}^1\| = 1$) whose associated principal component (PC) $\alpha_t^1 = \mathbf{X}\mathbf{e}^1$ is the linear combination of elements of $\mathbf{X}$ explaining the largest amount of variance. The second EOF $\mathbf{e}^2$ (which is orthogonal to the first EOF) provides the second PC α_t^2 explaining the largest amount of variance under the constraint of zero correlation with the first PC, and so forth. The EOFs are obtained by diagonalizing the cross-covariance matrix $\mathbf{X}^T\mathbf{X}$.

Since EOF analysis is an eigenvalue problem, the EOFs may be subject to degeneracy. North et al. (1982) illustrate this problem using synthetic data. Moreover, they provide a rule-of-thump, which allows to assess whether subsequent EOFs are mixed. North et al.'s rule-of-thump is used throughout this study.

Care has to be taken with respect to the interpretation of EOFs. If the EOFs are based on the cross-covariance matrix, then the patterns are constructed to maximize spatial *covariance* and not spatial *coherence* (correlation). Dominant patterns of spatial correlation can be obtained by normalizing $\mathbf{X}$ to unit variance prior to the decomposition, that is, by diagonalizing the cross-correlation matrix (Wallace and Gutzler, 1981). Examples illustrating the difference between spatial patterns of covariance and correlation are given, for instance, by Richman (1986).

2.2.4 Canonical Correlation Analysis (CCA)

The objectives and mathematics of canonical correlation analysis (CCA) are similar to those of EOF analysis. However, CCA is designed to find linear combinations within two vector series $\mathbf{X}$ and $\mathbf{Y}$ whose temporal correlation coefficients share maximal correlation. The first pair of *canonical correlation patterns* $\mathbf{f}_x^1$ and $\mathbf{f}_y^1$ (with $\|\mathbf{f}_x^1\| = 1$ and $\|\mathbf{f}_y^1\| = 1$) gives *canonical correlation coefficients* $\mathbf{X}\mathbf{f}_x^1$ and $\mathbf{Y}\mathbf{f}_y^1$ that share maximal correlation. Then, a second pair of canonical correlation patterns is found that gives a second pair of canonical correlation coefficients sharing maximal correlation under the constraint of no correlation with the first pair of canonical correlation coefficients, and so forth. Notice, that CCA does not require orthogonality between different pairs of canonical correlation patterns.

In the presence of small-scale noise the canonical correlation patterns may be poor estimates. As proposed by Barnett and Preisendorfer (1987), the impact of noise can be reduced if only a subset of the leading EOFs is used as input for CCA. Here, we follow Barnett and Preisendorfer's method.

Detailed introductions are given, for instance, by von Storch (1995), Bretherton et al. (1992), and von Storch and Zwiers (1999).

2.2.5 Multichannel Singular Spectrum Analysis (MSSA)

Multichannel singular spectrum analysis (MSSA) is a multichannel extension of SSA. As SSA does for univariate time series, MSSA approximates the (nonlinear) dynamics of a system by a linear system having oscillatory components. Thus, MSSA can also be used to draw spectral informations from multivariate (multichannel) time series. MSSA has been applied, for example, to study intraseasonal atmospheric variability (Plaut and Vautard, 1994), and the spectral characteristics of SST anomalies in the tropical Pacific (Allen and Robertson, 1996).

Consider a multivariate time series x_{it} having $i = 1, \ldots, L$ channels (grid points) and $t = 1, \ldots, N$ time steps. The objective of MSSA is to find typical sequences of x_{it} that are of (temporal) length M. Similar to SSA, this task reduces to diagonalizing the $L \cdot N' \times L \cdot N'$ (with $N' = N - M + 1$) lag-cross-covariance matrix formed from the sequences $(x_{1,t'}, x_{1,t'+1}, \ldots, x_{1,t'+M-1}; x_{2,t'}, x_{2,t'+1}, \ldots, x_{2,t'+M-1}; \ldots; x_{L,t'}, x_{L,t'+1}, \ldots, x_{L,t'+M-1})$ (with $t' = 1, \ldots N'$). The eigenvectors of the lag-cross-covariance matrix are called spatio-temporal EOFs (ST-EOFs). Similar to SSA, ST-PCs and ST-RCs can be determined. Notice, that for each eigenmode *and* each channel (grid point) one ST-PC and one ST-RC is obtained. The spatial degrees of freedom L (and thus the noise) can be substantially reduced if MSSA is applied to the leading PCs obtained from ordinary EOF analysis.

As for SSA, a Monte Carlo method (MC-MSSA) can be applied to make inference about the resulting eigenmodes (Allen and Robertson, 1996). Here, MC-SSA as proposed by Allen and Robertson (1996) is used, which is methodologically very similar to MC-SSA (see above). Since MSSA is applied to the leading L ordinary EOFs, the null hypothesis reads: The leading L ordinary PCs represent *independent* realizations of AR(1) noise.

Further details about MSSA are given, for instance, by Plaut and Vautard (1994), Ghil and Yiou (1996), and Allen and Robertson (1996).

3 Characteristics of the North Atlantic Oscillation

3.1 Introduction

The North Atlantic Oscillation (NAO) is a phenomenon that is well-known since many decades. It was indirectly identified by its characteristic to induce simultaneous out-of-phase temperature anomalies between Westgreenland and Europe (e.g. Hann, 1890). This temperature seesaw is known as either "Greenland below" or "Greenland above" mode (van Loon and Rogers, 1978). The term "North Atlantic Oscillation" was introduced in 1924 by Sir Gilbert Walker:

> *On the whole Iceland may be described as showing contemporary opposition with the northern belt of high pressure especially in the colder period of the year; and this fact will in future be expressed by saying that Iceland shares the "North Atlantic oscillation" (Walker, 1924).*

He and his colleagues already realized the importance of the NAO to influence regional climates over the neighbouring continents as well as the wind-driven circulation of the North Atlantic ocean. In the same year Defant (1924) presented results from zonally averaged sea level pressure data (SLP; $10°$–$60°W$) on a monthly basis. He identified two circulation types corresponding to low (typus a) and high (typus b) NAO states, which together were dominant in 83% of all analyzed cases.

It took additional forty years until J. Bjerknes (1964) published the first detailed analysis of North Atlantic air-sea interaction. On the basis of the difference between SLP at Ponta Delgada and southwest Iceland, Bjerknes presented evidence for the time scale dependent nature of North Atlantic air-sea interaction: Interannual variability of SST anomalies may be explained by a direct forcing from the NAO, whereas the explanation of interdecadal SST anomalies requires additional contributions from changed oceanic currents. Recent studies yield support for the time scale dependence of North Atlantic air-sea interaction (e.g., Deser and Blackmon, 1993; Kushnir, 1994; Delworth, 1996).

Rogers (1984) defined the NAO index as the difference between *normalized* SLP at the Azores and Iceland. He showed that the statistical connection between the wintertime NAO and the Southern Oscillation was weak during the period 1900–1983 and found significant power around 7–8-yrs for the winter-averaged NAO index. However, as noted by Rogers, the peaks may have occurred just by chance. Furthermore, his results support Bjerknes' finding that the NAO shows prounounced interdecadal variability.

Further motivated by several studies during the early 1990s (e.g., Cayan, 1992b; Deser and Blackmon, 1993; Kushnir, 1994; Latif and Barnett, 1994; Hurrell, 1995), the NAO has attracted considerable scientific interest in recent years. This can be inferred from the implementation plan for the Climate Variability and Predictability (CLIVAR, 1998) programme. The NAO is related to different topics of CLIVAR, that is, the Atlantic thermohaline circulation (e.g., Timmermann et al., 1998), tropical Atlantic variability (e.g., Rajagopalan et al., 1998; Xie and Tanimoto, 1998), paleoclimatology (e.g., Barlow et al., 1993; Appenzeller et al., 1998a,b), and even global change (e.g., Hurrell, 1996; Ulbrich and Christoph, 1999).

One of the major open scientific questions is whether the variability of the NAO is solely governed by internal atmospheric dynamics or whether some external forcing adds significant amounts of variance to the NAO. Especially the North Atlantic ocean is taken

into account as a possible external forcing candidate. From the observations alone it is difficult to decide in which direction air-sea interaction works[9]. In most cases the forcing pattern (SST anomalies), which is expected to influence the atmosphere, resembles the response pattern due to these atmospheric anomalies. Since time-averaged atmospheric parameters are occasionally considered, expected time-lags on much shorter times-scales are masked (e.g. Palmer, 1993). Furthermore, in most cases it is not sufficient to conclude from the occurrence of significant spectral peaks at specific frequencies in the atmosphere and ocean that a two-way coupling is involved. This is because spurious "oscillations" (just by chance occurrence) of the atmosphere may leave their imprints on the sea-surface via turbulent heat fluxes (Cayan, 1992b).

General circulation models provide valueable tools to investigate the nature of climate variability. The experiment with an atmospheric general circulation model by James and James (1989) shows that the atmosphere may produce low-frequency variability entirely by its own due to nonlinear internal dynamics. On the other hand, responses of the extratropical atmosphere to prescribed SST anomalies were found (e.g., Palmer and Sun, 1985; Latif and Barnett, 1994; Bresch, 1998), although some uncertainty remains with respect to the response pattern (for an overview, see Kushnir and Held, 1996). A somewhat controverse picture about an oceanic forcing of the NAO also arises from recent experiments with coupled general circulation models (CGCMs). There is evidence for a two-way interaction between the NAO and the North Atlantic subtropical gyre (Grötzner et al., 1998) in the ECHO simulation, which has its counterpart in the North Pacific ocean, as originally described by Latif and Barnett (1994). On the other hand, by analyzing the ECHAM4/OPYC3 model simulation, Christoph et al. (1999) found less indication for a noteworthy low-frequency forcing of the NAO by the North Atlantic ocean. A coupled air-sea mode on interdecadal time scales between the NAO and thermohaline circulation was proposed by Timmermann et al. (1998) (ECHAM3/LSG model). This is in contrast to the results by Delworth and Greatbatch (2000) from the coupled GFDL model, where thermohaline circulation variability is a passive response to interdecadal variability of the NAO. An overview about the dynamics of interdecadal variability in different CGCMs is given by Latif (1997).

In this chapter the basic characteristics of observed NAO variability are considered on a statistical basis. The focus is on the winter season. Moreover, attention is devoted to clarify whether there is statistical evidence against the null hypothesis that NAO variability is solely generated by internal atmospheric dynamics.

3.2 Data

As proposed by Rogers (1984), the NAO index is defined as difference between *normalized* SLP time series representative for the Azores High and Icelandic Low. Several NAO indices can be found in the literature. They differ in the choice of the southern station (proxy for the Azores High) and, therefore, in the length of the record. Since SLP measurements at the Azores start in 1865 but earlier measurements are available at Iceland and the Iberian Peninsula, longer NAO indices can be constructed by using, for example, SLP time series from Gibraltar as the southern proxy (Jones et al., 1997). Note, that these longer NAO indices are good proxies during the winter and early spring seasons only. This is because

[9]Notice, that the structure of the lag-correlation function allows to assess the nature of air-sea interactions (Frankignoul, 1985). This concept is applied in chapter 5.

the NAO's southern center of action (Azores High) is shifted considerable towards the west Atlantic during the other seasons (Hurrell and van Loon, 1997; Mächel et al., 1998).

Two different NAO indices are used in this study. The first NAO index, NAO1 hereafter, is based on the difference of normalized SLP observations between the Azores (Ponta Delgada) and a composite from different sites at south-west Iceland. NAO1 spans the period 1865–1997. The second NAO index, NAO2 hereafter, was constructed in a similar manner, except that SLP from Gibraltar was used instead of SLP from Ponta Delgada (Jones et al., 1997). By using SLP from Gibraltar the NAO index can be extended back by additional forty years (1825–1997). Furthermore, SLP time series for all three sites are analyzed separately along with the time series of the (non-normalized) SLP difference between the Azores and Iceland (dSLP1) as well as Gibraltar and Iceland (dSLP2). It is worth noting, that Jones et al. (1997) applied *ad hoc* adjustments to the raw SLP data from Gibraltar and Iceland in order to homogenize the time series. The homogenization has consequences for the subsequent discussions on the interdecadal variability (see below). For SLP at Gibraltar primarily changes in the station level are believed to be the source of these inhomogenieties. Adjustments of +0.8 hPa from 1931–1970 and +2.3 hPa before 1931 have been applied. Adjustments for the SLP proxy from southwest Iceland have their cause primarily in the composite nature of this time series, that is, SLP from different sites and therefore elevations enter this proxy. The SLP time series from Ponta Delgada (Azores) was also homogenized for the period 1894–1960 (Phil Jones, personal communication); the UK Met Office gridded SLP dataset served as the "truth". Note, that during the winter months uncertainties that are associated with the homogenization are relatively small compared to the standard deviation of natural fluctuations.

Spatial NAO characteristics were analyzed from gridded SLP data (5° × 5°) over the Northern Hemisphere north of $15°N$ for the period 1899–1997 (updated from Trenberth and Paolino, 1980). Errors and discontinuities are reported for this data set. These occur primarily during the period before 1922, particularly over parts of Asia. Problems also exist during World War II (1944 and 1945), especially north of $70°N$ due to sparse sampling and in low-latitudes where the signal-to-noise is relatively low.

3.3 Seasonality — On the Definition of the Winter

The annual cycle of the average and (interannual) standard deviation of the difference between monthly SLP from the Azores and Iceland[10] (dSLP1) is depicted in Fig. 3.1. On average dSLP1 is at its maximum during December and January. There is some indication that the average annual cycle lags behind the solar cycle by approximately one month. Such a phase-lag is well-known for average near-surface temperatures over the Northern Hemisphere (Trenberth, 1983), which is primarily caused by the thermal inertia of the ocean. The amplitude of interannual dSLP1 variability is clearly phase-locked to the annual-cycle and lags behind the average annual-cycle of dSLP1 by about one month (Fig. 3.1). There is less indication for this lag to depend on (i) the time scale under consideration (different frequency-ranges were checked), or (ii) the analyzed period (different epochs were checked). Furthermore, the SLP time series from the Azores, Gibraltar, and Iceland were analyzed in a similar manner; the phase-lag is evident at all three sites.

[10]Note, that the annual cycle of the average NAO index and its interannual standard deviation shows no seasonality by definition.

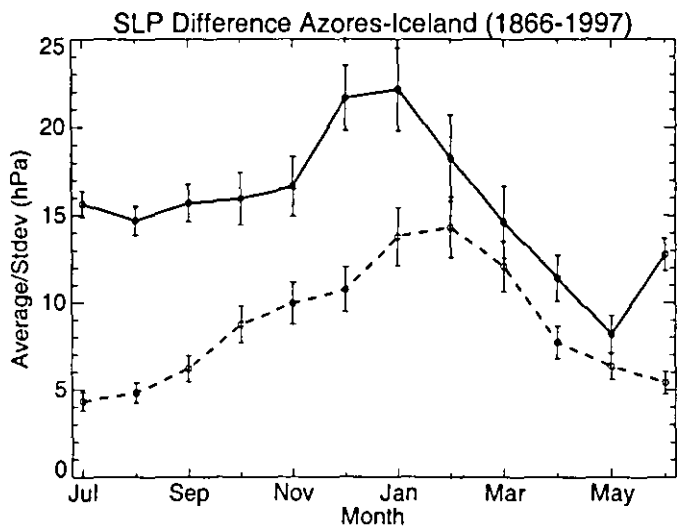

Figure 3.1: Annual cycle of the average SLP difference (hPa) between the Azores and Iceland (solid) and its interannual variability (dashed) for the period 1866–1997. Vertical bars denote 95% confidence intervals.

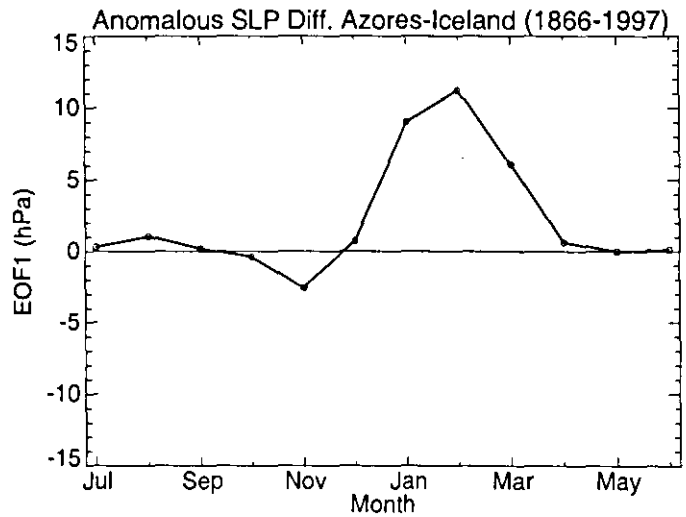

Figure 3.2: Leading EOF (hPa) of anomalous annual cycles of the SLP difference between the Azores and Iceland (dSLP1) estimated from the period 1866–1997.

In order to isolate the dominant modes of *covariability* during the winter months, ordinary EOF analysis was applied to anomalous annual cycles of dSLP1 for the period 1866–1997. The first EOF explains 24.5% of the total variance and describes anomalies of one sign during the winter months from January to March (Fig. 3.2). This mode explains 43%, 62%, and 26% of the variance for the individual winter months January, February, and March, respectively. During the other months between 0–7% of the interannual variance is explained by this EOF. The leading EOF is well-separated from the subsequent mode according to the criterion of North et al. (1982). The corresponding first PC is highly correlated with NAO1 for the winter season JFM ($r = 0.96$).

The same analysis was repeated for dSLP2 and SLP time series from the Azores, Gibraltar and Iceland separately as well as for different periods; the leading EOFs (not shown) are quite similar to those for dSLP1, except that EOF1 for SLP from Iceland is more biased towards February anomalies. It is worth noting, that the first EOF of dSLP1 does not necessarily imply intraseasonal coherence during JFM; it just represents the pattern that maximizes the total variance of the vector series in an effective manner (see Methods).

EOF analysis applied to *normalized* anomalous annual cycles of dSLP1 and NAO1 in order to investigate *coherent* structures on intraannual time scales does not yield conclusive results. This is because the leading EOFs may be mixed according to the criterion of North et al. (1982). The strength of intraseasonal coherence for NAO1 during the winter months from November to April can be inferred from the cross-correlation matrix shown in Tab. 3.1[11]. There is some tendency for NAO1 anomalies to persist into the following month, at least for November, January, and February (first off-diagonal in Tab. 3.1). Overall, although statistically significant, lag-1 month correlations are relatively small explaining less than 10% of the month-to-month variance.

The low-frequency character (5-yr running mean) of anomalous annual cycles of dSLP1 becomes apparent from Fig. 3.3. During the winter months from January to March interdecadal variability is evident: The westerlies were enhanced during the beginning and end of the 20th century and reduced during the period 1930–1960 (see also Hurrell, 1995). Note, that there seems to be relatively little interdecadal variability during the early winter months (OND) and during the late spring season (AMJ). On interannual time scales some agreement between anomalies in January and February is evident, at least during the 20th century ($r = 0.66$ from 1900 to 1997). Both months covary 180^o out-of-phase during the last part of the 19th century.

Throughout the remainder of this chapter further analyses of NAO characteristics during *winter* are based on JFM averages. Of course, other objective definitions are possible. However, the JFM season appears to account for the maximum of variance along with the maximum of intraseasonal coherency of low-frequency NAO variability, at least during the 20th century.

[11] During the preparation of this manuscript the author became aware of a similar analysis presented by Osborn et al. (1999). They show that for the NAO2 index (1865–1997) correlations are significant, but low, for one month ahead from November to March.

Table 3.1: Linear correlation coefficients between individual winter months of the NAO1 index for the period 1865–1997. Correlations significantly different from zero at the 95% confidence level are in bold (two-sided t-test).

	Nov	Dec	Jan	Feb	Mar	Apr
Nov	**+1.0**	**+0.29**	**−0.18**	−0.12	−0.02	0.00
Dec	—	**+1.0**	+0.13	−0.07	+0.04	**+0.17**
Jan	—	—	**+1.0**	**+0.17**	**+0.18**	+0.10
Feb	—	—	—	**+1.0**	**+0.21**	0.00
Mar	—	—	—	—	**+1.0**	−0.08
Apr	—	—	—	—	—	**+1.0**

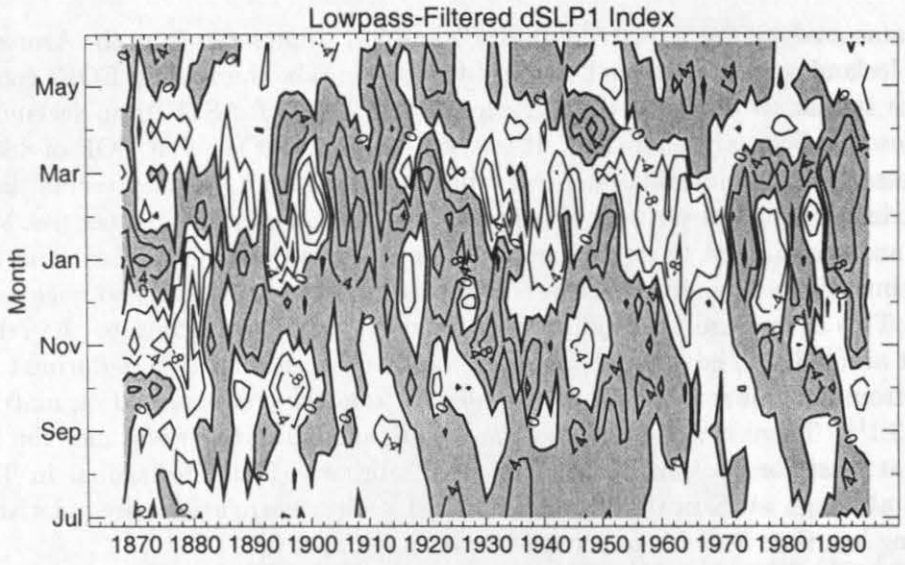

Figure 3.3: Lowpass-filtered (5-yr running mean) anomalous annual cycles of the difference between SLP at the Azores and Iceland (dSLP1, hPa) for the period 1866–1997. Contour interval is 4 hPa. Positive values are shaded. Years refer to Januaries. Lowpass-filtering was done for each month separately.

3.4 Distribution Characteristics

The NAO indices provide the basis for numerous statistical investigations throughout the remainder of this manuscript. For the interpretation of these results it is helpful to know how the indices are distributed.

Estimated probability density functions (PDF) for winter-averaged (JFM) NAO1 and NAO2 are depicted in Fig. 3.4. The distribution of these indices appears to be almost

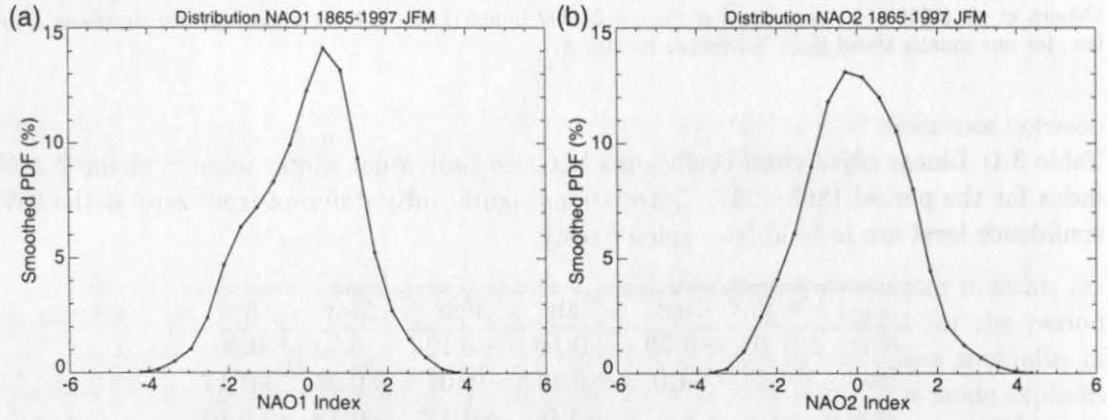

Figure 3.4: Probability density function (PDF) of winter-averaged (JFM): (a) NAO1 index (1865–1997) and (b) NAO2 index (1825–1997). PDFs were smoothed using a Gaussian Kernel (smoothing parameter is $h = 0.42$). Details are given by Silverman (1986).

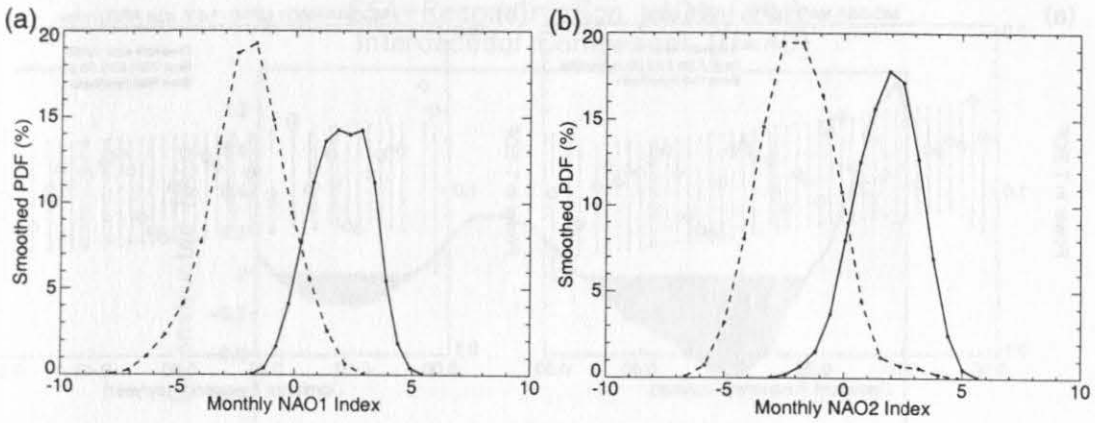

Figure 3.5: Probability density function (PDF) of monthly NAO indices (January through March) during high (solid) and low (dashed) NAO winters (JFM): (a) NAO1 index ($n_{high} = 39$ and $n_{low} = 60$ months) and (b) NAO2 index ($n_{high} = 69$ and $n_{low} = 60$ months). High (low) NAO winters are one standard deviation avove (below) the average. PDFs were smoothed using a Gaussian Kernel (smoothing parameter is $h = 0.62$).

Gaussian, especially for NAO2. NAO1 shows a negative coefficient of skewness[12] ($a_3 = -0.28$): Whereas high NAO1 winters are more frequently associated with relatively small anomalies, low index winters tend to be more extreme. Note, however, that the coefficient of skewness for NAO1 is not statistically significant (at 95% confidence) according to the method described by White (1980). For such a value of skewness to become significant at least 306 winters would be required. PDFs were also estimated using monthly data from January to March and the results are very similar (not shown) to those for JFM averages. Since more observations are available for monthly data, the negative coefficient of skewness ($a_3 = -0.41$) for NAO1 is significant (at 95% confidence). Significant positive (negative) coefficients of skewness for geopotential height anomalies at the 500 hPa level north (south) of the North Atlantic storm track on intraseasonal time scales were found by White (1980) and Nakamura and Wallace (1991). Since the NAO index is defined as the difference between (normalized) SLP time series from the south (Azores) and the north (Iceland) of the storm track, a negatively skewed distribution of the NAO is in agreement with results by White (1980) and Nakamura and Wallace (1991).

In the previous section it was shown that intraseasonal persistence of the NAO is relatively small during wintertime. In order to assess whether the persistence depends on the strength of the wintertime NAO, PDFs for monthly NAO1 and NAO2 were estimated for those winters (JFM) with weak and strong NAO1 and NAO2 anomalies, respectively (Fig. 3.5). Obviously, the bulk of monthly anomalies shows the same sign during high and low NAO winters although considerable scatter remains. Of course, this is what would be expected by construction. However, there is some indication that the intraseasonal variance is higher during low NAO winters than during high NAO winters. For NAO1 this difference (2.2 versus 1.3) is significant (90% confidence, two-sided F-test). It is worth noting, that over the North Pacific intraseasonal atmospheric variability is less pronounced

[12]That the distribution of the NAO index is negatively skewed has been brought to my attention by Axel Timmermann.

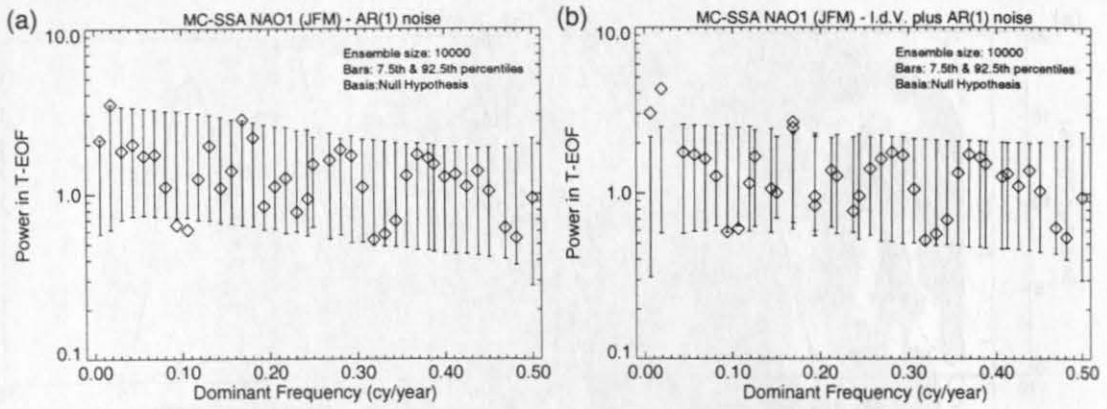

Figure 3.6: Test of the winter-averaged (JFM) NAO1 against (a) AR(1) noise and (b) interdecadal variability plus AR(1) noise by means of Monte Carlo SSA. *Diamonds* denote the projection of the lag-covariance matrix of NAO1 upon the T-EOFs of the null hypothesis, plotted against the dominant frequency (obtained by reduced Fourier transform of T-EOFs). Each vertical bar contains 85% of the eigenvalues out of 10000 realizations of the null hypothesis. A window length of forty years was used. The analysis is based on the period 1865–1997.

during winters with a more zonal circulation than during winters with more "blocked" flows (e.g., Molteni and Corti, 1998, and references therein). Due to the shortness of the observed NAO indices it is difficult to decide whether similar characteristics as over the North Pacific are also evident the North Atlantic. This item will be revisited in chapter 5, where the distribution of the NAO is investigated using a century-scale integration of a coupled general circulation model.

3.5 Frequency Characteristics

MC-SSA was applied in order to test winter-averaged NAO1 and NAO2 indices for deterministic components against (i) *AR(1) noise* and (ii) *signal(s) plus AR(1) noise.*

The eigenvalue spectrum of NAO1 (JFM, 1865–1997) using a window length of forty years is depicted in Fig. 3.6a. Two excursions above the *local* 92.5% confidence level (92.5*th* percentile) occur, one on interdecadal[13] time scales and one around 6-yrs. Note, that two or more excursions out of possible forty have a probability of 72% to occur just by chance under the *global* null hypothesis (determinded by a second run through the ensemble) that NAO1 represents a realization of AR(1) noise. As pointed out by Allen and Smith (1996), there is prior reason to focus attention onto the two low-frequency eigenvalues since they describe variability $\geq$40-yrs. This is in contrast to all other eigenvalues, which describe variability in a specific frequency-band (Allen and Smith, 1996). Therefore, interdecadal variability of winter-averaged NAO1 (1865–1997) is unusual at 92.5% confidence compared to realizations of AR(1) noise. Next, NAO1 was tested against the composite null hypothesis that it represents a segment of AR(1) noise plus interdecadal

[13] Actually, these eigenvalues represent a *nonlinear trend* since they are based on a window length of forty years. We shall call this nonlinear trend *interdecadal variability* due to the behaviour of the reconstruction (see below). Note, however, that there are 1.5 realizations at best for the time series under study.

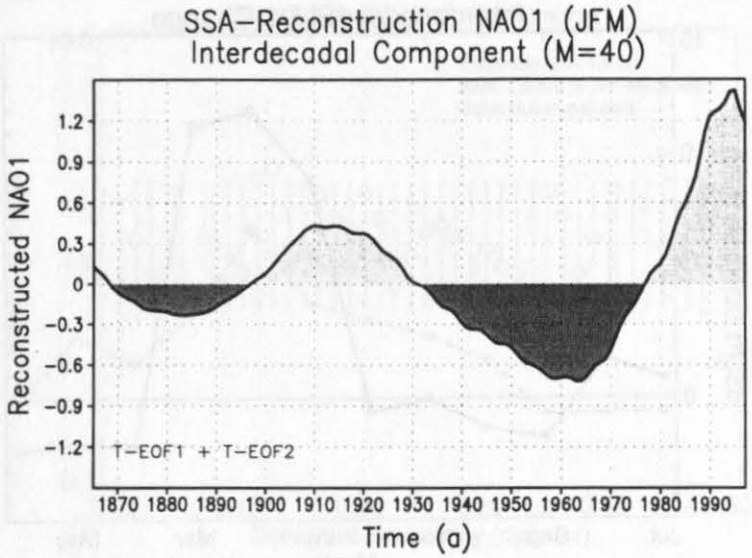

Figure 3.7: Interdecadal variability of the winter-averaged (JFM) NAO1 index. The reconstruction (T-RC) is based on the first two eigenmodes (Fig. 3.6) from a separate SSA using T-EOFs of the data. The reconstruction describes NAO1 variability on time scales longer than forty years.

variability. Both interdecadal eigenvalues were treated as signal although only one was found to be significant. Using this more specific null hypothesis the spectrum becomes approximately white (Fig. 3.6b). This is because the AR(1) parameters were estimated without taking into account the contribution from the *interdecadal signal*. Two significant excursions above the local 92.5% confidence level occur on interdecadal time scales as well as around 6-yrs[14]. The probability for at least two excursions (low-frequency eigenvalues due not enter the test) above the local 92.5% confidence level to occur just by chance is 69%. Since there was no *a priori* expectation about variability around 6-yrs, the more stringent *global* composite null hypothesis that NAO1 consists of interdecadal variability (at 92.5% confidence) plus AR(1) noise cannot be rejected with reasonable statistical confidence.

Reconstructed interdecadal NAO1 variability during wintertime, which is based on the leading two T-EOFs, is depicted in Fig. 3.7. The strong positive linear trend during the last three decades (Hurrell, 1996) with persistent high (low) NAO1 phases during the end of this century (around the sixties) is clearly evident. The interdecadal signal explains about 15% of the variance for NAO1 during the period 1865–1997. Obviously, there is no clear frequency associated with the interdecadal development: The decrease (increase) during the first (last) part of this century takes place relatively slow (fast). Note, that the amplitude of interdecadal NAO1 variability increases steadily as function of time. Our results are in general agreement with those described by Moron et al. (1998), who applied MC-SSA to DJFM averages of NAO1. Here, additionally the confidence level for interdecadal variability is given. Moron et al. (1998) conclude that NAO1 shows a robust oscillation with a period of 7–8-yrs. Results from the global test applied in this study do

[14]The eigenvalues for NAO1 have slightly changed, because of the more specific null hypothesis and therefore slightly changed $\mathbf{E}_N$ in Eqn. 2.8.

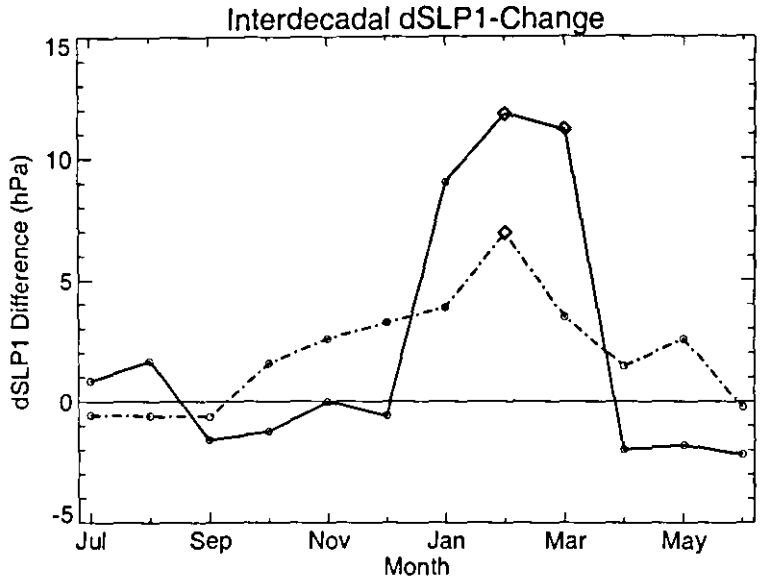

Figure 3.8: Epoch-difference of monthly dSLP1 (hPa): 1980–1997 minus 1950–1970 (solid) and 1905–1925 minus 1866–1900 (dash dot). Diamonds denote statistically significant differences at the 95% confidence level (two-sided t-test).

not support the notion that this "oscillation" is robust.

In order to clarify during which winter months interdecadal NAO variability is most pronounced, epoch differences for dSLP1 between interdecadal high and low NAO1 states were calculated (Fig. 3.8). Obviously, the strong increase of dSLP1 ($\approx$ 10 hPa) from the sixties onwards is evident during *all* individual winter months from January to March. This is in agreement with the more qualitative discussion of Fig. 3.3. The increase of dSLP1 during the turn of the last century is less pronounced and the early winter months are also somewhat (although not significantly) involved. A similar picture is obtained if NAO1 is used instead of dSLP1 (not shown). This analysis further enhances our confidence that the JFM definition is not merely motivated from the point of view of variance-compression, as might be suggested by the EOF technique.

The MC-SSA test of NAO2 against the null hypothesis of AR(1) noise yields somewhat different results (Fig. 3.9), even if the overlapping period (1865–1997) is considered (not shown). There is less "redness" for NAO2 compared to NAO1. This is primarily due to relatively low power of NAO2 on interdecadal time scales. Two excursion above the *local* 92.5% confidence level occur around 8-yrs. The probability for at least two such excursions to occur just by chance is 72%. Since there was no *a priori* expectation regarding 8-yr variability, NAO2 is not unusual (at 28% confidence) compared to realizations of AR(1) noise.

A direct comparison of the eigenvalue-spectra for NAO1 and NAO2 (Fig. 3.6 and 3.9) reveals that the former index shows significant power for slightly higher frequencies than the latter does (0.169 versus 0.136 cy/yr^{-1}). Since the spectral resolution of SSA is limited by $1/M$ (M=40-yrs in this study) these two peaks cannot be distinguished from a broad-band phenomenon.

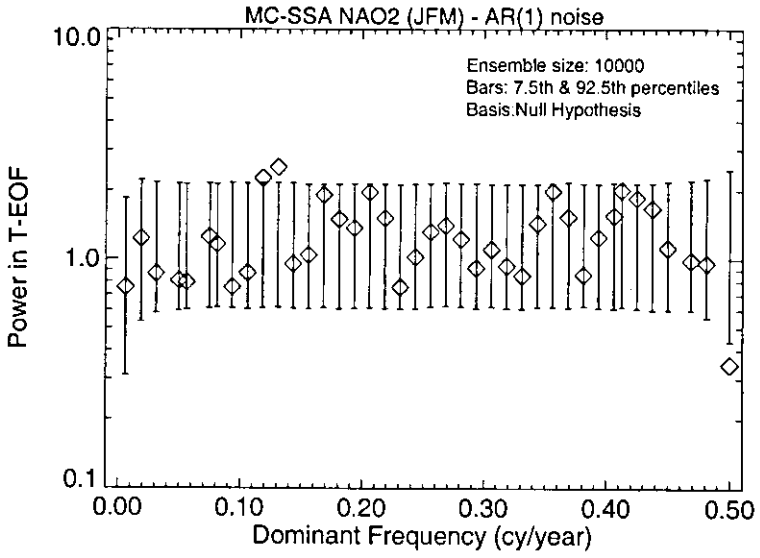

Figure 3.9: As in Fig. 3.6a except for NAO2 (1825-1997).

3.6 Time-Frequency Characteristics

In order to investigate whether the NAO's spectral characteristics are time-dependent, Wavelet analysis was applied.

Normalized local wavelet power for winter-averaged NAO2 and NAO1 is depicted in Fig. 3.10. Note, that averaging local wavelet *spectra* over the whole record (time) yields essentially the same results as described in the previous section. Neither for NAO2 nor for NAO1 there is strong evidence for the presence of a distinct mode of variability in any frequency-band throughout the whole record. This finding is in agreement with results by Appenzeller et al. (1998b), who applied Wavelet analysis to an *annual-mean* NAO index. Local wavelet power is enhanced on inderdecadal time scales during the 20th century for NAO1 and NAO2 (Fig. 3.10). Only for the former index, however, power estimates exceed the *local* 95% confidence level. Interdecadal variability was less pronounced during the 19th century. This feature becomes particularly evident for the longer time series NAO2 (Fig. 3.10a). It is worth noting, that power estimates on these longer time scales are strongly influenced by side-effects (underestimated, the bias which increases towards the sides). A comparison between the interdecadal NAO1 reconstruction by SSA (Fig. 3.6) and the results from the Wavelet analyis indicates that the decrease of local wavelet power on interdecadal time scales since 1960 or so is an artifact of the wavelet method due to side-effects. Nevertheless, we think that it is reasonable to discuss local wavelet power on interdecadal time scales, at least qualitatively. Differences between the results from SSA and Wavelet analysis show the importance to use different methods.

Results from Wavelet analysis applied to NAO1 and NAO2 suggest that frequency-characteristics have changed during the turn of the last century, that is, the spectrum became "redder". This reddening has already been noted by Hurrell and van Loon (1997), who used windowed Fourier analysis with a window-length of 60-yrs. The advantage of Wavelet analysis compared to windowed Fourier analysis lies in the better (data-adaptive) resolution on interannual time scales. Note, that using the latter method a single spike-

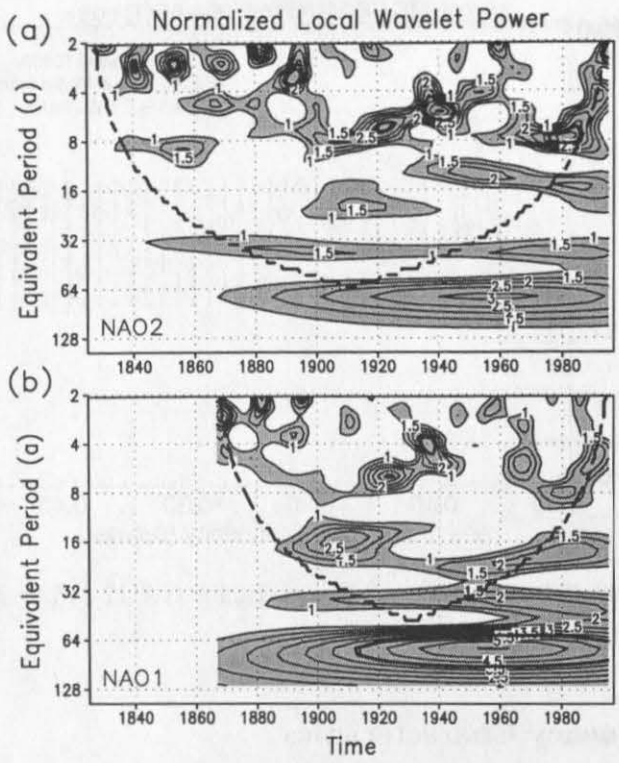

Figure 3.10: Normalized (by variance) local wavelet power for winter-averaged (JFM) (a) NAO2 and (b) NAO1. Power exceeding 1.0 stands above the background noise (shaded regions). Contour interval is 0.5 for local wavelet power exceeding 1.0. The cone of influence (bold-dashed), within side effects become important, and local wavelet power estimates exceeding the local 95% confidence level (bold-solid) are also shown. Power estimates are smoothed in time (5-yr smoothing).

like event on interannual time scales would be smeared over the whole window-length. The Wavelet analysis reveals that actually the frequency of occurrence of spike-like events on interannual time scales (2–4-yrs) was enhanced for NAO2 during the 19th century (Fig. 3.10a).

Of course, some agreement between NAO1 and NAO2 can be expected by construction, since they are based on measurements at the same location for the NAO's northern center of action (southwest Iceland). Nevertheless, differences are obvious between NAO1 and NAO2, especially with respect to variability on interdecadal time scales. Wavelet analysis separately applied to the winter time series of normalized SLP from Iceland, Gibraltar, and the Azores (Fig. 3.11) shows that strong interdecadal SLP variability is evident at Iceland and the Azores, but missing at Gibraltar. There remain, however, some uncertainties for the SLP time series from Gibraltar, because *ad hoc* corrections were applied that may interfere with natural variability on interdecadal time scales. If, for example, the adjustment of $+0.8\ hPa$ for the epoch 1931–1970 (Jones et al., 1997) is removed from the SLP time series at Gibraltar, then local wavelet power reveals enhanced interdecadal variability during the 20th century (not shown). Nevertheless, even without these adjustments power estimates for SLP at Gibraltar are still 2–3 times smaller than those for SLP

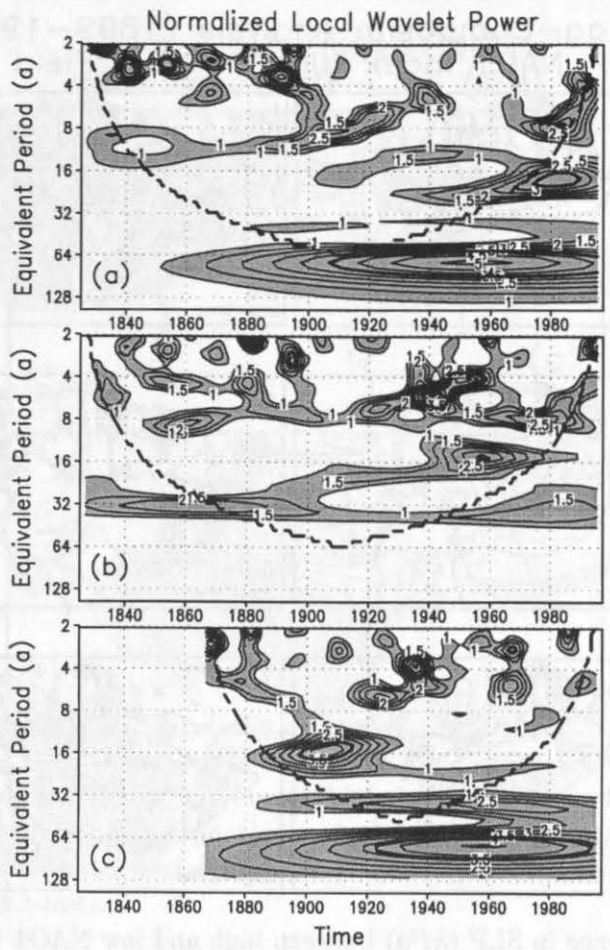

Figure 3.11: As in Fig. 3.10, except for SLP time series from (a) Iceland, (b) Gibraltar, and (c) the Azores. No data are available in (c) before 1865.

at Iceland and the Azores. The relatively strong reddening during the turn of the last century seems to be most pronounced for SLP at Iceland (Fig. 3.11a).

3.7 Winter-to-Winter Persistence

As shown in previous sections, the spectrum of the winter-averaged NAO is slightly red. This "redness" is primarily due to enhanced low-frequency variability (>5-yrs or so) of the NAO during the 20th century. The lag-1 auto-correlation coefficient for NAO1 (NAO2) amounts to 0.25 (0.18) for the period 1899–1997. Although the auto-correlation between subsequent winters explains (linear) less than 7% of the winter-to-winter variance the presence of this auto-correlation is surprising having in mind that the auto-correlation for the seasonal[15] NAO1 (NAO2) index is -0.07 (-0.08). In order to shed further light onto the persistence of wintertime NAO anomalies, lag-composite analyses were performed.

The typical evolution of SLP anomalies through the annual march during years when there was a strong wintertime NAO1 anomaly is depicted in Fig. 3.12. Simultaneous

[15]Seasonal indices are based on the sequence JFM, AMJ, JAS, OND, JFM and so forth.

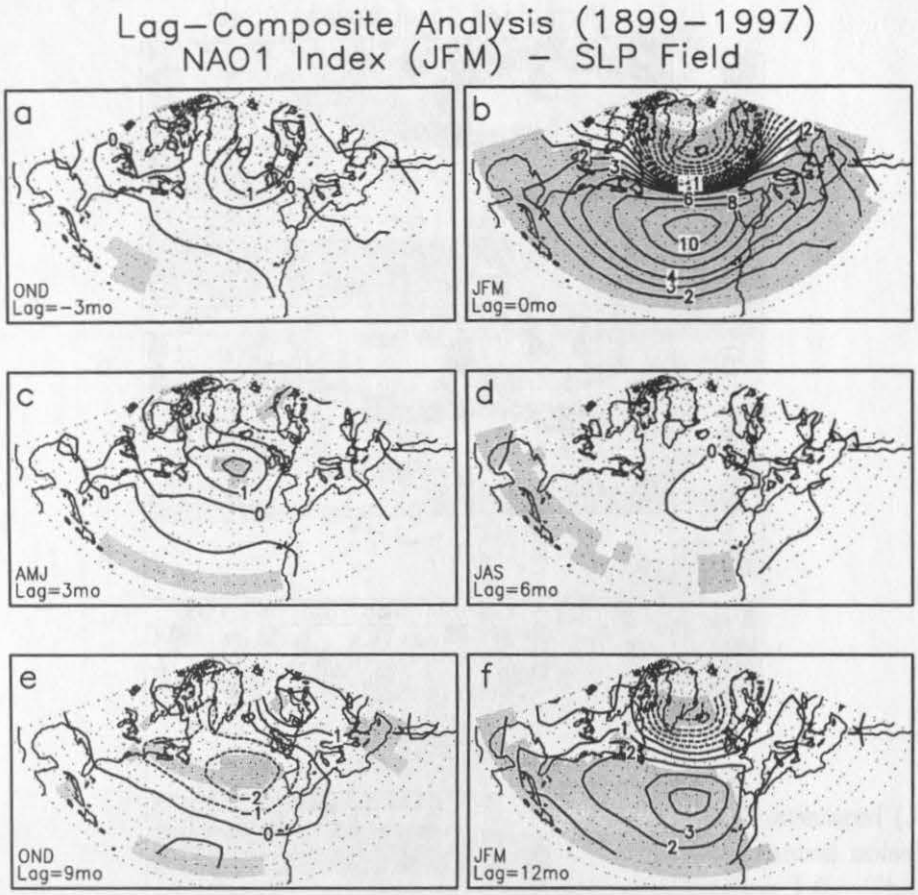

Figure 3.12: Difference in SLP (hPa) between high and low NAO1 winters (JFM) for (a) the autumn before, (b) the same winter, (c) the following spring, (d) the following summer, (e) the following autumn, and for (f) the following winter. A threshold of one standard deviation was used. Results are based on the period 1899–1997. Differences non-zero at 95% confidence are shaded (two-sided t-test).

SLP anomalies show the typical NAO pattern with centers of action near Iceland and the Azores (Fig. 3.12b). During the subsequent non-winter seasons the NAO anomaly disappears (Fig. 3.12c–e). A significant NAO anomaly having the same sign as in the previous year reappears one winter later (Fig. 3.12f); its magnitude, however, is reduced by more than a factor of two compared to the previous winter. Furthermore, no NAO-like precursor is evident from the anomalous SLP field during the autumn before the occurrence of a winter with a strong NAO anomaly (Fig. 3.12a). Note, that the null hypothesis of no persistence of winter NAO anomalies through the subsequent seasons can be rejected on the basis of *local* significance descisions at the NAO's centers of action. To test the significance of different patterns like that in Fig. 3.12c, for instance, a *global* test (Livezey and Chen, 1983) would be required. Such an analysis goes beyond the scope of this study. Rogers and van Loon (1979) and Meehl and van Loon (1979) analyzed SLP fields for the autumn before and spring after there were strong seesaw years in air temperature between Westgreenland and Scandinavia. Missing NAO anomalies for these seasons in

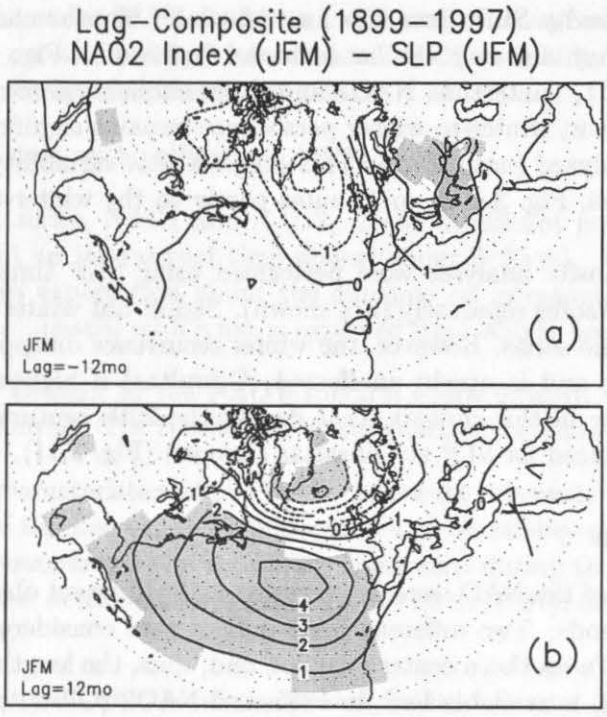

Figure 3.13: Difference in SLP (hPa) between high and low NAO2 winters (JFM) the (a) winter before and (b) for the following winter. A threshold of one standard deviation was used. Results are based on the period 1899–1997. Differences non-zero at 95% confidence are shaded (two-sided t-test).

Fig. 3.12a,c are in agreement with their results. It is worth noting, that the recurrence of strong wintertime NAO anomalies one year later is most pronounced over oceanic regions (Fig. 3.12f), particularly over the subtropical ocean large areas of statistical significance are evident.

We have checked that the winter-to-winter persistence is stable with respect to changes in (i) the threshold used for compositing (others than ± 1 standard deviation) and (ii) the epoch under investigation (1899–1949 and 1950–1997 compared to 1899–1997). Separate analyses for high and low NAO1 (JFM) index years indicates that the recurrence is slightly more pronounced after *high* index winters.

The MC-SSA spectra (Fig. 3.6) and the local wavelet spectra (Fig. 3.10a) of NAO1 suggest that particularly variability on interdecadal time scales contributes to the winter-to-winter persistence of NAO1. To test this hypothesis, both, NAO1 and SLP anomalies at each grid point were highpass-filtered retaining variability in the range 2–30-yrs. This was done using a wavelet-based filter (e.g., Torrence and Compo, 1998). The response function has its halfpower-width at about 30-yrs. The response for 2-yr variability amounts to approximately 40% increasing to 100% for 3-yr variability. Lag-composite analysis for highpass-filtered data (not shown) reveals no significant winter-to-winter persistence. Thus, winter-to-winter persistence of NAO1 seems to be primarily governed by processes taking place on interdecadal time scales.

Significant winter-to-winter persistence also occurs if NAO2 is used for compositing

(Fig. 3.13b). For brevity SLP anomalies for non-winter months and the base winter are not shown, since they are very similar to those depicted in Fig. 3.12. In contrast to the results for NAO1, wintertime NAO2 anomalies show no precursors one year before (Fig. 3.13a). Moreover, winter-to-winter persistence remains significant even if highpass-filtered data are analyzed (not shown). This suggests that variability on interannual time scales (about 5–9-yrs, Fig. 3.10a) contributes partly to the winter-to-winter persistence, at least for NAO2.

Finally, lag-composite analyses were performed using SLP time series from Iceland, Gibraltar, and the Azores separately (not shown). Significant winter-to-winter persistence is found for each time series. However, the winter recurrence disappears (Azores), is only moderate (Iceland), and is nearly unaffected (Gibraltar) if highpass-filtered (2–30-yrs) data are used. Note in this context, that during the 20th century 5–9-yr variability is most (least) pronounced for SLP at Gibraltar (Azores) (Fig. 3.11).

3.8 Conclusions

The characteristics of the NAO were investigated using different observational time series and statistical methods. Two different NAO indices were considered, which differ in the location of the NAO's southern center of action and, thus, the length of the record. NAO1 (Azores and Iceland) is available back to 1865, and NAO2 (Gibraltar and Iceland) covers the period 1825–1997. Historical SLP analyses spanning the 20th century were used to investigate spatial characteristics of the NAO.

First, the seasonality of the NAO was investigated. From these analyses the following conclusions can be drawn:

- Covariability of the NAO between individual winter months is most pronounced for January, February and March (JFM) explaining about 25% of the total variance.
- Monthly coherence of the NAO is very low explaining less than 10% of the month-to-month variability.
- During the 20th century the NAO's monthly coherence is relatively strong for lower-frequency variability. Interdecadal NAO variability during the last five decades is only evident during the winter months from January through March.

Second, the distribution of the NAO was investigated from estimated probability density functions (PDFs). Having in mind the shortness of the observational record and, thus, possible sampling problems, evidence for the following conclusions is presented:

- The wintertime NAO1 index shows a negative coefficient of skewness. The negative skewness of NAO1 is significant for monthly data (January through March).
- Intraseasonal variability is more pronounced for low NAO1 winters compared to high NAO1 winters.

These results provide at least working assumptions that can be evaluated using century-scale integrations of coupled general circulation models (see chapter 5).

Third, spectral characteristics of the NAO were investigated by means of Monte Carlo SSA. The conclusions are as follows:

- NAO1 is consistent (at 92.5% confidence) with realizations of interdecadal variability superimposed on AR(1) noise. Interdecadal NAO1 variability explains 15% of the total variance during the period 1865–1997.

- NAO2 is consistent with realizations AR(1) noise.

- For both time series, NAO1 and NAO2, *locally* significant power (at 92.5% confidence) is found on interannual time scales (about 5–9-yrs). However, since there was no *a priori* expectation about the outcome on interannual time scales, their existence is not unusual with what is expected from AR(1) noise.

Fourth, temporal changes of the NAO's spectral characteristics were investigated by means of Wavelet analysis. The results can be summarized as follows:

- The spectral characteristics of the NAO underwent relatively abrupt changes during the turn of the last century. Whereas 2–4-yr variability dominated during the 19th century, lower-frequency variability dominated during the 20th century. This "reddening", first described by Hurrell and van Loon (1997), is most pronounced for SLP at Iceland.

- Natural variability of SLP is relatively weak in low-latitudes of the North Atlantic basin. Thus, inhomogenieties of SLP time series representing variability of the Azores High lead to considerable uncertainties (especially at Gibraltar) for SLP variability on interdecadal time scales.

- Interdecadal NAO variability is captured most efficiently if SLP time series from the Azores and Iceland are used.

Finally, the analysis how wintertime NAO anomalies during the 20th century evolve through the annual march leads to the concept of winter-to-winter persistence[16]:

- NAO anomalies show significant persistence from winter-to-winter. During the in-between non-winter seasons no significant NAO anomalies are evident.

- Although primarily interdecadal NAO variability is responsible for the winter-to-winter persistence, enhanced variability on interannual time scales (about 5–9-yrs) appears to contribute to this phenomenon. Due to the shortness of the time series a quantification of the relative contributions is difficult to carry out.

3.9 Discussion

The main objective of the analyses decribed in this chapter was to clarify whether there is *statistical* evidence for the presence of deterministic components from the observational NAO record.

The presence of significant NAO variability around periods of 2–2.5-yrs and 24-yrs was reported in the literature (e.g., CLIVAR, 1998; Cook et al., 1998). From the results of this study, there is less indication for noteworthy power of the NAO around 24-yrs. Enhanced quasi-biennial variability (2–2.5-yrs) of the NAO is only found during the 19th century

[16] J. W. Hurrell (personal communication) and M. McCartney arrived at a similar conclusion.

(Fig. 3.10; see also Walker, 1924; Hurrell and van Loon, 1997). Quasi-decadal variability (12–14-yrs) in the North Atlantic region is another phenomenon that has attracted considerable attention in recent years (e.g., Deser and Blackmon, 1993; Sutton and Allen, 1997). In agreement with the results by Deser and Blackmon (1993) we found less evidence for the NAO to be strongly involved, because spectral power is relatively low in this frequency-band (Fig. 3.10). Furthermore, the quasi-decadal atmospheric SLP pattern (e.g., Deser and Blackmon, 1993; Sutton and Allen, 1997; Jung et al., 1998) bears more resemblence with the near-surface signature of the West Atlantic teleconnection pattern originally described by Wallace and Gutzler (1981) rather than the NAO pattern.

It is shown that the NAO index, defined as the difference between normalized SLP time series from the Azores and Iceland, shows significant interdecadal variability (at 92.5% confidence) during the period 1865–1997. This low-frequency variability of the NAO was most pronounced during the last four decades or so. It may surprise that interannual NAO variability (5–9-yrs) is not interpreted as a determinstic component although spectral analysis reveals local significance. This is because no *a priori* expectation was available, thus, requiring a more stringent *global* test in order to reject the null hypothesis that, apart from interdecadal variability, the NAO represents a segment of red noise (see Livezey and Chen, 1983; Allen and Smith, 1996, for a detailled discussion). It it worth mentioning, that even the well-known El Niño/Southern Oscillation phenomenon just passes the red noise null hypothesis at the global 95% confidence level. Summarizing, *"red noise is hard to beat"* (Allen and Smith, 1996), especially for variability of the extratropical atmosphere.

An important item for the discussion of wintertime NAO variability is its winter-to-winter persistence (Fig. 3.12). It is difficult to explain how internal variability of the atmosphere ("randomness") leads to the reemergence of NAO anomalies from one winter to the following one, although no NAO anomalies were evident during the inbetween non-winter seasons. From a dynamical point of view the autumn following a strong NAO anomaly provides an initial condition for the subsequent winter season that is random in character (Fig. 3.12e). Thus, there is less reason to expect recurrence of NAO anomalies (Fig. 3.12f) if the NAO is solely governed by internal atmospheric dynamics. From the above discussion the following two hypotheses may be formulated: First, the appropriate null hypothesis for wintertime NAO variability is "white noise". The "red noise" null hypothesis leads to conclusions that are too conservative. Second, the recurrence of the wintertime NAO anomalies during the 20th century results from some external forcing.

The North Atlantic ocean represents an attractive candidate for such an external forcing of the NAO. Namias and Born (1970) found recurrence of North Pacfic wintertime SST anomalies. They speculated that wintertime SST anomalies are capped by a shallow summer mixed-layer so that much longer lifetimes for wintertime SST anomalies result in comparison to those predicted by the stochastic climate model (for an overview, see Frankignoul, 1985). This mechanism — the Namias-Born mechanism — was confirmed by Alexander and Deser (1995) from the analysis of sub-surface data. The Namias-Born mechanism may explain the winter-to-winter persistence of the NAO. If, for example, a positive wintertime NAO anomaly has developed (randomly or externally forced), then associated turbulent heat flux anomalies change the heat content of the upper-ocean. This heat content anomaly is preserved from the sea-surface through the summertime mixed-layer. During the subsequent (autumn) winter season enhanced mechanical mixing brings the heat content anomaly back to the sea-surface. The recurrence of the SST anomaly may help to lock the NAO in the same state as during the winter one year before. For

this mechanism to operate it is crucial that the anomalous SST pattern generated by the NAO resembles the anomalous SST pattern that forces the NAO. Recent results from the modelling study by Rodwell et al. (1999) yield support for such a two-way interaction between the NAO and North Atlantic SST anomalies. The Namias-Born mechanism has difficulties, however, to explain low-frequency *variability* in the North Atlantic region. Moreover, winter-to-winter peristence of the NAO was presumably missing during the 19th century (Hurrell and van Loon, 1997, their Fig. 7). The reconstruction of the annual-mean NAO index from paleoclimatic data by Appenzeller et al. (1998b) suggests that the spectral characteristics of the NAO as observed during the 20th century are even unusual in a longer-term context (since 1650). It has to be kept in mind, however, that this NAO proxy explains only 27% of the NAO's low-frequency variability during wintertime for the overlapping period.

Externally forced low-frequency *variability* of the NAO may be explained, for example, if North Atlantic oceanic dynamics are taken into account. Such two-way coupled modes of air-sea interaction were found in different integrations of coupled general circulation models (e.g., Latif and Barnett, 1994; Timmermann et al., 1998; Grötzner et al., 1998). Although these coupled modes of variability differ in the oceanic physics that are involved, their basic concept — the delayed-action oscillator — is very similar: Instantanously, atmosphere and ocean form a positive feedback. At the same time, however, changes in the ocean are induced reversing SST anomalies and, thus, the atmospheric anomaly after some delay. From the analyses presented in this chapter it cannot be decided whether low-frequency variability of the observed NAO resulted from an external forcing by the North Atlantic ocean. This item is revisited in chapter 4, where the modelled response of the North Atlantic ocean to a forcing by the NAO over the period 1865–1997 is described. From this experiment it will be argued that the phase-relationship between interdecadal variability of the NAO and the variability of the North Atlantic ocean does not support the existence of a two-way coupled mode of interdecadal variability.

Recently, Palmer (1993, 1999) proposed a nonlinear paradigm for the extratropical atmosphere. From this paradigm it may be expected that atmospheric changes due to increasing greenhouse gas concentrations primarily manifest as changes in the frequency of occurence of natural modes of atmospheric variability. Having in mind the strong increase of the NAO during the last three decades (Fig. 3.7) it cannot be excluded that a greenhouse gas forcing contributed to the observed low-frequency variability of the NAO. As for the Namias-Born mechanism, an anthropogenic forcing may have difficulties to explain low-frequency *variability*, although it has be kept in mind that the coupled climate system may respond with multi-decadal oscillations to an externally imposed forcing (Manabe and Stouffer, 1999). A more detailed discussion of possible changes of the NAO under increasing greenhouse gas concentrations is given in chapter 6.

4 North Atlantic Interdecadal Variability

4.1 Introduction

In his pioneering article Bjerknes (1964) introduced the concept of the time scale dependent nature of air-sea interaction in the North Atlantic. He suggested that sea surface temperature (SST) anomalies on interannual time scales may solely be explained by a local forcing from the atmosphere. On the other hand, the explanation of interdecadal SST anomalies along the Gulf Stream extension requires additional contributions from oceanic dynamics (altered currents). This conclusion was supported by the observed development/persistence of interdecadal SST anomalies against the local damping influence from the atmosphere. According to Bjerknes, therefore, on interannual time scales the ocean reacts merely passively to changes of the overlying atmosphere; whereas on interdecadal time scales the ocean plays an active role in generating SST anomalies. Bjerknes' hypothesis has been essentially supported by recent observational (Deser and Blackmon, 1993; Kushnir, 1994) and modelling studies (Delworth et al., 1993; Delworth, 1996; Christoph et al., 1999). From the observations, however, it is still unclear whether interdecadal changes of the subtropical gyre (Bjerknes, 1964) or the Atlantic thermohaline circulation (THC) (Kushnir, 1994) contributed to the development of interdecadal SST anomalies. There is consensus, however, that interdecadal changes of the NAO were involved (Bjerknes, 1964; Deser and Blackmon, 1993; Kushnir, 1994). The NAO is the dominant atmospheric mode of variability in the North Atlantic region (Cayan, 1992a) and describes the simultaneous strengthening and weakening of the Icelandic Low and Azores High (Walker, 1924; Hurrell, 1995).

In recent years coupled general circulation models (CGCMs) of different complexity became valueable tools in climate research. Among others they were used to investigate the physics of extratropical air-sea interaction. Latif and Barnett (1994) found evidence for the presence of a two-way interaction between the Aleutian Low and North Pacific subtropical gyre in an integration of the coupled ECHO model. By analyzing the same integration Grötzner et al. (1998) found evidence for the existence of a very similar mode in the North Atlantic ocean. Due to geometrical differences between the North Pacific and North Atlantic basin, however, the North Atlantic subtropical gyre interacts primarily with the Azores High. The dominant time scale of this two-way coupled air-sea mode as simulated by the ECHO model is about 17-yrs, whereas the realization of interdecadal variability, as described by Bjerknes, rather points towards time scales of about 40-yrs and longer. As noted by Grötzner et al. (1998), both, the modelled patterns and dominant time scale of the coupled air-sea mode bear more resemblence with the quasi-decadal mode originally described by Deser and Blackmon (1993). Moreover, the relaxation of SST and sea surface salinity towards climatology north of 60°N in the ECHO model biases the oceanic response towards the wind-driven circulation.

Kushnir's suggestion that interdecadal variability of the THC was of importance during the 20th century is supported by the spatial pattern of North Atlantic interdecadal SST variability. He notes that the centers of action in the interdecadal SST pattern occur in areas known for their unique role in oceanic dynamics, that is, the Labrador Sea, the surroundings of Iceland and the area northeast of Bermuda. Moreover, the observed interdecadal SST pattern shows a striking similarity to those obtained from the coupled GFDL model for an anomalously strong THC (Delworth et al., 1993). In this model, however,

the relationship between the SST pattern and the NAO is reversed compared to the observations (Delworth et al., 1993). Further evidence for the importance of interdecadal THC variability is put forward by Timmermann et al. (1998) from an integration of the coupled ECHAM3/LSG model. Although the mechanisms for the generation of THC variability seem to be somewhat different compared to the GFDL model, Timmermann et al. (1998) find a relationship between the interdecadal SST pattern and the NAO closely resembling those in the GFDL model. The results by Timmermann et al. (1998) suggest that the warming trend along the Gulf Stream extension from 1894 to 1924, as described by Bjerknes (1964), can be explained by an enhancement of the THC.

Although the results from different CGCMs share some common features with respect to interdecadal THC variability, physical mechanisms seem to differ among the CGCMs. In a very recent study, Delworth and Greatbatch (2000) show that in contrast to previous studies (Delworth et al., 1993, 1997) interdecadal variability of the THC in the GFDL model may be explained by a passive response of the ocean to internally generated (by the atmosphere) interdecadal NAO variability. Moreover, associated surface heat flux anomalies appear to dominate over associated freshwater and momentum flux anomalies. This is in contrast to the ECHAM3/LSG model, where interdecadal SST anomalies feed back onto the NAO and interdecadal freshwater flux (primarily evaporation) and windstress (Ekman transports) variability dominates over the heat flux component in forcing the ocean (Timmermann et al., 1998). In the coupled ECHAM4/OPYC3 model the mechanisms how the NAO forces interdecadal oceanic variability seem to be more elaborate, since the NAO appears to affect the THC by two inversely operating processes (Christoph et al., 1999), that is, the advection of density anomalies into the subpolar sinking regions and the modification of the vertical stratification in the Greenland/Icelandic/Norwegian Seas through freshwater flux anomalies. Sensitivity experiments with a mixed layer model that was coupled to the atmospheric component of ECHAM4/OPYC3 indicate that in this coupled model integration interdecadal changes of the North Atlantic ocean circulation add little additional low-frequency variability to the NAO.

The advantage of using CGCMs to investigate air-sea interaction comes from the fact that atmosphere and ocean can freely interact. Moreover, long-term statistics about interdecadal oceanic variability can be obtained from CGCM integrations. A direct comparison with observational results, however, is difficult to carry out. This is because modelled climate trajectories obtained from CGCM integrations are difficult to merge with the observed realization of North Atlantic interdecadal variability during the 20th century.

Such a comparison is possible for integrations of ocean general circulation models (OGCMs) that are forced with observed fields of heat, freshwater and momentum fluxes (or near-surface atmospheric parameters). These atmospheric forced OGCM experiments are not suited, however, to investigate possible oceanic feedbacks onto the atmosphere. An increasing body of literature deals with this kind of experiments in the North Atlantic (e.g., Halliwell, 1998; Häkkinen, 1999; Kushnir et al., 1999; Eden and Willebrand, 2000). To our knowledge, however, all of the studies are restricted to the post World War II period, when the relatively good sampling in North Atlantic allows to construct reliable atmospheric forcing fields. Since a possible model drift during the course of these integrations may interfere with the interdecadal signal, these experiments were primarily conducted to investigate variability from interannual to quasi-decadal time scales.

The objective of this study is to contribute to our understanding about *interdecadal* variability of the North Atlantic ocean circulation. For this purpose we make use of the

following items: First, numerous observational studies (e.g., Bjerknes, 1964; Deser and Blackmon, 1993; Kushnir, 1994; Dickson et al., 1996; Curry et al., 1998) and modelling studies (e.g., Timmermann et al., 1998; Delworth and Greatbatch, 2000; Häkkinen, 1999; Eden and Willebrand, 2000) point towards the importance of the NAO in forcing the oceanic circulation. Second, sea level pressure (SLP) measurements from the Azores and Iceland (thus, the NAO index) are available back to the mid-19th century (Hurrell, 1995; Jones et al., 1997). Third, after World War II the sampling in the North Atlantic region became relatively good and NCEP/NCAR reanalysis data (Kalnay et al., 1996) provide a full coverage of the surface flux fields for the period 1958–1997. Finally, since interdecadal changes of the North Atlantic ocean seem to leave their imprint on SST anomalies (see above) and SST is a relatively well-sampled parameter during the 20th century in the North Atlantic, the model results can be assessed.

In this study the following strategy is used: Spatial patterns of anomalous surface flux fields associated with the NAO are estimated from reanalyzed data (1958–1997). Then, the Atlantic OGCM is forced by combining the *temporal* behaviour of the NAO from 1865 to 1997 with the associated surface flux *patterns* (estimated using data from 1958 to 1997). Modelled and observed interdecadal SST anomalies are compared and, finally, interdecadal variability of the North Atlantic circulation that is forced by the NAO is investigated from the OGCM.

The OCGM integrations discussed throughout the remainder this chapter were performed by Dr. Carsten Eden. The development of the forcing strategy and the analysis of the model results is based on collaboration with Dr. Carsten Eden.

4.2 Model and Forcing

The OGCM is an extended version of the GFDL MOM2.1 code (Pacanowski, 1995) developed as part of a hierarchy of models for the Atlantic Ocean (FLAME group, 1999)[17]. The resolution of the present model is $4/3^o$ in longitudinal direction and $4/3^o \cos\phi$ in latitudinal direction, where ϕ denotes latitude. In the vertical 45 levels are used. The model domain spans the entire Atlantic from 100^oW to 30^oE and from 70^oS to 70^oN. Further model details are given by Eden (1999) (see also references therein).

The spatial resolution and the domain of the model was chosen as a compromise between realism of the model solution compared to observations and computational costs to perform century-scale integrations. The spatial resolution of the model is considerably higher than in most oceanic components of CGCMs used so far. Starting from a state of rest and climatological values for temperature and salinity the model was forced with monthly climatological windstress and heat flux fields taken from Barnier et al. (1995) over 50 years of the spin-up phase. Sea surface salinity was restored towards a monthly climatology during the first 40 years of the spin-up. Thereafter, the model was driven with diagnosed freshwater flux fields taken from year 40. Diagnosed freshwater fluxes were used to reduce the model drift, which may be considerable if observed freshwater fluxes are prescribed. For the heat flux forcing a Haney-type (Haney, 1971) boundary condition is used. A flux correction term is added to the net heat flux forcing in this formulation acting as a restoring towards climatological SSTs with temporally and spatially varying time scales. The time scales were determined from a linearization of the heat flux bulk formulae (Barnier et al., 1995).

[17] *http://www.awi-bremerhaven.de/Modelling/FLAME/*

Once the spin-up was finished, surface flux anomalies were added to the climatologies during the course of the integrations. For the heat flux forcing the anomalies were added to the heat flux term only; climatological SSTs and the time scales of the flux correction term were not changed. Details about the model spin-up and the boundary conditions are given by Eden (1999).

For each month NAO-related *spatial* forcing patterns were obtained by regressing fields of anomalous surface heat, momentum and freshwater fluxes, taken from the NCEP/NCAR reanalysis (Kalnay et al., 1996), onto the normalized NAO index for the relatively well-sampled period 1958–1997. The NAO-related monthly *spatio-temporal* forcing was reconstructed by multiplying the (monthly) normalized NAO index for the period 1865–1997 with the associated (monthly) anomalous flux patterns. By constructing the forcing fields on a monthly basis the annual cycle of the NAO (Hurrell and van Loon, 1997; Barnston and Livezey, 1987) is taken into account. Here, the NAO index is defined as the difference between normalized SLP from the Azores and Iceland (Rogers, 1984). By using the SLP time series from the Azores instead of Gibraltar or Lisboa as a proxy for the southern center of NAO variability, it is ensured that out-of-phase variability between the Azores High and Icelandic Low is captured even during the summer months (Hurrell and van Loon, 1997).

Observed SST fields (Rayner et al., 1996) during the period 1900–1996 were used to evaluate the realism of the modelled SST anomalies during wintertime.

4.3 Model Evaluation

The mean-state of the model is typical for medium-resolution GFDL-type Atlantic OGCMs. The maximum annual-mean strength of the THC at 45^oN and a depth of 1000 m amounts to 18 Sv ($1Sv = 1{\cdot}10^6 m^3/s$); the maximum annual-mean northward meridional heat transport (MHT) amounts to approximately 0.9 PW ($PW = 10^{15}W$) at 25^oN and decreases towards 0.6 PW at 48^oN.

The variability of these integral oceanic parameters from the OGCM's long-term integration (1865–1997) with reconstructed NAO forcing is in good agreement with estimates from an integration of the same OGCM using the full forcing fields from the NCEP/NCAR reanalysis during the overlapping period 1958–1997 (for details on the latter integration, see Eden and Willebrand, 2000): Cross-correlations between the modelled THC strengths amount to 0.7–0.8 in the northern North Atlantic, and cross-correlations for MHT reach 0.9 near the North Atlantic subpolar front (C. Eden, personal communication).

Local correlations between modelled and observed SST anomalies for winter seasons (JFM) from 1900 to 1996 are depicted in Fig. 4.1a. Statistically significant correlations, locally exceeding $r = 0.5$, are evident in the northern North Atlantic and the eastern subtropical North Atlantic. The western subtropical North Atlantic is another area of relatively high correlations. Common to all of these centers of action is the fact that the NAO explains relatively large amounts of the total surface heat flux variability during wintertime (Fig. 4.1b). Hence, the agreement between modelled and observed SST anomalies may simply result from a realistic local heat flux forcing of the model's mixed layer by the wintertime NAO (see also Cayan, 1992a; Delworth, 1996; Christoph et al., 1999). An exception from this simple explantion, that is, a local forcing of the upper-ocean by NAO-related heat flux anomalies, is evident along the North Atlantic Current between 40^o–50^oN. Here, significant correlations are apparent although no local heat flux

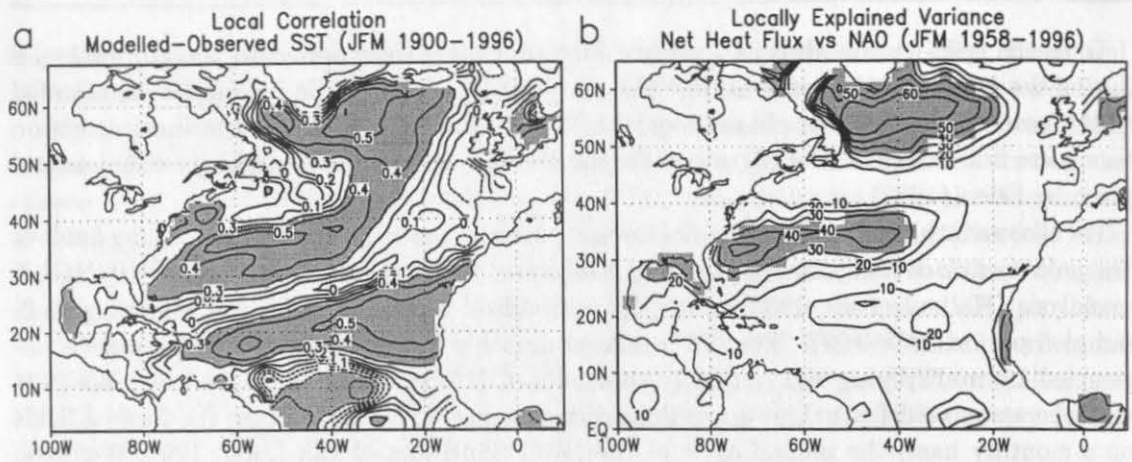

Figure 4.1: (a) Local correlations between modelled and observed SST anomalies for winters (JFM) from 1900 to 1996. Correlations significant at the 95% confidence level are shaded. (b) Percentage of observed net heat flux variance ($r^2 \cdot 100$ in %) explained by the NAO index (JFM from 1958 to 1996). Values exceeding 30% are shaded.

forcing was applied to the model. Therefore, relatively high correlations in this region indicate a reasonable model response to a *non-local* forcing by the NAO. In the following it is shown that the realistic non-local model response may be understood in terms of a successful simulation of interdecadal changes of the North Atlantic circulation during the 20th century.

4.4 Observed and Modelled Interdecadal Variability

4.4.1 NAO and SST Anomalies

The focus of this study is on interdecadal variability in the North Atlantic. To draw spectral characteristics from univariate and multivariate time series and to objectively separate interdecadal variability from higher-frequency fluctuations, Singular Spectrum Analysis (SSA) and Multichannel Singular Spectrum Analysis (MSSA), respectively, were applied. Methodological details are given in chapter 2. Since a window-width of thirty years was used for SSA and MSSA, hereafter, the term "interdecadal variability" refers roughly to variability with time scales longer than 30-yrs.

Spectral characteristics of observed and modelled North Atlantic wintertime SST anomalies become evident from Fig. 4.2. The MSSA spectra are based on the leading ten normalized ordinary principal components (PCs) explaining 85% (96%) of the total observed (modelled) SST variance. Both, observed and modelled North Atlantic SST anomalies show very similar red noise background spectra. Thus, primarily the high-frequency stochastic forcing by the NAO seems to be responsible for the redness of North Atlantic SST anomalies. Moreover, the observed and modelled structure of the spectra is quite similar: Significant power on interdecadal and interannual (around 5–8, 2.5–3 years) time scales is clearly evident from both, the observations and the model. We do not want to go into too much statistical detail since this study is primarily based on physical argumentation. However, it is worth mentioning that the probability for 4 (Fig. 4.2a) or more local excursions above the local 95% confidence level (out of 68 possible), as obtained from

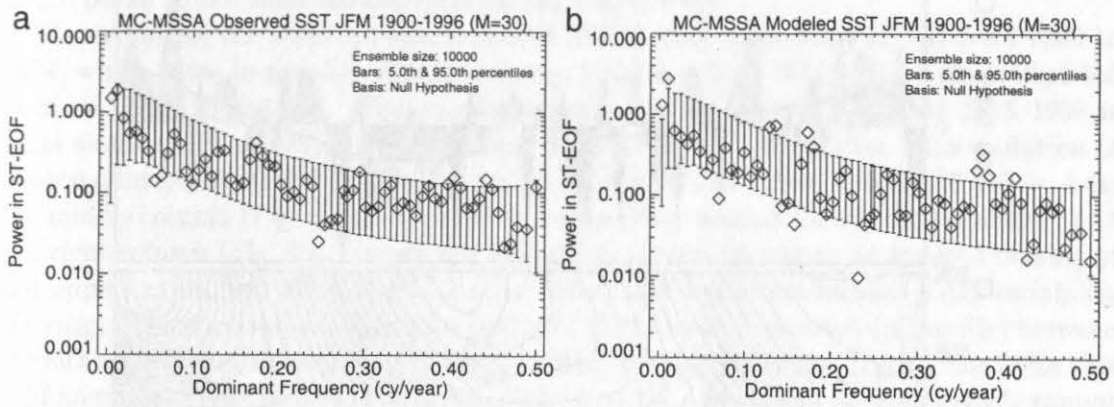

Figure 4.2: Spectral characteristics of (a) observed and (b) modelled North Atlantic (100^oW–20^oE, 5^oN–65^oN) SST anomalies for winters (JFM) from 1900 to 1996, obtained by means of MC-MSSA. Diamonds denote the eigenvalues (power) of the data, plotted versus the dominant frequency ($cy/year$). Percentiles ($5.0th, 95.0th$) were estimated from 10000 realizations of the null hypothesis, i.e., the leading ten PCs ($L = 10$) of North Atlantic SST anomalies represent independent realizations of AR(1) noise. Both, data and ensemble members were projected onto the ST-EOFs of the null hypothesis. A window-length of 30-yrs ($M = 30$) was used.

the observations, to occur just by chance is greater than 43%. Therefore, without any *a priori* expectations the leading ten PCs from the observations are not unusual (at 57% confidence) compared to independent realizations of AR(1) noise. On the other hand, ten excursions above the local 95% confidence level are found for the modelled SST (Fig. 4.2b). The probability for 10 or more local excursions to occur just by chance under the global null hypothesis is less than 1%. This indicates that other processes than the integration of high-frequency atmospheric noise (Hasselmann, 1976) contribute to the spectral structures in Fig. 4.2.

Summarizing, variability on interdecadal time scales dominates observed and modelled SST anomalies. Notice, that the same holds for the observed NAO index (see chapter 3, Fig. 3.6). Once the spectral characteristics of modelled and observed North Atlantic SST anomalies are described, subsequently, SSA and MSSA are applied to separate interdecadal variability from higher-frequency fluctuations. This is achieved by reconstructing interdecadal variability from the leading two eigenmodes (see, e.g., Fig. 4.2 for SST) following the methods decribed in chapter 2. Note, that for all univariate and multivariate time series discussed in this study the leading two (most energetic) eigenmodes represent interdecadal variability. These were used to objectively lowpass-filter the data retaining interdecadal variability.

The wintertime NAO index and its interdecadal variability is shown in Fig. 4.3 together with zonally-averaged (20^oW–40^oW) observed interdecadal SST variability during wintertime (JFM) from 1900 to 1996. Interdecadal NAO (SST) variability explains 15% (25%) of the total variance. At the first glance Fig. 4.3 may suggest a local relationship between the atmospheric forcing by the NAO and North Atlantic SST anomalies on interdecadal time scales. The persistent positive phases of the NAO during the beginning and end of

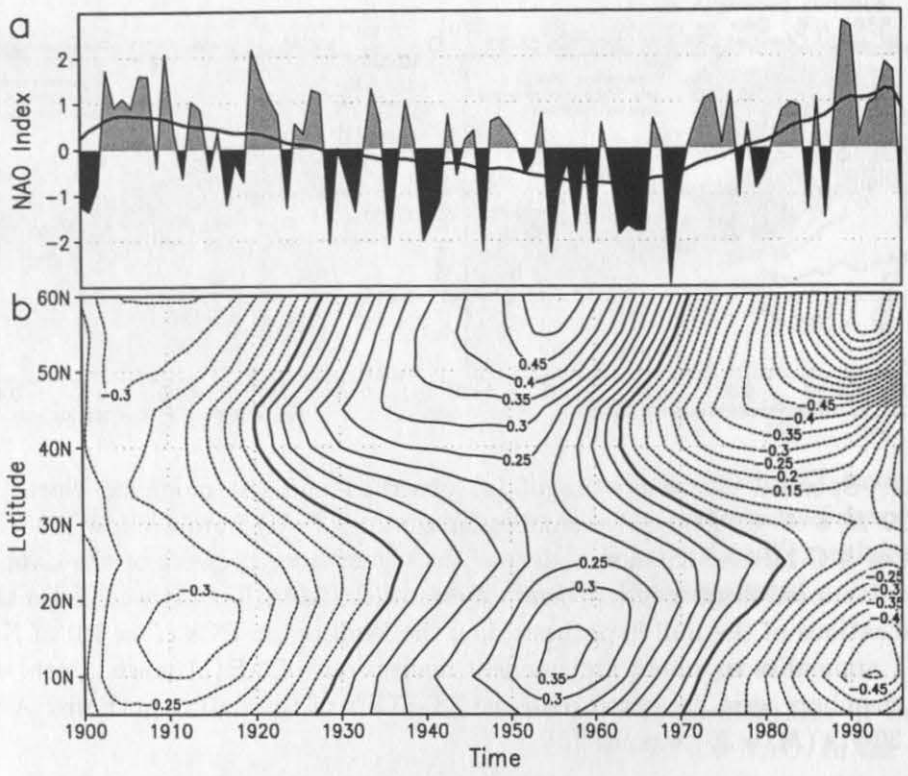

Figure 4.3: Observed interdecadal variability of the NAO index and North Atlantic SST during the period 1900–1996 and wintertime (JFM). (a) Unfiltered NAO index (shaded) along with its interdecadal variability (solid). (b) Zonal average (20^oW–40^oW) of the observed interdecadal SST variability (^oC). Interdecadal NAO (SST) variability is based on the leading two SSA (MSSA) eigenmodes (see Fig. 4.2a for SST). A window-width of 30-yrs ($M = 30$) was used. The leading ten normalized PCs of North Atlantic SST anomalies, explaining 85% of the total SST variance, were used.

the 20th century (see also Hurrell, 1995; Moron et al., 1998; Jung and Ruprecht, 1999) are accompanied by an anomalously cold subpolar and eastern subtropical North Atlantic. In both regions interdecadal SST anomalies are positive during the persistent negative phase of the NAO (≈1930–1975). Hence, the existence of these SST anomalies may partly be explained by corresponding atmospheric changes (see also Cayan, 1992b).

The latitudinal dependence of the nodes, maxima, and minima of the observed interdecadal SST anomalies (Fig. 4.3b), which has been already noted by Kushnir (1994), indicates that other processes than a passive response of the North Atlantic ocean to an atmospheric forcing are involved in the generation of interdecadal SST anomalies. In the northern North Atlantic (50^o–60^oN) there is the tendency for interdecadal SST anomalies to lead the NAO by a few years. The earliest precursors of theses SST anomalies appear in the mid-latitude North Atlantic (40^o–45^oN). The fact that SST anomalies lead the NAO by a few years in the northern North Atlantic may be understood as an indicator that the ocean forces the atmosphere (e.g., Wohlleben and Weaver, 1995). However, another possible explantion can be based on the superposition of two different processes, that is, an *instantaneous local forcing* of the ocean by the atmosphere along with the *lagged response*

of the ocean to the same atmospheric forcing (see below).

The cooling of the observed and modelled SST during wintertime (JFM) from 1960 to 1984, which came in parallel with the change towards a high NAO (Fig. 4.3), is depicted in more detail in Fig. 4.4. The corresponding warming during the period 1915–1939 is quite similar (not shown), except for smaller observed SST anomalies. The evolution of observed interdecadal SST variability during the period 1960–1984 is depicted in Fig. 4.4a; the middle column (Fig. 4.4b) shows the corresponding changes for the modelled SST; and the right column (Fig. 4.4c) shows anomalous heat fluxes (positive: anomalous heating of the upper-ocean) and 10 m winds that are associated with interdecadal NAO variability (forcing). The observed cooling of the northern North Atlantic started (primarily) between the subtropical and subpolar gyre along the NAC during the 1960s. During the 1970s this cold anomaly spread towards the north. Note, that the appearence of this anomaly cannot entirely be explained by a local forcing from the NAO: First, there is no heat flux forcing associated with the NAO near 40^oN. Second, north of 40^oN the anomalous heat flux and windstress fields worked in such a way (1960–1974) to maintain the positive SST anomaly. Third, despite of a missing forcing from the NAO during the pentade 1975–1979 the observed cold SST anomaly continued to grow. Note, that extratropical SST anomalies show typical e-folding times of a few months in the absence of any forcing (e.g. Frankignoul, 1985).

The modelled development of interdecadal SST anomalies is in good agreement with those obtained from the observations (Fig. 4.4a,b). The intensification of the cold anomaly and its subsequent spread (intensification) into the subpolar gyre, for example, is clearly evident. The magnitudes of the observed interdecadal SST anomalies, however, are about twice as large as those from the model. These differences tend to be even more pronounced in the eastern part of the subtropics. Smaller amplitudes for modelled SST anomalies are presumably due to the relaxation towards climatological SSTs (surface boundary conditions). Note, however, that changing the relaxation values for SST would be inconsistent with the linearization of the bulk parameterization of the heat flux components, and SST would be hardly a prognostic model variable anymore. Although absolute values between modelled and observed SST anomalies differ, relative contributions from interdecadal time scales to the total variance are comparable. Both, modelled and observed interdecadal SST anomalies explain approximately 25% of the total SST variance in the North Atlantic during the winters from 1900 to 1996.

4.4.2 NAO and Oceanic Dynamics

The development of observed and modelled SST anomalies (i) despite of a missing NAO-related forcing along the NAC near 40^oN and (ii) against the damping atmospheric forcing in the subpolar region (50^o–60^oN) supports the hypothesis of an active contribution from the North Atlantic ocean to the generation (maintainence) of interdecadal SST anomalies. Moreover, the agreement of the phase-relationship between observed and modelled SST anomalies on interdecadal time scales enhances our confidence that the model results can be used to assess interdecadal variability of the North Atlantic ocean circulation during the 20th century.

The (unfiltered) wintertime NAO index and the strength of the annual-mean THC at 48^oN and 1000 m depth (THC_{48^oN}) is shown in Fig. 4.5a. Obviously, interdecadal changes of the NAO lead those of THC_{48^oN} by several years. The phase-relationship

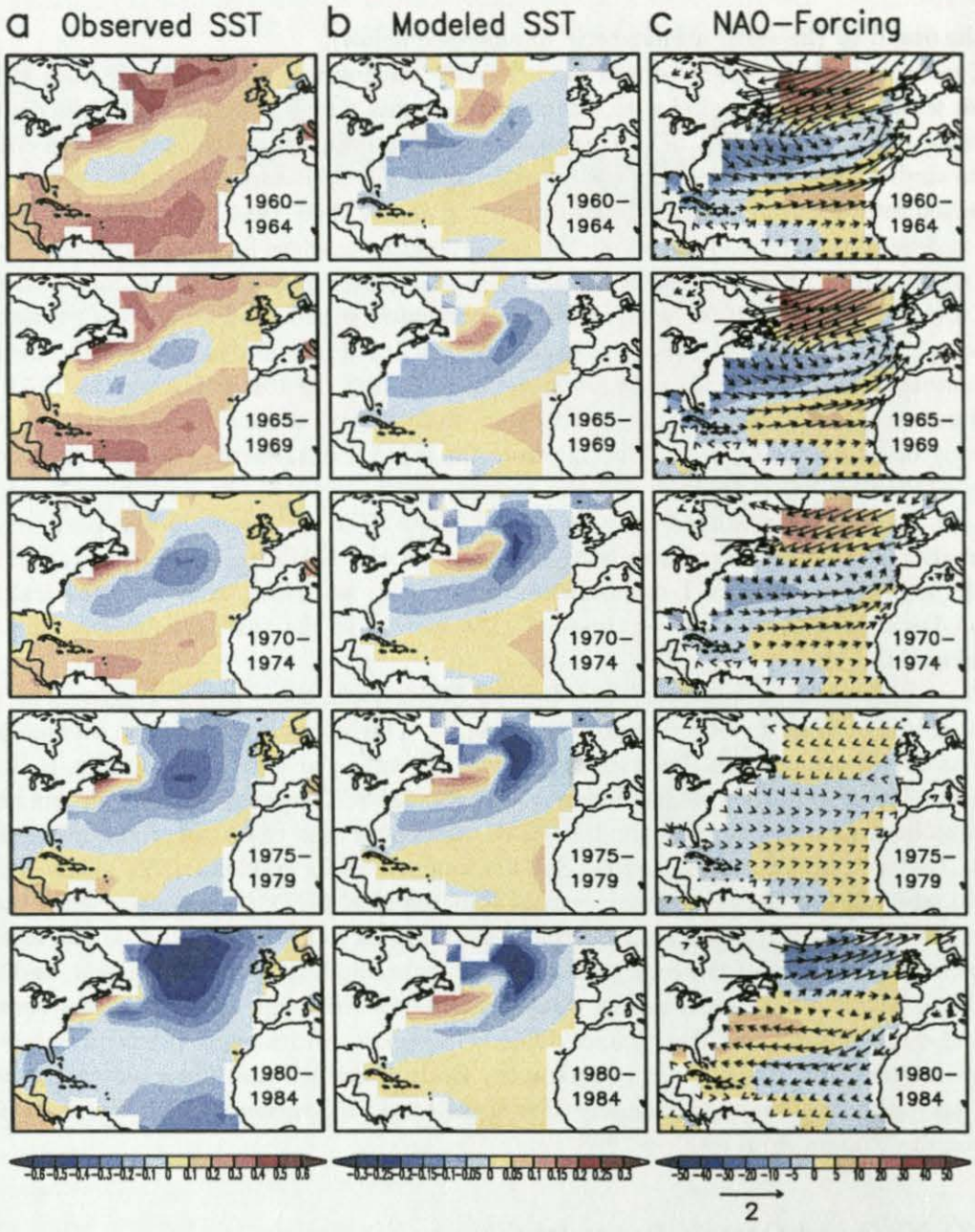

Figure 4.4: Interdecadal modes of (a) observed and (b) modelled SST anomalies (^oC) for subsequent pentades during the period 1960–1984 and wintertime (JFM), along with (c) NAO-related interdecadal heat flux (W/m^2) and near-surface wind (m/s) fields. Interdecadal modes in (a) and (b) were reconstructed in the same manner as described in Fig. 4.3b. The leading ten normalized PCs of observed (modelled) North Atlantic SST anomalies explain 86% (95%) of the total variance. In (c) interdecadal variability of the NAO index (Fig. 4.3a, solid) was multiplied by the anomalous fields of heat flux as well as zonal and meridional wind components associated with the NAO index (see Model and Forcing). Note the different contour-spacing in (a) and (b).

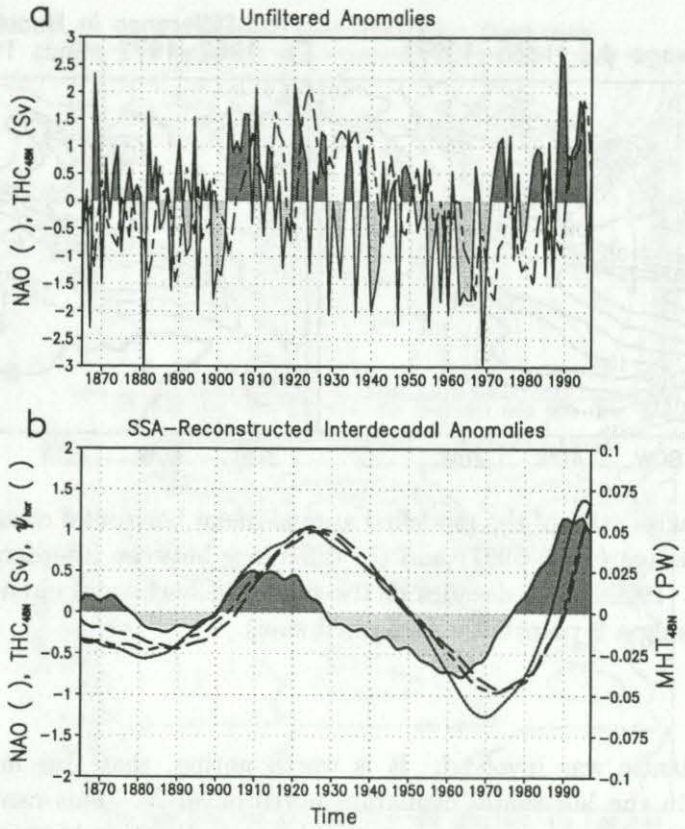

Figure 4.5: Time series of the observed winter-averaged (JFM) NAO index and different modelled annual-mean oceanic parameters during the period 1865–1997. (a) Unfiltered NAO index (shaded) and Atlantic thermohaline circulation strength at 48^oN (THC_{48N} in Sv; long short dash). (b) Interdecadal variability of the NAO index (shaded), THC_{48N} (in Sv; long short dash), total meridional heat transport at 48^oN (MHT_{48N} in PW; long dash), along with the strength of the subtropical and subpolar gyres (ψ_{hor}; solid). Interdecadal variability was reconstructed as decribed in Fig. 4.3a. From each of the oceanic time series the linear trend was removed prior to the analysis.

on interdecadal time scales between the NAO and modelled time series of the THC_{48^oN}, annual-mean meridional heat transport at 48^oN and 1000 m depth (MHT_{48^oN}), as well as the North Atlantic horizontal gyre strength[18] (ψ_{hor}) becomes evident from Fig. 4.5b. All these integral oceanic parameters lag behind the NAO by 10–20-yrs during the 20th century. Furthermore, all oceanic time series are approximately in-phase on interdecadal time scales. The persistent high NAO period at the beginning of the 20th century, for example, is followed (after ≈20-yrs) by an enhanced meridional and horizontal circulation in the North Atlantic and, therefore, an enhanced MHT_{48^oN}. The persistent negative phase of the NAO during the early 1960s is followed by a minimum of MHT_{48^oN} about 10-yrs later.

The gyre-strength index (Fig. 4.5b) suggests that the complete horizontal gyral-circulation

[18]The (North Atlantic) gyre strength was obtained by projecting anomalous annual-mean fields of the barotropic stream function onto the long-term mean stream function. Hence, this index gives a measure for the anomalous strength of the "mean" gyral circulation.

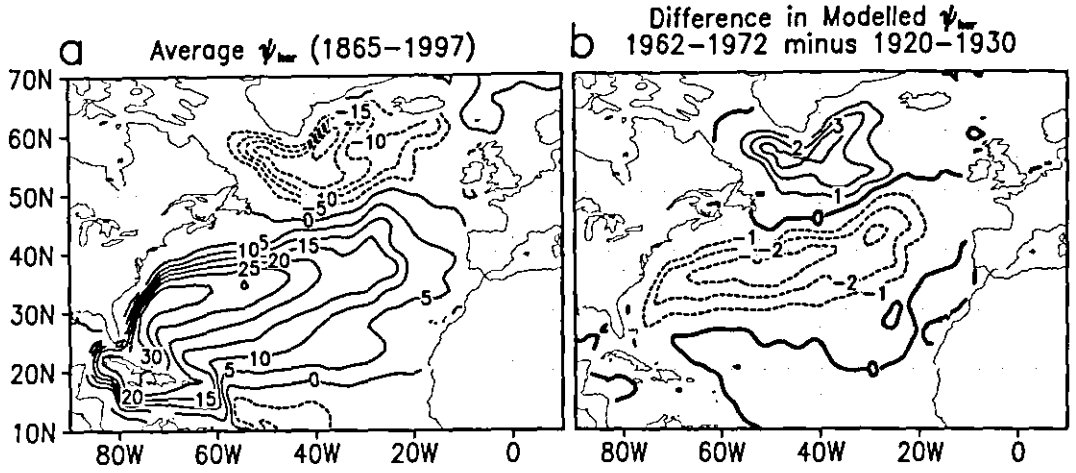

Figure 4.6: Characteristics of the modelled annual-mean horizontal stream function (Sv): (a) Long-term average (1865–1997) and (b) difference between interdecadal weak (1962–1972) and strong (1920–1930) decades of the modelled horizontal circulation. The fields were smoothed using a 9 point filter (weighted sum).

in the North Atlantic was involved. It is worth noting, that this index primarily reflects variability in the horizontal ciculation north of $30°N$. This can be inferred from Fig. 4.6 showing the difference of the horizontal stream function between its interdecadal low (1962–1972) and high (1920–1930) epochs (compare Fig. 4.5) along with the long-term mean stream function.

In order to assess the relative contributions from the anomalous meridional and horizontal circulation to the total meridional heat transport, the total MHT was decomposed into its THC-related (MHT_{over}) and gyre-related (MHT_{gyre}) components. Here, MHT_{over} is defined as the product between the zonally-averaged potential temperature and meridional velocity. The zonal-average of the product between the corresponding deviations from the zonal average yields the gyre-related component of the total MHT. In the long-term mean MHT_{over} dominates over MHT_{gyre} in the North Atlantic south of 45°N. MHT_{gyre} contributes approximately equally to the total MHT north of 45°N (not shown). Obviously, the same holds for variability of the MHT components on interdecadal time scales (Fig. 4.7). Furthermore, interdecadal variability of MHT_{over} spans the whole North Atlantic basin. This is in contrast to NAO-related *interannual* variability of the meridional overturning circulation, where a dipole-structure is involved (Eden and Willebrand, 2000).

The observed and especially the modelled cooling during the period 1960–1984 (Fig. 4.4) may suggest that a propagation of the cold SST anomaly that was generated in the western subtropical North Atlantic by anomalous heat fluxes out of the ocean during the 1950s and 1960s played a crucial role (Sutton and Allen, 1997). To quantify the relative contributions from temperature anomalies to anomalies of the total MHT, a decomposition of the MHT into the transport of temperature anomalies by the mean currents ($\overline{v}T'$), the anomalous transport of mean temperatures ($v'\overline{T}$), and the covariance between anomalous currents and temperatures ($v'T'$) was performed (not shown). The results suggest that the bulk of interdecadal MHT variability in the North Atlantic is governed by changes of the circulation ($v'\overline{T}$), whereas $\overline{v}T'$ and $v'T'$ played a minor role. This is in agreement

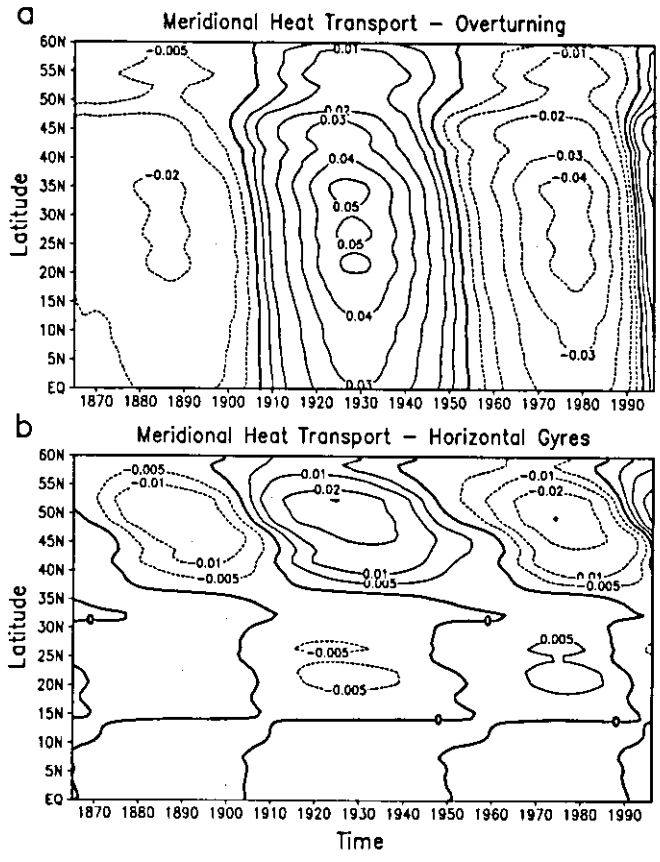

Figure 4.7: Interdecadal variability of the modelled North Atlantic meridional heat transport (MHT) components: (a) Overturning ($\mathrm{MHT}_{over}; 10^{15}W$), calculated from the products between zonal mean meridional velocities, $[v]$, and zonal mean temperature, $[T]$. (b) Gyre component ($\mathrm{MHT}_{gyre}; 10^{15}W$), i.e., covariance between the departures from the zonal mean, $[v^*T^*]$. Interdecadal variability was reconstructed as described in Fig. 4.3b, except that the first five normalized PCs, explaining 99.5% (98%) of the total MHT_{over} (MHT_{gyre}) variance, were used. Linear trends were removed prior to the analysis.

with the notion of a lagged response of the oceanic circulation to interdecadal changes of the NAO (Fig. 4.5). Moreover, the amplification of the cold SST anomaly north of 40^oN can hardly be explained by a propagation of SST anomalies along the Gulf Stream/NAC extension.

Summarizing, the cooling in the northern North Atlantic during the 1960s and 1970s was presumably caused by a lagged response of the ocean to the persistent low NAO phase during the mid-20th century, that is, the lagged anomalously weak total MHT due to a reduced strength of the meridional and horizontal oceanic circulation. Similar arguments hold for the warming during the 1920s and 1930s. As mentioned above, there is some indication that SST anomalies in the northern North Atlantic lead the NAO on interdecadal time scales by some years (Fig. 4.3). This lead-relationship may be explained by the superposition of the instantanous thermal response of the upper-ocean and the lagged response of the North Atlantic circulation to an interdecadal forcing by the NAO. During

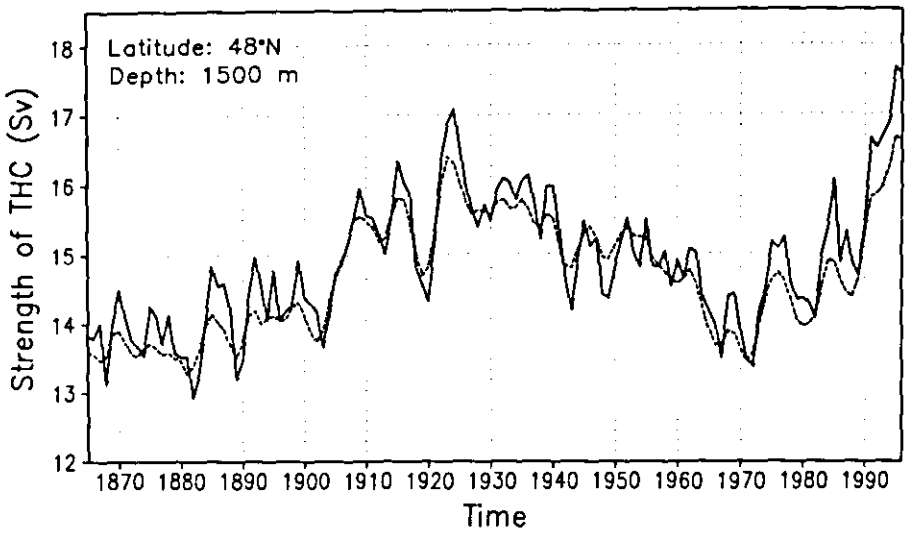

Figure 4.8: Modelled strength of the annual-mean thermohaline circulation (Sv) at 48^oN and 1500 m depth with NAO-related heat flux, wind stress, and freshwater flux forcing (solid) and with NAO-related heat flux forcing only (dashed).

the 1960s, for example, the westerly winds were reduced, which supported a warming of the northern North Atlantic. At the same time the oceanic MHT decreased. This oceanic response to the low NAO contributed to the cooling of the northern North Atlantic. The increase of the NAO, which contributed to a further cooling of the northern North Atlantic through anomalous heat fluxes out of the ocean, started later, that is, during the 1970s. Therefore, SST anomalies lead the NAO on interdecadal time scales. Note, however, that this phase-relationship may simply be the result of a *lagged* response of the oceanic circulation.

4.5 Sensitivity Experiments

4.5.1 Role of Turbulent Heat Fluxes

For the experiment described in previous sections (EXMAIN, hereafter) the model was forced with NAO-related heat flux, freshwater flux, and windstress variability. To assess the relative importance of different surface flux components to the modelled interdecadal variability of the North Atlantic circulation, an additional experiment (EXHEAT, hereafter) was performed. In EXHEAT the model was solely forced by NAO-related heat flux variability; freshwater flux and windstress fields were prescibed as climatological annual cycles during the course of the integration.

Annual-mean values of the THC at 48^oN and a depth of 1500 m are shown in Fig. 4.8 for EXMAIN (solid) and EXHEAT (dashed). Obviously, interdecadal changes of the THC are mainly driven by heat flux variability. NAO-related changes of freshwater and momentum fluxes are of minor importance on *interdecadal* time scales. The mechanisms which are responsible for enhanced *interannual* variability of the THC in EXMAIN compared EXHEAT are described by Eden and Willebrand (2000).

For EXHEAT the same analyses as described for EXMAIN were repeated. The inter-

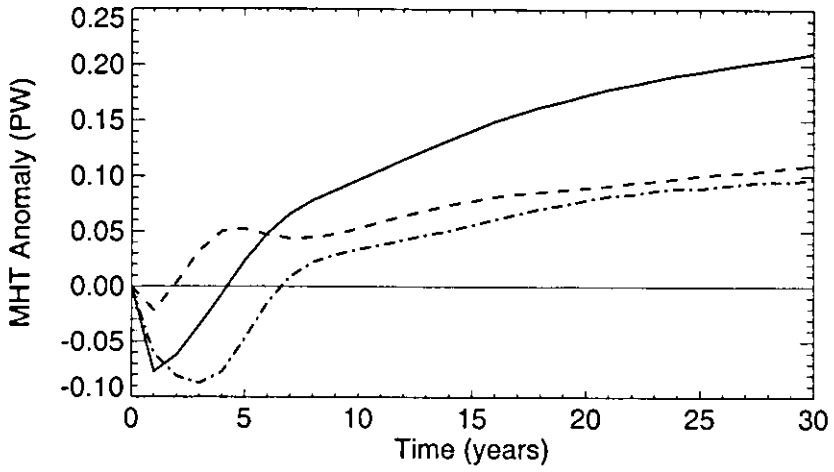

Figure 4.9: Changes of the total meridional heat transport (MHT in PW; solid) and its overturning (dashed) and gyre (dash-dotted) components at $48^{o}N$ under a steady positive NAO-like net heat flux, wind stress, and freshwater flux forcing over 30-yrs. The magnitudes of the forcing field anomalies are associated with a NAO index three standard deviations above the average. Year 0 is the last year of the spin-up (from C. Eden, personal communication).

decadal SST development for EXMAIN (Fig. 4.4) and EXHEAT (not shown) are very similar. This similarity suggests that *locally* forced SST anomalies are primarily driven by surface heat flux anomalies associated with the NAO. Other atmospheric forcing components like wind-driven currents, mixed-layer depth variations, and entrainment (for an overview, see Frankignoul, 1985) were of minor importance for the local generation (damping) of modelled SST anomalies.

4.5.2 Steady Forcing by the NAO

To further test the hypothesis of a lagged response of the meridional and horizontal oceanic circulation to persistent NAO anomalies and to assess the physics of the oceanic response, two additional integrations with idealized NAO forcings were performed[19]. In the first experiment (EXHIGH, hereafter) the model was forced with NAO-related anomalous patterns of heat flux, freshwater flux, and windstress (as in EXMAIN) over thirty years. The magnitudes of these anomalies are associated with a NAO index three standard deviations above normal (i.e., NAO index $= 3 \cdot \sigma$). The second experiment (EXLOW, hereafter) is similar to EXHIGH, except for reversed anomalies (i.e., NAO index $= -3 \cdot \sigma$).

Changes of the total $\mathrm{MHT}_{48^{o}N}$ for EXHIGH are depicted in Fig. 4.9 along with the contributions from the gyre and overturning component to the total $\mathrm{MHT}_{48^{o}N}$. Instantaneously, a positive NAO anomaly is accompanied by a reduced total $\mathrm{MHT}_{48^{o}N}$. This reduction is due to an instantaneous barotropic oceanic response in form of an anomalous anticyclonic gyral circulation between the subpolar and subtropical gyre and due to anomalously southward Ekman transports. Both, the overturning and gyre component contribute to the delayed increase of the total $\mathrm{MHT}_{48^{o}N}$. Enhanced convective activity

[19]These integrations were performed by Carsten Eden, who kindly provided me with the results.

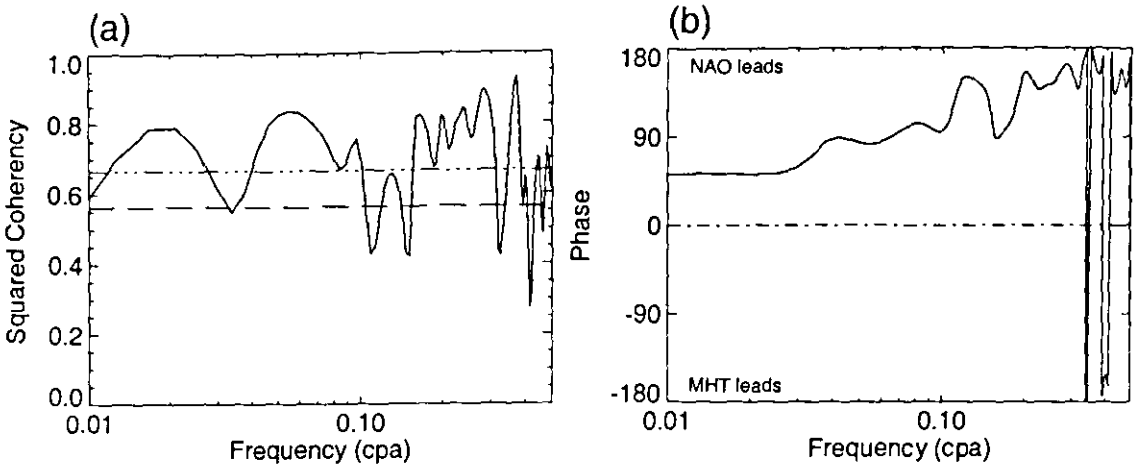

Figure 4.10: Cross-spectral characteristics between the winter-averaged (JFM) NAO index and the modelled annual-mean meridional heat transport (MHT) at 48^oN for the period 1865–1997: (a) Estimated squared coherency spectrum with 95% (dashed) and 99% (dash dot) confidence levels and (b) estimated phase spectrum. The NAO index leads for positive phases. A Tukey-window with a maximum lag of $M = 40$-yrs was used for smoothing (8.9 degrees of freedom). Time series were prewhitened. Methodological details are given by Jenkins and Watts (1968).

in the Labrador Sea due to anomalously strong heat fluxes out of the ocean leads to a baroclinic boundary wave response which propagates southward. As a consequence the subpolar THC is enhanced after 3-yrs. Moreover, the subpolar and subtropical gyres are enforced after a lag of 3–5-yrs due to baroclinic processes. Both components are working in such a way to increase the total MHT_{48^oN}. This response is discussed im more detail by Eden and Willebrand (2000). After a lag of 10-yrs or so the baroclinic adjustment has completed and there is a basin-wide enhancement of the THC (see also Fig. 4.7). Moreover, the strength of the subpolar and subtropical gyre further increases.

The oceanic response to a steady forcing by a negative NAO (EXLOW) is quite similar to the response in EXHIGH, except for opposite signs (not shown). Therefore, we conclude that the oceanic response to persistent NAO anomalies is symmetric with respect to the sign.

This time scale dependent relationship between the NAO and the MHT becomes also evident from the model integration with the reconstructed NAO-like forcing (EXMAIN). Estimated coherency and phase spectra between the NAO index and the modelled total MHT_{48^oN} are shown in Fig. 4.10. On interannual time scales the NAO and the total MHT_{48^oN} are approximately 180^o out-of-phase, that is, years with a high NAO index are accompanied by a reduced MHT at 48^oN and vice versa. On interdecadal time scales, however, the NAO leads the total MHT_{48^oN} by approximately 60^o–80^o (i.e., $\approx$10–20-yrs for variability around 60–80-yrs).

4.6 Conclusions

A general circulation model for the Atlantic ocean (OGCM) was forced with a realistic monthly NAO-like forcing during the period 1865–1997 in order to understand those

oceanic processes that contributed to the observed interdecadal SST variability in the North Atlantic region during the 20th century. The following conclusions can be drawn:

- Apart from those regions where the OGCM was *locally* forced by NAO-related fluxes of heat, freshwater and momentum, the modelled SST anomalies are consistent with the observations near the subpolar front along the North Atlantic Current (NAC), despite of a missing local forcing by the NAO. Hence, we conclude that the response of the upper-ocean to a *non-local* forcing by the NAO was successfully simulated, at least in this part of the North Atlantic.

- The development of observed and modelled SST anomalies during the periods 1915–1939 and 1960–1984 (i) against a direct local heat flux forcing by the NAO north of 50^oN and (ii) despite of a missing forcing from the NAO along the NAC near 45^oN can be traced back to a lagged response ($\approx$ 10–20-yrs) of the thermohaline circulation and the subpolar gyre to interdecadal changes of the NAO. The contribution from interdecadal variability of the subtropical gyre to the meridional heat transport was of minor importance.

- The oceanic response to interdecadal changes of the NAO is primarily driven by surface heat flux variability. This finding is different compared to the variability on interannual time scales, where the oceanic response depends on surface heat flux *and* windstress variability (Eden and Willebrand, 2000).

- Interdecadal variability of modelled oceanic quantities like the strength of the thermohaline circulation, meridional heat transport, and gyral circulation amounts to approximately 10% of their long-term mean values.

4.7 Discussion

Interdecadal variability of the North Atlantic ocean circulation and its relationship to the NAO is investigated using an OGCM that was solely forced with anomalous surface fluxes associated with the NAO over the period 1865–1997. Several simplifying assumptions are inherent to our experimental setup. First, it is assumed that the bulk of interdecadal oceanic variability is governed by the NAO. As noted above, this assumption is justified by previous observational and modelling studies. Our results provide further (*a posteriori*) evidence for the validity of this assumption. Second, it is assumed that interdecadal atmospheric variability can be described by the standing pattern of the NAO. We applied MSSA to wintertime (JFM) fields of North Atlantic SLP anomalies (update from Trenberth and Paolino, 1980) for the period 1900–1997. The dominant mode describing interdecadal NAO variability (14% explained SLP variance) closely resembles the standing pattern of the NAO (not shown). Thus, we are confident that the forcing fields used in this study account for the bulk of interdecadal atmospheric variability in the North Atlantic region. Third, surface heat fluxes from the NCEP/NCAR reanalysis that were used to force the OGCM are to some degree influenced by the model physics of the reanalysis system (Kalnay et al., 1996). A comparison between surface net heat fluxes from the reanalysis and voluntary observing ship (VOS) data reveals a fair agreement in the spatial patterns and temporal characteristics of North Atlantic heat flux variability (Gulev et al., 2000b). Thus, we are confident that reanalyzed surface heat fluxes capture the bulk of NAO-related variability in the North Atlantic region. Finally, we have to note that any

direct impacts from the variability of the overflow and freshwater intrusions from high-latitudes (north of $70°N$) were neglected. We did not take into account, for example, the *direct* effect of the "Great Salinity Anomaly" (GSA) which passed the Labrador Sea during the early 1970s (Dickson et al., 1988). We cannot exclude that the effect of the GSA is inherent to the forcing fields through an impact onto the SST and/or atmospheric parameters. However, according to our OGCM experiments the *direct* influence from the GSA in the Labrador Sea region was presumably of minor importance for interdecadal North Atlantic variability. Although some of the simplifications may appear rather crude, the agreement between observed and modelled key-aspects of interdecadal SST variability enhances our confidence that the modelled interdecadal variability of the North Atlantic circulation as a response to a forcing by the NAO is realistically.

It is shown that interdecadal changes of the North Atlantic circulation leave their imprint on the sea surface (SST anomalies) and that oceanic changes lag behind the NAO. This may explain why previous observational studies (Bjerknes, 1964; Deser and Blackmon, 1993; Kushnir, 1994) successfully identified oceanic dynamics to play an important role for North Atlantic interdecadal variability. Moreover, the appearence of interdecadal oceanic variability on the sea surface allows to assess forced OGCM experiments during the 20th century, at least to some degree. Our results essentially confirm Kushnir's hypothesis that interdecadal variability of the North Atlantic ocean is primarily governed by changes in the THC and NAO. Changes in the meridional heat transport due to interdecadal variability of the subpolar gyre, however, seem to be of importance too.

Our finding that interdecadal oceanic changes lag behind the NAO by several years (Fig. 4.5, 4.9) imply that the definition of epochs for subsequent composite analyses, which are based on sea surface data alone, may mix the instantaneous impact from the NAO and the delayed impact from the ocean. Hence, such composite analyses may neither describe the extreme anomalies in the atmosphere nor those in the ocean effectively. Provided that the model performed realistically, stongest interdecadal changes in the North Atlantic ocean should be found by analyzing sub-surface data for the epoch difference 1990s versus late 1960s to early 1970s (Fig. 4.5). Such an analysis, however, goes beyond the scope of this study.

A relatively strong two-way interaction between the NAO and THC on interdecadal time scales was found by Timmermann et al. (1998) in an integration of the coupled ECHAM3/LSG model. In agreement with the results from this study, in their model the NAO alters the strength of the THC after some delay. On the other hand, in the ECHAM3/LSG model the NAO and THC are approximately in-phase on interdecadal time scales. This is because the atmospheric response to an anomalously strong (weak) THC involves a strengthened (weakened) NAO in the ECHAM3/LSG model. From our results there is less indication that the NAO and THC covary in phase on interdecadal time scales, because there were no pronounced interdecadal NAO anomalies during periods of an anomalously strong (1925–1935) and weak (1965–1975) THC (Fig. 4.5b). This may indicate that the instantaneous response of the NAO to interdecadal variability of the THC is rather weak. From the results of this study the simplest way to explain interdecadal variability in the North Atlantic ocean is as follows: Interdecadal variability of the North Atlantic ocean circulation is the lagged (passive) response to a surface heat flux forcing associated with interdecadal variability of the NAO. A similar explanation has been put forward by Delworth and Greatbatch (2000).

5 Variability as Simulated by a Coupled Climate Model

5.1 Introduction

Coupled general circulation models (CGCMs) became important tools for climate research in recent years. They are primarily used to assess possible future climate changes under an increasing greenhouse gas forcing (e.g., Houghton et al., 1996). The realism of these future projections, however, depends crucially on the CGCM's capability to realistically simulate major feedbacks between different components of the climate system.

CGCM integrations under present-day climate conditions are also used to improve our knowledge about possible mechanisms giving rise to low-frequency climate variability (e.g., Latif and Barnett, 1994; Grötzner et al., 1998; Timmermann et al., 1998). One advantage of using CGCMs when studying natural climate variability comes from the fact that they can provide relatively long time series of the full three-dimensional flow field. In contrast, the observational record is relatively short and gappy, especially when the ocean is considered. On the other hand, however, the modelled variability may suffer from model deficiencies in representing important key-processes.

In order to assess modelled mechanisms giving rise to natural climate variability, it is possible to compare the results from different CGCMs and to search for robust features. Moreover, the results can be compared with hindcast integrations of ocean general circulation models and with what is known from the observations.

Here, North Atlantic climate variability as simulated by the coupled atmosphere-ocean-sea ice model ECHAM4/OPYC3 is investigated. The ECHAM4/OPYC3 model was used to study the El Niño/Southern Oscillation phenomenon (Roeckner et al., 1996) along with its future changes under increasing greenhouse gas concentrations (Timmermann et al., 1999). Corresponding analyses were also performed for North Atlantic climate variability (Christoph et al., 1999; Ulbrich and Christoph, 1999; Latif et al., 2000). The role of oceanic dynamics in the coupled model for low-frequency fluctuations of the NAO was investigated by Christoph et al. (1999). The results from their analyses suggest that modelled variability of the North Atlantic ocean is consistent with the stochastic climate model (Hasselmann, 1976), and that the North Atlantic ocean adds little additional low-frequency variability to the NAO.

Here, the same integration is revisited. In contrast to the study by Christoph et al. (1999), however, the focus is on the characeristics of the NAO and its role for North Atlantic air-sea interaction over a broader range of frequencies. Moreover, variability of the North Atlantic overturning circulation (and its relationship to the NAO) is explicitely investigated.

5.2 Model Description

Climate variability in the North Atlantic region is investigated from a control integration of the coupled general circulation model ECHAM4/OPYC3 under present-day climate conditions.

The atmospheric component ECHAM4 is the fourth generation of a hierarchy of models that was further developed at the Max-Planck-Institut für Meteorologie (MPI) in Hamburg from the former European Center for Medium Range Weather Forecast (ECMWF) model. ECHAM4 has a horizontal resolution of T42 (approx. 2.8° by 2.8°) and 19 hybrid levels in the vertical. Further details about this integration are given by Roeckner et al. (1996).

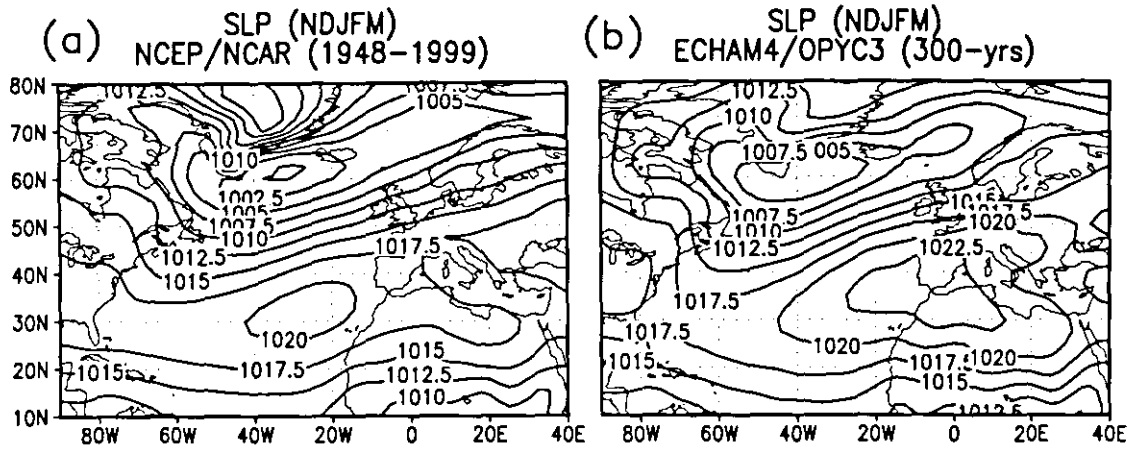

Figure 5.1: Average SLP pattern during wintertime (NDJFM) from (a) observations (NCEP/NCAR reanalysis) and (b) the coupled model. Contour interval is 2.5 *hPa*. Averaging periods are given in the titles.

OPYC3 is a three-component model including an interior ocean, a mixed-layer component, and a sea ice model (Oberhuber, 1993a,b). Prognostic variables for the interior ocean are momentum, mass, heat and salt. These quantities are determined on isopycnal levels solving the primitive equations in flux form. The model for the interior ocean is coupled to a mixed-layer model and a dynamic-thermodynamic sea ice model. A viscous-plastic rheology is used to parameterize the stress tensor for sea ice. The governing equations are solved on an Arakawa B-grid. The horizontal resolution is identical to that of the atmospheric model poleward of 38°. The meridional resolution increases towards the equator (0.5°) to properly resolve the equatorial wave guide. Vertically, 11 layers were used (see Oberhuber, 1993a,b, for details).

OPYC3 has been spun up for 1000-yrs prior to the coupling by using a combination of observed and ECHAM4 simulated fluxes and variables. Then, the coupled model has been spun-up over 100-yrs. During this spin-up annual mean flux correction terms for heat and freshwater have been determined for the subsequent control integration. The residual drift of the coupled model is relatively small over the first 100-yrs of the control integration (Roeckner et al., 1996).

Here, we investigate North Atlantic climate variability as simulated by the coupled ECHAM4/OPYC3 using the first 300-yrs (100-399) from the control integration. Time series of oceanic surface parameters and the North Atlantic meridional stream function are available from the first 280-yrs (100-379) of this integration.

5.3 Model Climatology

The observed and simulated average sea level pressure (SLP) distribution over the North Atlantic region during wintertime (NDJFM) is shown in Fig. 5.1. The gross features of the observed and simulated average SLP field are very similar. Differences are primarily associated with the Azores High that is stronger than observed and biased towards the east. The simulated Icelandic Low is less pronounced compared to the observations, especially its extension towards the northeast North Atlantic. These systematic differences, however,

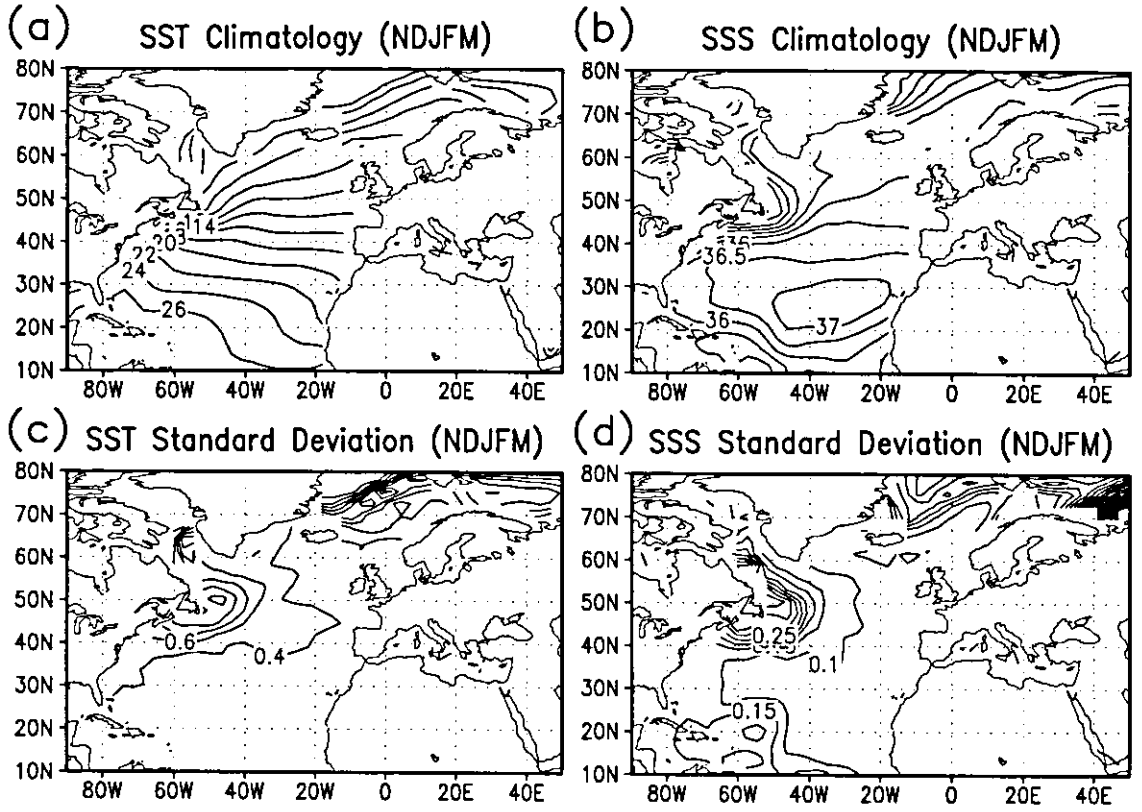

Figure 5.2: Average (a) SST and (b) sea surface salinity (SSS) along with interannual (c) SST and (d) SSS variability during wintertime (NDJFM) from the coupled model. Contour interval is (a) 2 K, (b) 0.5 *psu*, (c) 0.2 K, and (d) 0.05 *psu*.

tend to compensate each other with respect to the meridional pressure gradient over the northern North Atlantic (about 40^o-60^oN), at least over the ocean. This compensation vanishes over northeastern Europe leading to a weaker simulated climatological west-southwesterly flow compared to the observations.

Since an annual-mean flux correction scheme was applied during the course of the CGCM's integration, wintertime net heat fluxes and freshwater fluxes at the sea surface as seen by the atmospheric and the oceanic component of the coupled model are different. A comparison between net surface heat fluxes from the NCEP/NCAR reanalysis and those seen by the atmospheric component of the coupled model during wintertime (not shown) reveals a relatively good agreement within the range of uncertainty[20]. Essentially the same holds for North Atlantic surface freshwater fluxes (evaporation minus precipitation). For both, the NCEP/NCAR reanalysis and the coupled model, average freshwater fluxes are directed out of the ocean in the subtropical North Atlantic (about 2–4 *mm/day*), freshwater fluxes vanish north of about 40^oN (not shown).

Average SST and sea surface salinity (SSS) fields during wintertime (NDJFM) along with their interannual standard deviations from the coupled model are shown in Fig. 5.2. As for other coarse resolution CGCMs (e.g., Delworth et al., 1993; Timmermann et al.,

[20]A detailed discussion about the uncertainty of observational surface net heat flux climatologies (and variability) is given by Gulev et al. (2000b).

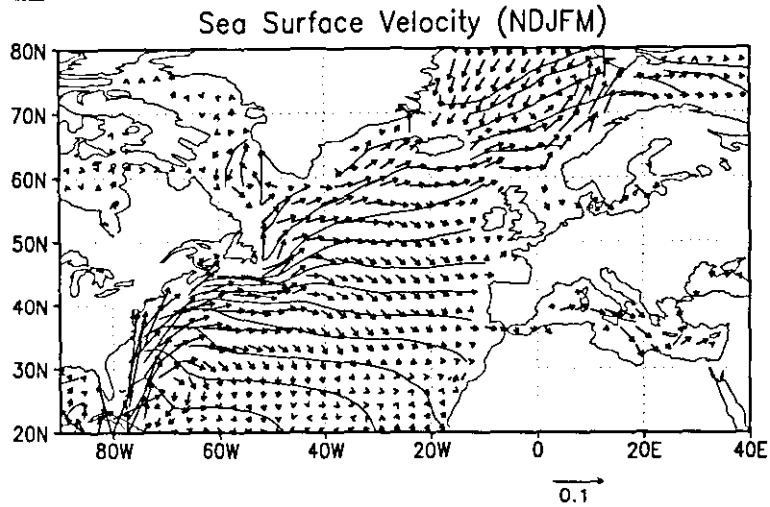

Figure 5.3: Average sea surface velocity during wintertime (NDJFM) from the coupled model. A reference arrow is given (0.1 ms^{-1}). Average SST is shown as contour lines (compare Fig. 5.2a).

1998), the average SST gradient across the Gulf Stream is too weak compared to the observations[21]. The relatively small SST gradient is partly due to a warm SST bias in the Labrador Sea region and south of Greenland in the coupled model. Moreover, simulated isotherms are too zonal in the mid-latitude eastern North Atlantic compared to the observations. The climatological field of wintertime SSS is in relatively good agreement with the observations, apart from a too weak SSS gradient across the Gulf Stream.

The bulk of simulated interannual SST and SSS variability during wintertime takes place in two regions (Fig. 5.2), that is, around Newfoundland and along the ice edge in the Greenland/Icelandic/Norwegian Seas (GIN Seas) and Barents Sea. In the northeastern North Atlantic interannual changes in the position of the ice edge contribute to the pronounced interannual SST and SSS variability. It is worth noting, that the simulated SST variability in the mid-latitude North Atlantic is biased towards Newfoundland, and too strong compared to the observations (see Timmermann et al., 1998, their Fig. 5a, for observed SST variability).

The long-term average surface flow field during wintertime as simulated the coupled model is shown in Fig. 5.3. The Gulf Stream follows the eastern U.S. seaboard from Florida towards Newfoundland. Moreover, there is no cyclonic surface-circulation in the subpolar gyre. Missing cyclonic circulation in the subpolar gyre is associated with a North Atlantic Current that is biased towards the western part of the northern North Atlantic and whose flow direction is too zonal between about $50°N$ to $60°N$. Notice, that these differences may partly explain the differences between observed and simulated SST characteristics just discussed. Near-surface water in the Labrador Sea region, for example, originates primarily from the relatively warm south, rather than from the relatively cold Irminger Sea. A relatively strong cyclonic circulation is evident in the GIN Seas, which is composed of the North Atlantic Current extensions and surface outflow from the Arctic.

In the coupled model deep convection primarily takes place in the GIN Seas (Christoph

[21] Observed climatologies for SST, SSS, and surface drift velocity are given, e.g., by Peixoto and Oort (1992).

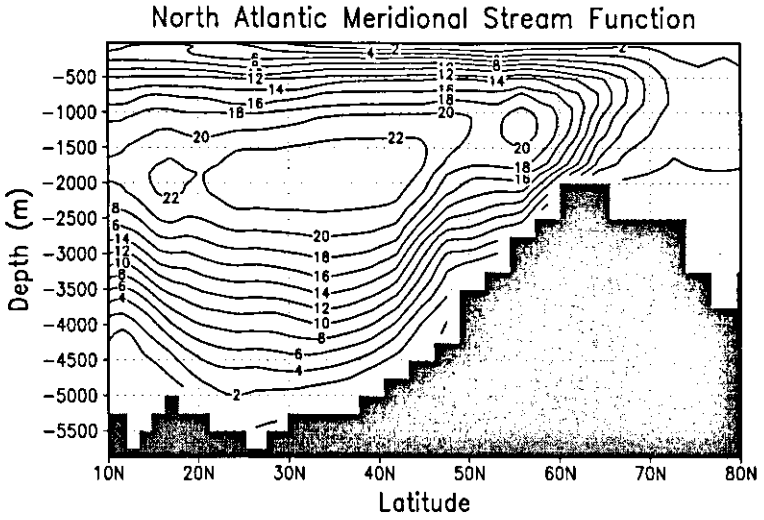

Figure 5.4: Long-term average of the annual-mean North Atlantic meridional stream function (Sv) from the coupled model. The average was estimated from 280-yrs (100–379).

et al., 1999; Latif et al., 2000). This can be inferred from Fig. 5.4 showing the long-term average of the annual-mean meridional overturning circulation in the North Atlantic. Positive values stand for a clockwise rotation. In agreement with other studies (e.g., Delworth et al., 1993; Timmermann et al., 1998) the maximum strength of the meridional overturning amounts to 22 Sv from about 15^oN to 50^oN. North Atlantic Deep Water is primarily produced north of 60^oN. This is in contrast to the CGCMs analyzed by Delworth et al. (1993) and Timmermann et al. (1998), where the bulk of sinking takes place south of 60^oN. Moreover, Antarctic Bottom Water does not reach the deep subtropical North Atlantic.

Summarizing, the simulated mean oceanic circulation shows considerable differences compared to the observations, to other CGCM integrations (e.g., Delworth et al., 1993; Timmermann et al., 1998), and to simulations with ocean general circulation models (e.g., Oberhuber, 1993c; Eden, 1999; Eden and Willebrand, 2000).

5.4 The North Atlantic Oscillation

In this section NAO variability as simulated by the ECHAM4/OPYC3 model is evaluated by a comparison with the observational results described in chapter 3.

Following the methodology for the observations the NAO index is defined as the difference between *normalized* SLP of the Azores High and the Icelandic Low. For the definition of the NAO's centers of action we follow closely Christoph et al. (1999), that is, variability of the Icelandic Low (Azores High) is described by SLP time series averaged over the region 17.5^o–20^oW and 65^o–67.5^oN (10^o–15^oW and 40^o–42.5^oN). These regions show the strongest teleconnectivity in the North Atlantic region (negative correlations, see Wallace and Gutzler (1981)) and represent the centers of action of the first EOF of anomalous wintertime SLP. Additionally, the difference between *non-normalized* SLP of the Azores High and Icelandic Low is considered (dSLP).

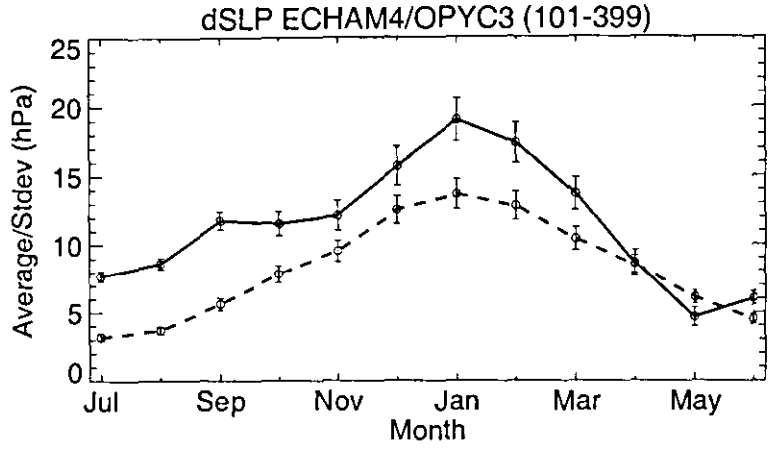

Figure 5.5: Annual cycle of the average SLP difference (hPa) between the Azores and Iceland (solid) and its interannual standard deviation (dashed) from the coupled model (300-yrs). Vertical bars denote 95% confidence intervals.

5.4.1 Seasonality — On the Definition of the Winter

The modelled annual cycle of average dSLP along with its (interannual) standard deviation is depicted in Fig. 5.5. As for the observations (Fig. 3.1), interannual dSLP variability is phase-locked to the annual cycle. The observed time lag of one month between the average and standard deviation of dSLP, however, is missing in the model. Overall, the agreement between the observed and modelled annual cycles is reasonable within the range of uncertainties.

The NAO describes the simultaneous strengthening and weakening the Azores High and the Icelandic Low, that is, the NAO *signal* is represented by a negative correlation between the two time series (see Hurrell and van Loon, 1997). The observed and simulated annual cycle of the correlation between SLP at the Azores and Iceland is depicted in Fig. 5.6. For

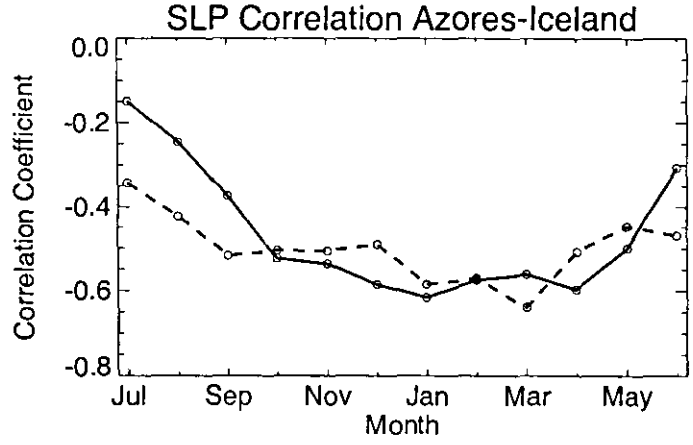

Figure 5.6: Annual cycle of the simulated (solid) and observed (dashed) correlation coefficient between monthly SLP at the Azores and Iceland.

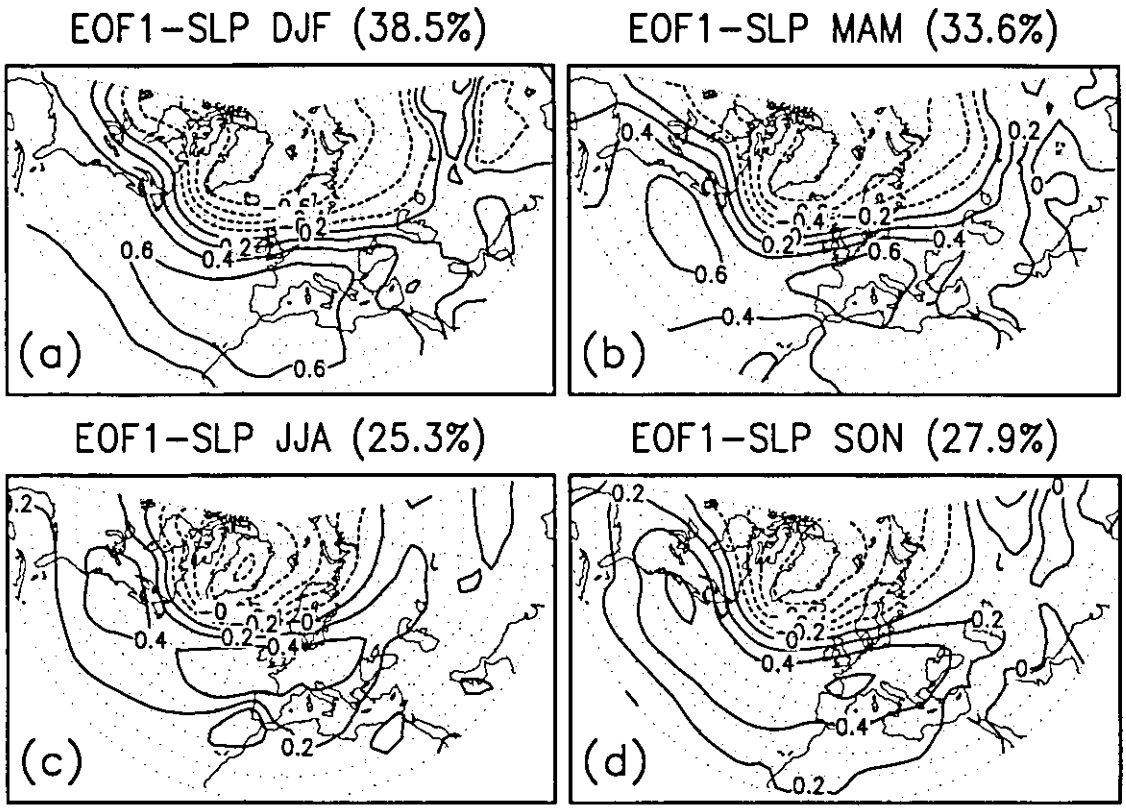

Figure 5.7: First EOF of *normalized* North Atlantic SLP anomalies for (a) DJF, (b) MAM, (c), JAS, and (d) OND from the coupled model. EOFs were estimated from 300-yrs of the simulation (100–399). The contour interval is 0.2. Values in parentheses give the percentage of total variance explained by the EOF.

the observations and the model correlations range between -0.5 and -0.6 from October to April. Thus, from late autumn to early spring the monthly NAO signal explains about 30% ($r^2 \cdot 100$) of the variance. In agreement with the results by Hurrell and van Loon (1997), the NAO signal is lower during the summer months.

Applying EOF analysis to observed North Atlantic SLP anomalies for different seasons, Hurrell and van Loon (1997) showed that the NAO pattern undergoes changes through the annual march, both, with respect to its magnitude and with respect to the longitudinal position of the NAO's southern center of action (their Fig. 4). We performed a similar analysis for modelled North Atlantic SLP anomalies. The annual cycle of the modelled strength of the NAO pattern is quite similar to the observations. The observed westward migration of the anomalous Azores high during spring and summer, however, is almost missing in the model. This can be inferred from Fig. 5.7 showing the first EOFs of *normalized* SLP anomalies in the North Atlantic region. By applying EOF analysis to normalized SLP anomalies the leading eigenvectors represent patterns of *spatial coherency* (strength of spatial teleconnectivity). In constrast to the observations SLP over the Iberian Peninsula remains a good proxy of the NAO's southern center of action throughout the whole year. The areal extend of regions of strong teleconnectivity are highest during wintertime. Especially during the summer season the spatial coherence of NAO anomalies

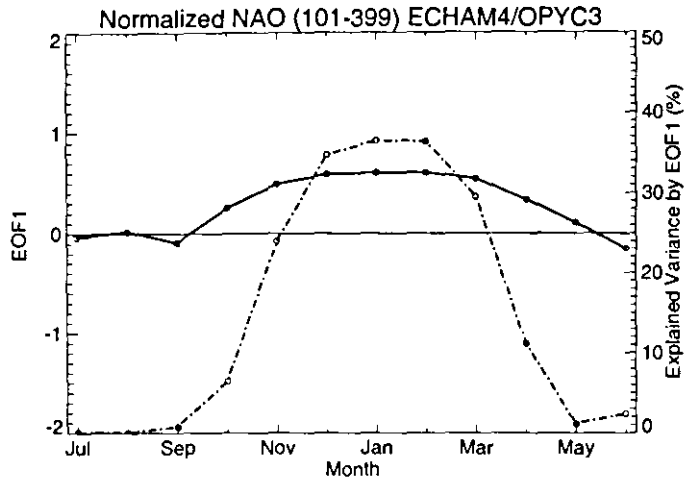

Figure 5.8: Leading EOF (solid) of anomalous *normalized* annual cycles of the NAO and proportion of explained variance (%) for each month (dash-dotted) from the coupled model (299-yrs).

is much lower. Moreover, reduced magnitudes of the first EOF over the subtropical North Atlantic (Fig. 5.7c) reflect a reduced teleconnectivity between the anomalous Azores High and the anomalous Icelandic Low during the summer months (see also Fig. 5.6).

In order to investigate intraseasonal coherence of the simulated NAO during wintertime, EOF analysis was applied to anomalous *normalized* annual cycles of the NAO index. The first EOF (Fig. 5.8, solid) describes temporally coherent NAO anomalies of one sign during the winter months from November to April. This EOF, which shows no indication for degeneracy with higher order EOFs according to the criterion of North et al. (1982), explains 15.3% of the total variance. For the individual winter months from November to March this EOF explains about 20–40% (Fig. 5.8, dash-dot). The correlation between the corresponding first PC and the wintertime NAO index (NDJFM) amounts to $r = 0.96$.

Throughout the remainder of this section, thus, the NAO index, averaged over the winter months from November through March, is used. This choice ensures (i) that the bulk of interannual NAO variability is captured (Fig. 5.5), (ii) that the NAO signal is strongest (Fig. 5.6), (iii) that the NAO index is based on the centers of maximum teleconnectivity (Fig. 5.7a and Christoph et al. (1999)) and (iv) that the wintertime NAO index describes a maximum of intraseasonal coherence. The temporal evolution of the simulated NAO index during wintertime is depicted in Fig. 5.9 along with the associated anomalous SLP pattern over the Northern Hemisphere. This pattern shows the typical NAO signature over the North Atlantic region. In this model the Aleutian Low covaries out-of-phase with the Icelandic Low. Over the North Pacific locally more than 30% of the SLP variance is explained by the NAO index. Thus, the spatial NAO pattern as simulated by the ECHAM4/OPYC3 model resembles the Arctic Oscillation pattern as described by Thompson and Wallace (1998).

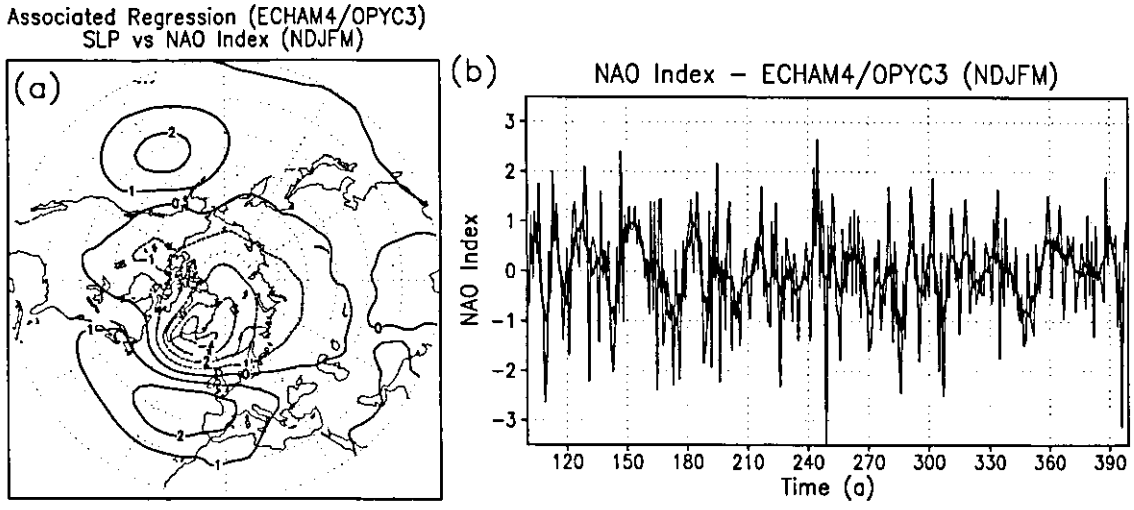

Figure 5.9: Modelled spatial and temporal behaviour of the NAO during wintertime (NDJFM): (a) SLP anomalies (hPa) that are associated with the (b) NAO index. SLP anomalies were regressed onto the normalized NAO index. The lowpass-fitered NAO index (5-yr running mean, bold) is also shown in (b).

5.4.2 Distribution Characteristics

The distribution characteristics of the oberved NAO index were described in section 3.4. There, evidence was presented that the distribution of the observed wintertime NAO index is almost Gaussian with a slight tendency towards a negative coeffcient of skewness. The probability density function (PDF) of the simulated wintertime NAO index reveals

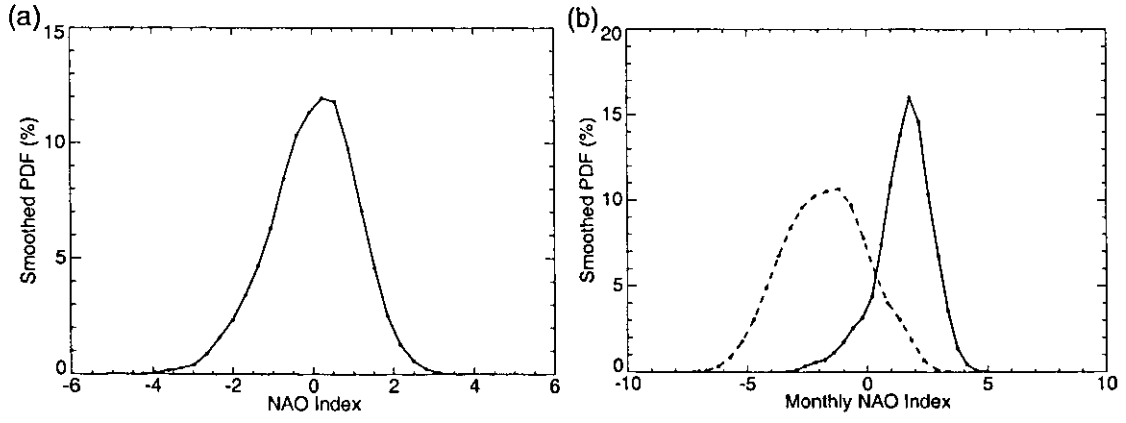

Figure 5.10: Probability density function (PDF) of (a) the wintertime NAO index (NDJFM, $n = 300$) and (b) monthly NAO indices (November to March) during high (solid, $n_{high} = 215$) and low (dashed, $n_{low} = 225$) NAO winters from the coupled model. High (low) NAO winters are one standard deviation above (below) the average. PDFs were smoothed using a Gaussian Kernel. Smoothing parameter is $h_a = 0.32$ in (a) and $h_b = 0.51$ in (b).

a quite similar picture (Fig. 5.10a). As for the observations, in the model positive NAO anomalies occur more frequently with smaller magnitudes compared to negative NAO anomalies. Negative NAO winters tend to be more extreme. This asymmetry is quantified by a negative coefficient of skewness of -0.38. Due to the length of the simulated NAO index this value is statistically significant (at 95% confidence). The negative skewness of the NAO is even more pronounced (-0.5) if monthly data from November to March are analyzed (not shown).

Moreover, observational evidence was presented in section 3.4 that intraseasonal variability is more pronounced during low NAO winters compared to high NAO winters. This difference in intraseasonal variance is very pronounced for the simulated NAO (Fig. 5.10b). The variance is 1.23 (2.82) for all winter months from November to March when the winter-averaged NAO index (NDJFM) is one standard deviation above (below) the average. This implies that NAO-like variability on intraseasonal time scales is more persistent during high NAO winters compared to low NAO winters.

Summarizing, the main PDF features are very similar for the observed and modelled NAO index.

5.4.3 Frequency Characteristics

In order to clarify whether there is statistical evidence for the presence of deterministic components for simulated NAO variability, Monte Carlo SSA was applied to the wintertime NAO index (40-yr window, see Methods). The eigenvalue spectrum is shown in Fig. 5.11. Similar to the results by Christoph et al. (1999), who estimated Fourier spectra from the simulated NAO index, significant excursions above the local 92.5% confidence level are observed for periods of about 2–2.5, 7.5, and 30-yrs. Note, however, that the probability for the occurrence of five or more excursions above the 92.5th percentile is 23% to occur just by chance under the global null hypothesis of AR(1) noise[22]. Thus, as long as there are no *a priori* reasons to focus on variability around 2–2.5, 7.5, and 30-yrs the wintertime NAO index as simulated by ECHAM4/OPYC3 is not strongly unusual (at 77% confidence) compared to realizations of AR(1) noise. Notice, that the spectrum of the simulated wintertime NAO index is almost "white".

It is worth mentioning, that locally significant excursions above the 92.5th percentile around 2–2.5-yrs and 5–9-yrs were also found for the observed NAO index (section 3.5). Thus, one might speculate that the same physical mechanisms are responsible for the generation of these spectral peaks[23]. Christoph et al. (1999) show that the spectral peaks around 7.5-yrs and 30-yrs vanish if a coarser-resolution component (T30) of the atmosperic model (ECHAM4) is coupled to a mixed layer model. In contrast, the peak around 2–2.5-yrs is evident in both integrations, with and without a dynamical ocean. The disappearence of the spectral peaks around 7.5-yrs and 30-yrs, if oceanic dynamics are neglected, may be indicative for the presence of two-way coupled air-sea modes on these time scales. On the other hand, these differences are in accordance with what is expected from realizations of AR(1) noise, that is, different realizations may show different randomly generated peaks. Thus, from a statistical point of view the results from the sensitivity experiments

[22]Due to a vanishing auto-correlation of the simulated winter-averaged NAO index this is equivalent to "white noise".

[23]From this point of view *local* excursions above the 92.5th percentile would suffice to have evidence (at 92.5% confidence) against the null hypothesis.

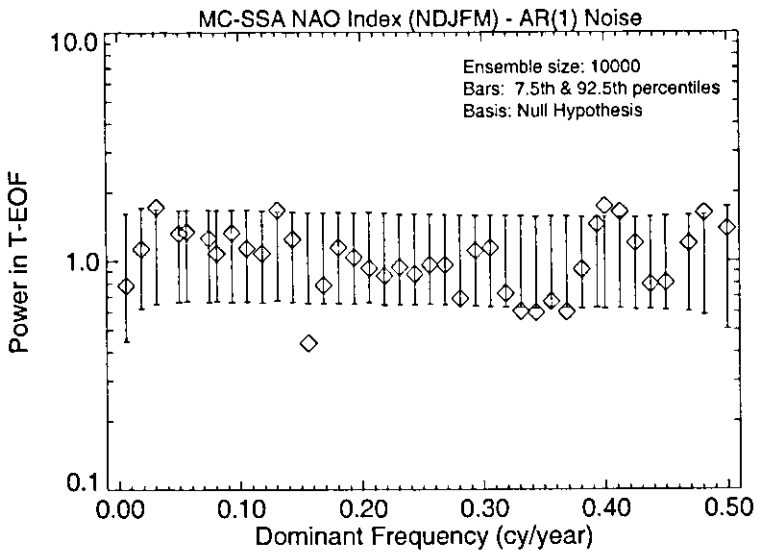

Figure 5.11: Test of the simulated wintertime NAO index (NDJFM) against AR(1) noise by means of Monte Carlo SSA (see Methods). *Diamonds* denote projections of the NAO's lag-covariance matrix upon the T-EOFs of the null hypothesis, plotted against the dominant frequency (obtained by reduced Fourier transform of T-EOFs). Each vertical bar contains 85% of the eigenvalues out of 10000 realizations of the null hypothesis. A window length of forty years was used. The analysis is based on 300-yrs.

described by Christoph et al. (1999) are not conclusive with respect to the existence of two-way interactions between the NAO and the North Atlantic ocean on interannual (7.5-yrs) and interdecadal (30-yrs) time scales.

5.4.4 Time-Frequency Characteristics

Normalized local wavelet power of the simulated NAO index during wintertime giving rise to the spectral characteristics described in the previous section is depicted in Fig. 5.12. Variability of the NAO seems to be more powerful during the first part of the simulation. Furthermore, there is less indication for a distinct mode of variability. Enhanced activity around 30-yrs is most pronounced during the first century of the simulation. Note, that even a spike-like event on this time scale would show enhanced local wavelet power during an episode of approximately 90-yrs (two-sided cone-of-influence). Interannual variability around 8-yrs shows an epoch of enhanced power during the middle of the simulation (approx. from the model year 180 to 300) which is much longer than two-times the cone-of-influence. During the years 210–270 of the simulation NAO variability on this time scale contributes more than 15% to the total NAO variance, as revealed by an analysis of the *local variance fraction* (Plaut et al., 1995), which was estimated from the SSA-reconstructed 7.5-yr component. Finally, there is no evidence for changes of the NAO's "redness".

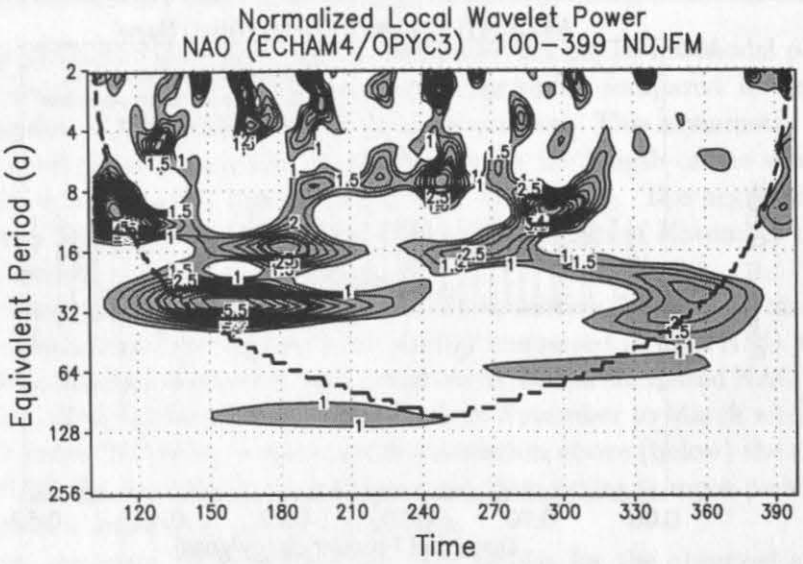

Figure 5.12: Normalized (by variance) local wavelet power of the modelled wintertime NAO index. Power exceeding 1.0 stands above the background noise (shaded regions). Contour interval is 0.5 for local wavelet power exceeding 1.0. The cone of influence (bold-dashed), within side effects become important, and local wavelet power estimates exceeding the local 95% confidence level (bold-solid) are also shown. Power estimates are smoothed in time (5-yr average).

5.4.5 Winter-to-Winter Persistence

In chapter 3 it is shown that observed wintertime NAO anomalies during the 20th century tended to recur one winter later although the NAO pattern disappeared during the inbetween non-winter seasons. It was argued that this winter-to-winter persistence is suggestive for an external forcing of the wintertime NAO.

In contrast to the observed NAO during the 20th century, the simulated NAO shows no significant winter-to-winter persistence (Fig. 5.13)[24], that is, during the subsequent non-winter seasons (Fig. 5.13c–e) the wintertime NAO anomaly (Fig. 5.13b) disappears, and there is no recurrence one winter later (Fig. 5.13f). Missing winter-to-winter persistence of the simulated NAO implies that in the coupled model there is no significant external forcing of the NAO on interannual and longer time scales (variability with time scales >4-yrs). This finding supports the conclusions by Christoph et al. (1999) that possible two-way feedbacks between ocean and atmosphere — if existent — add little additional variance to the NAO.

As for the observations, it was checked that the results are not sensitive against the sign of the wintertime NAO anomaly (high and low NAO events were considered separately) and against changes in the threshold. Moreover, in accordance with the results from wavelet analysis of the wintertime NAO index (Fig. 5.12), winter-to-winter persistence is missing for different subsets (not shown).

In agreement with the results from EOF analysis of anomalous annual cycles of the

[24]For the model the seasons were defined as DJF, MAM, JJA, and SON. Notice, that the DJF season captures the bulk of the NAO's interannual variability and intraseasonal coherence (Fig. 5.8). The conclusions, however, are not sensitive against changes in the definiton of the seasons.

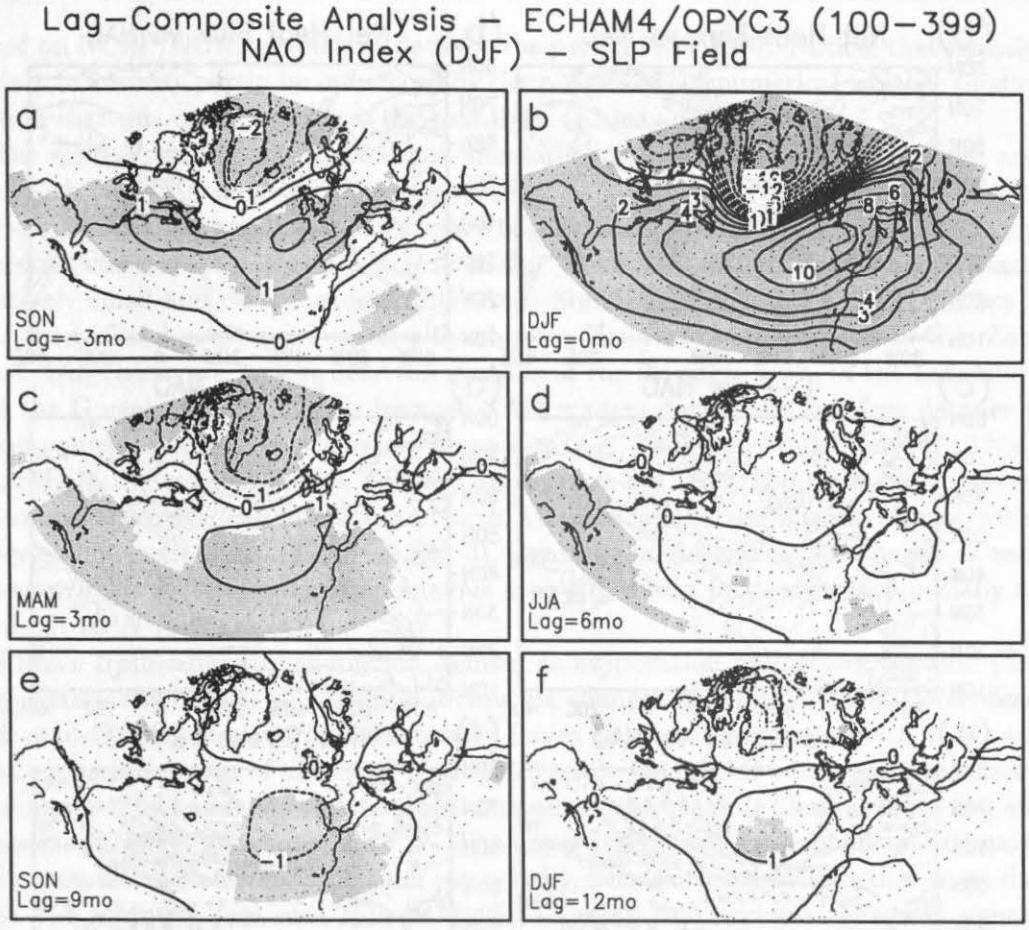

Figure 5.13: Difference in SLP (hPa) between high and low NAO winters (DJF) for (a) the autumn before, (b) the same winter, (c) the following spring, (d) the following summer, (e) the following autumn, and for (f) the following winter from the coupled model. A threshold of one standard deviation was used. Results are based on 300-yrs (100-399). Differences at the 95% confidence level are shaded (two-sided t-test).

normalized monthly NAO index (Fig. 5.8), the results from the lag-composite analysis confirm some persistence of the NAO within the extended winter season (Fig. 5.13a–c).

5.5 NAO and Air-Sea Interaction

Atmosphere and ocean interact at the sea surface through the fluxes of heat, freshwater, and momentum. Thus, a thorough understanding of the air-sea fluxes is a prerequisite to improve our knowledge about possible interactions between atmosphere and ocean. In this subsection the question is addressed, how the NAO modulates air-sea fluxes in the ECHAM4/OPYC3 model. Furthermore, by analyzing lag-correlation relationships between the atmosphere (SLP) and the ocean (SST) the direction of possible interactions between the two subsystems is considered.

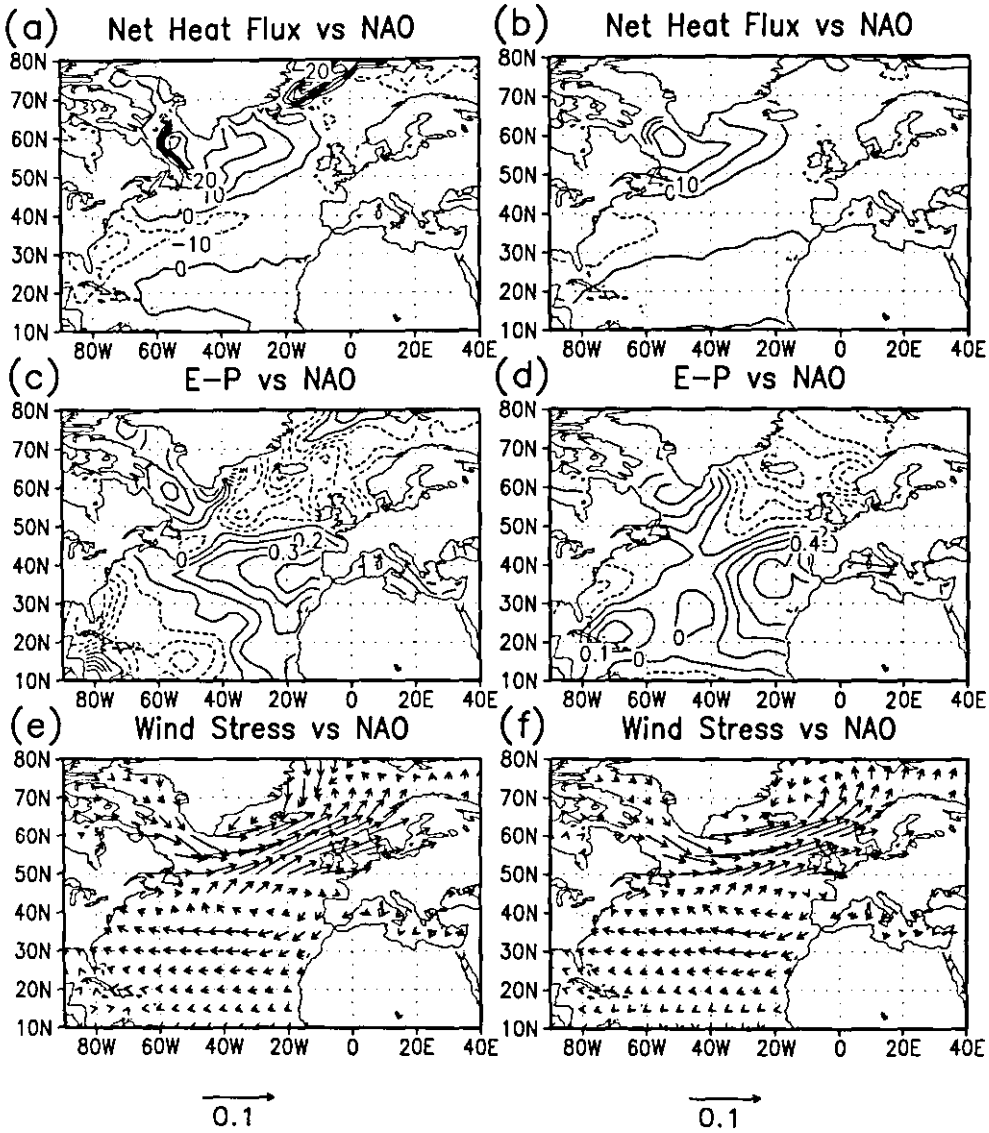

Figure 5.14: Linear response of North Atlantic surface parameters to a forcing by the NAO during wintertime (NDJFM) for the observations (left column, NCEP/NCAR reanalysis, 1958–1996) and the coupled model (right column). Anomalous fields of (a)–(b) net surface heat flux (W/m^2), (c)–(d) net surface freshwater flux (E−P in mm/day), and (e)–(f) zonal and meridional surface wind stress (N/m^2) were regressed onto the normalized NAO indices. Positive fluxes are directed out of the ocean. Contour interval is (a)–(b) 5 W/m^2 and (c)–(d) 0.1 mm/day. A reference vector for wind stress ($0.1N/m^2$) is given in (e) and (f). For clarity every second vector in latitudinal and longitudinal direction was omitted.

5.5.1 Instantaneous Relationships

Anomalous North Atlantic net heat flux, freshwater flux, and wind stress fields at the sea surface that are associated with the wintertime (NDJFM) NAO index are shown in Fig. 5.14. The analysis was performed for both, the observations and the coupled model, in order to evaluate the results from the coupled model. "Observational" estimates are

based on NCEP/NCAR reanalysis data for the period 1958–1997. Notice, that reanalyzed surface fluxes may partly be influenced by the physics of the numerical weather prediction system that was used to perform the reanalysis (Kalnay et al., 1996).

The spatial patterns of observed and simulated net surface heat flux anomalies associated with the NAO are in good agreement (Fig. 5.14a,b). High NAO winters, for example, are accompanied by anomalous net surface heat fluxes out of (into) the ocean in the northwestern (western subtropical) North Atlantic. Anomalies off the East African coast are relatively small and do not exceed 10 W/m^2. Simulated magnitudes of net surface heat flux anomalies, however, are smaller by about a factor of two compared to the observations. Differences are largest near the margins of the ice edge, both, in the Labrador Sea and the Greenland Sea. This is because NAO winters during the last four decades were accompanied by respective ice extent anomalies (e.g., Fang and Wallace, 1994). This is in contrast to the coupled model, where NAO winters are not accompanied by noteworthy ice extent anomalies in the northern North Atlantic (not shown). In agreement with the observations (see Cayan, 1992b, his Fig. 3), primarily latent and sensible heat flux anomalies contribute to the simulated anomalous net surface heat flux patterns, especially north of about 20^oN (not shown).

Surface freshwater flux anomalies, defined as evaporation minus precipitation (E−P), may change the density of the upper-ocean via changes in salinity. Anomalous observed and modelled fields of surface freshwater fluxes that are associated with NAO are in good agreement north of about 20^oN (Fig. 5.14c,d). High NAO winters, for instance, are accompanied by anomalous freshwater fluxes out of the ocean in the Labrador Sea and in the eastern North Atlantic near 40^oN. The upper-ocean faces an anomalous freshening in the northeastern North Atlantic and, secondarily, near the southeastern U.S. coast during high NAO winters (see also Hurrell, 1995). Taking into account the mean simulated North Atlantic surface drift (Fig. 5.3) freshwater flux anomalies in the Labrador Sea and the northeastern North Atlantic associated with the NAO are presumably most effective in (subsequently) changing the upper-ocean density in the sinking regions via salinity anomalies. Note, that in the Labrador Sea region, both, anomalous net surface heat fluxes and freshwater fluxes are working in such a way to either enhance or to reduce the sea surface density. In the GIN Seas freshwater flux anomalies presumably dominate over net surface heat flux anomalies in changing the upper-ocean density during high and low NAO winters.

Whereas simulated surface freshwater flux anomalies during NAO winters in the western part of the North Atlantic basin are primarily governed by changes in evaporation, associated changes in precipitation dominate surface freshwater flux anomalies in the eastern North Atlantic (Fig. 5.15). Similar results are found for the observations (not shown). The excess of NAO-related evaporation variability over that of precipitation in the western North Atlantic is due to relatively strong humidity gradients across the eastcoast of North America. Strong precipitation anomalies in the eastern North Atlantic are presumably related to systematic changes in the position and strength of the North Atlantic storm track (e.g., Rogers, 1990; Christoph et al., 1999; Gulev et al., 2000a).

In the previous section it was shown that the spatial pattern of simulated NAO variability agrees well with those estimated from the observations. Thus, it does not surprise that observed and simulated wind stress anomalies, which are associated with the NAO (Fig. 5.14e,f), are also very similar. Differences are largest over the Greenland Sea. There, in contrast to the coupled model, observed high NAO winters, for example, are accompa-

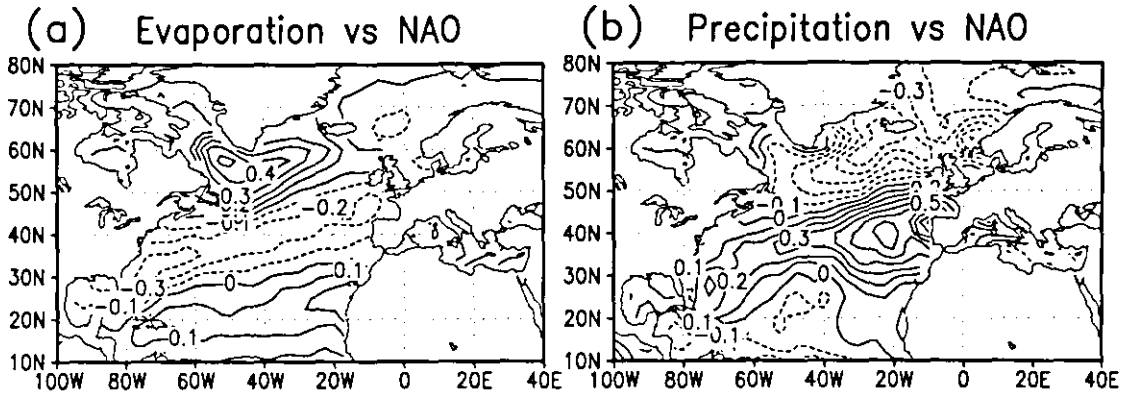

Figure 5.15: Same as in Fig. 5.14d, except for the simulated surface (a) evaporation and (b) precipitation response to the NAO. Contour interval is 0.1 mm/day.

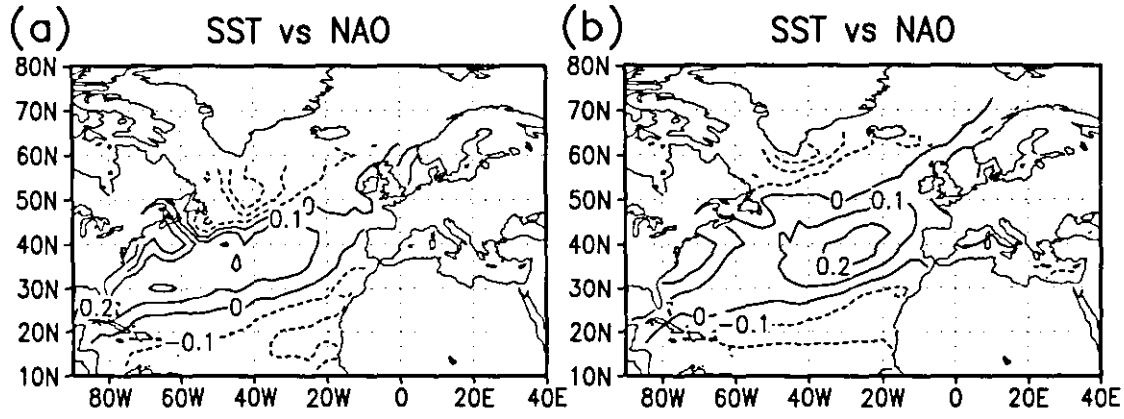

Figure 5.16: Same as in Fig. 5.14a and 5.14b, except for (a) observed and (b) simulated SST anomalies. Contour interval is 0.1 K. Reconstructed historical SST data (1958–1996) from Smith et al. (1996) were used in (a).

nied by southward wind stress anomalies[25]. However, as will be discussed in chapter 6, the observed NAO's centers of interannual variablity during the last two decades were located further downstream compared to previous decades. This shift may explain the differences between observed and simulated wind stress anomalies over the Greenland Sea.

In the North Atlantic, simulated high and low NAO winters are accompanied by anomalous surface drifts that can largely be explained by wind-driven Ekman transports (not shown, see Eden and Willebrand, 2000, for further details). Maxima of the anomalous North Atlantic meridional streamfunction near $55^{o}N$, however, are located at a depth of about 300 m. This indicates that in the coupled model baroclinic processes are also partly involved in the northern North Atlantic. These baroclinic signatures are associated with processes taking place in the low-frequency part of the spectrum (Christoph et al., 1999).

Apart from SLP, SST is another widely used parameter in studies on extratropical climate variability. This is because SST is a relatively well-sampled parameter and SST is a

[25]Note, that this southerly flow advects dry and cold air of Arctic origin over the Greenland Sea. This may explain the large net surface heat flux response to a forcing by the NAO (Fig. 5.14a).

good proxy for the North Atlantic upper-ocean heat content, at least during boreal winter (e.g., Deser and Blackmon, 1993). On the other hand, SST is also a parameter that is influenced by a number of different forcings like (i) net surface heat flux, (ii) temperature advection by anomalous current, and (iii) anomalies in the entrainment velocity and mixed layer depth (see Frankignoul, 1985, for a detailed discussion). Observed and modelled SST anomalies, which are associated with the wintertime NAO, are depicted in Fig. 5.16. Observed SST anomalies are consistent with the notion that they are locally generated by NAO-related net surface heat flux and wind stress anomalies (Cayan, 1992a). In the northern North Atlantic, for example, high NAO winters are associated with anomalously strong heat fluxes out of the ocean and anomalously strong mixing due to enhanced westerlies (Figs. 5.14a,c and 5.16a), thus, explaining the presence of the cold SST anomaly. In the coupled model, the gross features can be explained in a similar manner. However, there are differences compared to the observations (Fig. 5.16). From the surface flux forcing patterns (Fig. 5.14) the presence of a cold SST anomaly east of Newfoundland would be expected under a local oceanic forcing by the NAO. Since no pronounced SST anomaly is found east of Newfoundland, one might speculate that oceanic dynamics offset the local cooling by the NAO. Christoph et al. (1999) performed a similar analysis using lowpass-filtered data (10-yr running-mean). They show that modelled low-frequency changes of the NAO are associated with a strengthened northward drift along the western part of the North Atlantic giving rise to the formation of a positive SST anomaly. This SST anomaly vanishes if the atmospheric model is coupled to a mixed-layer ocean. Thus, in accordance with the observations (Bjerknes, 1964), air-sea interaction in the coupled model is time scale dependent.

Differences between observed and simulated SST anomalies during high NAO winters are also evident west of the Iberian Peninsula. There, the simulated positive SST anomaly is relatively pronounced compared to the observations, although a local net surface heat flux and wind stress forcing is missing. The existence of this SST anomaly might be explained by an anomalous downwelling. It remains unclear why this SST anomaly is less pronounced in the observations.

5.5.2 Nature of Air-Sea Interaction — Cross-Correlation Functions

In the previous section the *instantaneous* relationship between the NAO and North Atlantic air-sea interaction was considered. This kind of analysis cannot reveal the existence and nature of possible feedbacks between atmosphere and ocean without additional model experiments (see, e.g., Latif and Barnett, 1994; Rodwell et al., 1999, for such experiments). However, the existence and nature of possible air-sea feedback *can* be assessed even for CGCM integrations (and observations) by analyzing cross-correlation functions (see Frankignoul, 1985, for details). Results from such analyses for the ECHAM4/OPYC3 model are presented in this section.

Canonical correlation analysis (CCA, see Methods) was applied to anomalous North Atlantic SLP and SST fields during wintertime (NDJFM) from the coupled model. The leading five EOFs explaining 88% (57%) of the total SLP (SST) variance were used as input. It was tested that the results are not sensitive against the number of EOFs retained for CCA. The spatial patterns of the first and second canonical correlation pair for SLP and SST are depicted in Fig. 5.17. The temporal correlation between the canonical correlation coefficients amounts to $r = 0.80$ ($r = 0.68$) for the first (second) canonical correlation

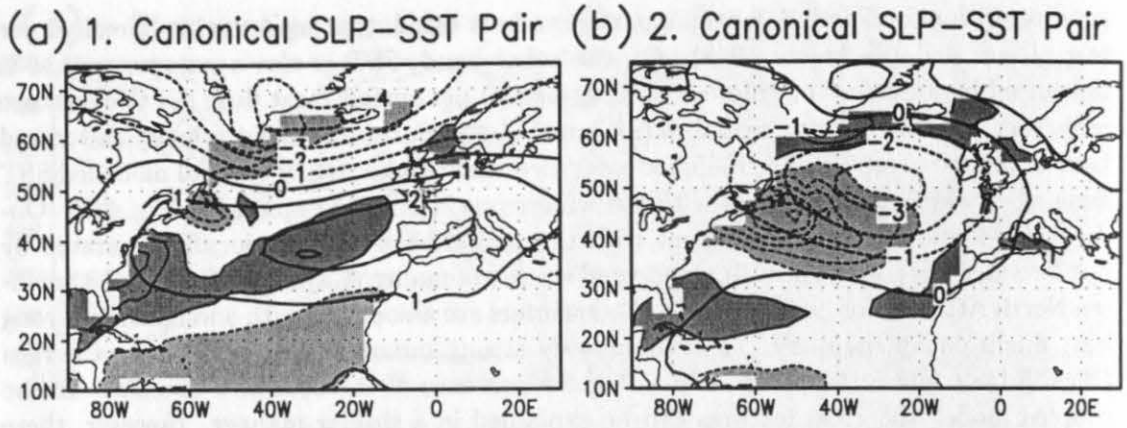

Figure 5.17: The patterns of the (a) first and (b) second canonical correlation pair of SLP (hPa) and SST (K) during wintertime (NDJFM) from the coupled model. SLP anomalies are given as contours (1 hPa). The contour interval for SST anomalies is 0.1 K and anomalies larger (smaller) than 0.1 K ($-0.1K$) are heavy (light) shaded. The leading five EOFs explaining 88% (SLP) and 57% (SST) of the total variance were used. The correlation between the coefficient time series is (a) $r = 0.80$ and (b) $r = 0.68$. The first (second) canonical SLP mode explains 46.9% (13.6%) of the total SLP variance. The first (second) canonical SST mode explains 9.6% (10.6%) of the total SST variance.

pair. Temporal correlations for higher-order coupled modes are almost zero. The first coupled mode of simulated coherent SLP-SST variability (Fig. 5.17a) describes variability of the NAO along with its associated anomalous SST pattern (compare Figs. 5.9a and 5.16b). The second coupled SLP-SST mode is associated with a SLP monopole near 50^oN and 30^oW. As for the NAO, anomalous net surface heat fluxes and wind stresses associated with this SLP monopole may explain the existence of the canonical SST pattern (Fig. 5.17b).

CCA was also applied to observational SLP and SST data. The leading two canonical correlations patterns as well as the correlation between the canonical time series coefficients are very similar to those for the coupled model (not shown). Thus, the model appears to successfully simulate the bulk of North Atlantic air-sea interaction.

The cross-correlation function between the canonical correlation time series of the first and second canonical SLP-SST pair is shown in Fig. 5.18 for time lags from −7- to +7-yrs. SLP anomalies lead for negative lags. Both correlation functions peak at lag of 0-yrs (instantaneous coupling). The cross-correlation function shows a slight asymmetry. The cross-correlation is slightly higher if SLP leads SST than vice versa. However, even if SLP leads SST by 1–2-yrs, the percentage of variance explained by a linear relationship is very low. Notice, that the existence of a noteworthy positive (negative) feedback between the NAO and North Atlantic SST on interannual time scales would require significant positive (negative) cross-correlations if SST leads SLP. Thus, the results from the cross-correlation analysis can be summarized as follows: The NAO generates North Atlantic SST anomalies within one winter, primarily via anomalous net surface heat fluxes. These North Atlantic SST anomalies, however, do not feed back onto the NAO in subsequent years.

From the above analyses it remains unclear whether the NAO and its canonical SST

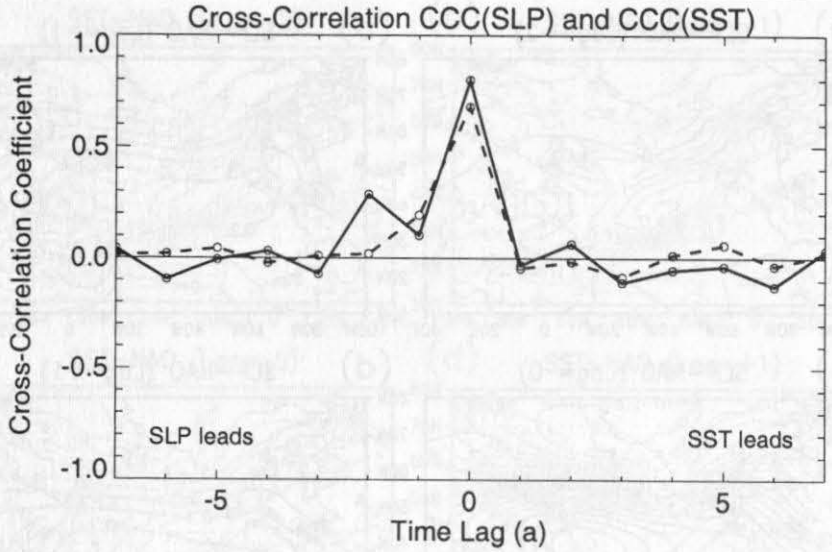

Figure 5.18: Cross-correlation function between the first (solid) and second (dashed) canonical SLP and SST time series during wintertime (NDJFM) from the coupled model. The solid (dashed) line refers to the patterns depicted in Fig. 5.17a (Fig. 5.17b). SLP leads for negative lags.

pattern form a positive (or negative) feedback within the winter seasons. Thus, cross-correlation functions for monthly data during wintertime (November through March) were analyzed in a similar manner.

CCA applied to *monthly* SLP and SST data from November through March yields canonical correlation patterns that are very similar to those for NDJFM averages (not shown). Estimated cross-correlations for the leading two coupled pairs for time lags from -3 months to $+3$ months are summarized in Tab. 5.1. The cross-correlation functions of the first and second canonical SLP-SST pair are clearly asymmetric. Whereas less than 4% ($r^2 \cdot 100$) of the variance is explained when SST leads SLP, more than 25% of the variance is explained when SLP leads SST by one or two months. Very similar canonical SLP-SST pairs and associated cross-correlation functions were found by Zorita et al. (1992), who analyzed observational *monthly* data from December through February for the period 1950–1986. Thus, in the observations and the coupled model the dominant coupled modes

Table 5.1: Lagged correlation between the first and second monthly (November to March) canonical correlation coefficients of SLP and SST. A lag of -1 indicates that SLP leads by one month.

	SLP-SST						
CCA pair	-3	-2	-1	0	1	2	3
First	+0.45	+0.58	+0.70	+0.52	+0.20	+0.16	+0.13
Second	+0.35	+0.47	+0.61	+0.44	+0.14	+0.10	+0.06
n	598	897	1196	1495	1196	897	598

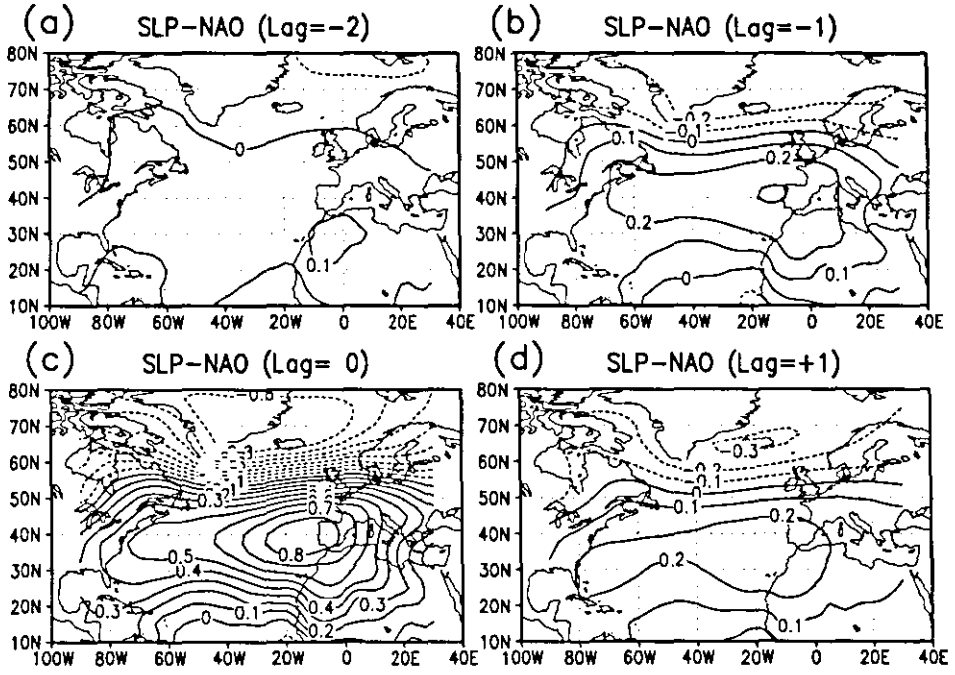

Figure 5.19: Lagged correlations between North Atlantic SLP anomalies and the NAO index from the coupled model. Correlations were computed using monthly data from November through March. The average annual cycle was removed before. A lag of -1 indicates that the NAO leads SLP by 1 month. (a) Lag -2 months, (b) lag -1 months, (c) lag 0 months, and (d) lag $+1$ month. Contour interval is 0.1.

of SLP-SST variability as revealed by CCA are primarily *one-way*, that is, the existence of the canonical SST pattern can be explained by the existence of the SLP pattern and not vice versa.

The structure of the cross-correlation functions described above is based on fixed SLP and SST patterns (the canonical correlation patterns). To further test the hypothesis of a missing feedback between the NAO and North Atlantic SST anomalies in the coupled model, the monthly NAO index (November–March) was correlated with monthly North Atlantic SLP anomalies (Fig. 5.19) and SST anomalies (Fig. 5.20), respectively, for different time lags. The NAO index leads for negative lags. Consistent with the results described in section 5.4, the NAO memorizes about 10% of the month-to-month variance (Fig. 5.19b,d). Note, that this memory does not depend on the sign of the lag, that is, the cross-correlation function between monthly SLP anomalies and the monthly NAO index is symmetric. For longer time lags the NAO signal disappears. In agreement with the results from Tab.5.1, the same analysis applied to North Atlantic SST instead of SLP reveals considerable asymmetry. This asymmetry is associated with the *magnitude* of SST anomalies; the anomalous SST *patterns* do not depend on the sign of the lag (Fig. 5.20). A direct comparison between the associated correlation patterns in Fig. 5.19 and Fig. 5.20 supports the hypothesis that the NAO generates the associated SST pattern (Fig. 5.20c), and this SST pattern does not feed back onto the NAO, neither positively nor negatively. Note that two months after a high NAO month, for example, there is still a very pronounced SST anomaly (Fig. 5.20a); a pronounced NAO anomaly, however, is clearly missing.

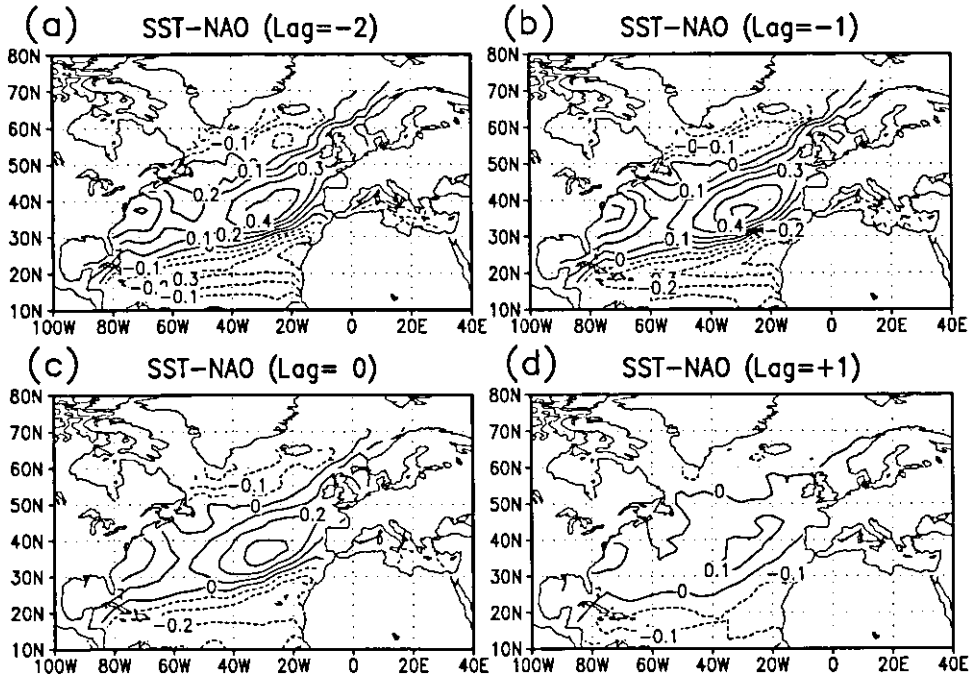

Figure 5.20: Same as in Fig. 5.19, except for North Atlantic SST anomalies and the NAO index.

5.6 NAO and Thermohaline Circulation

In this section variability of the North Atlantic meridional overturning circulation and its relationship to the NAO is investigated by analyzing the ECHAM4/OPYC3 integration. Annual-mean values for the North Atlantic overturing circulation are considered to reduce the impact from wind-driven variability during wintertime.

The first two EOFs and PCs of the anomalous North Atlantic meridional overturning circulation are shown in Fig. 5.21. Linear trends were remove prior to the decomposition. The first (second) mode accounts for 41.5% (15.2%) of the total variance. Although there is some resemblence between the first EOF and the long-term average meridional stream function (see Fig. 5.4), differences show up, especially for the depth of the maximum overturning and the latitude of deep water formation. The magnitude of overturning variability that is associated with the first EOF mode amounts to about 5% of the long-term average meridional overturning. The first EOF and PC were compared with a "THC-index"[26] as used by Delworth et al. (1993) and Timmermann et al. (1998). The temporal correlation between the THC index and the first PC is $r = 0.88$. Thus, the anomalous meridional overturning associated with the THC index resembles the first EOF (not shown). However, since the first EOF mode describes about twice as much of the total meridional overturning variance compared to the THC index the former is used for subsequent analyses.

The second EOF (Fig. 5.21c) involves two centers of action with opposite signs. In contrast to the first EOF, the second EOF is associated with deep water formation in the high-latitude North Atlantic (about 70^oN).

[26]The THC index is defined each year as the maximum stream function value representing the annual-mean meridional circulation.

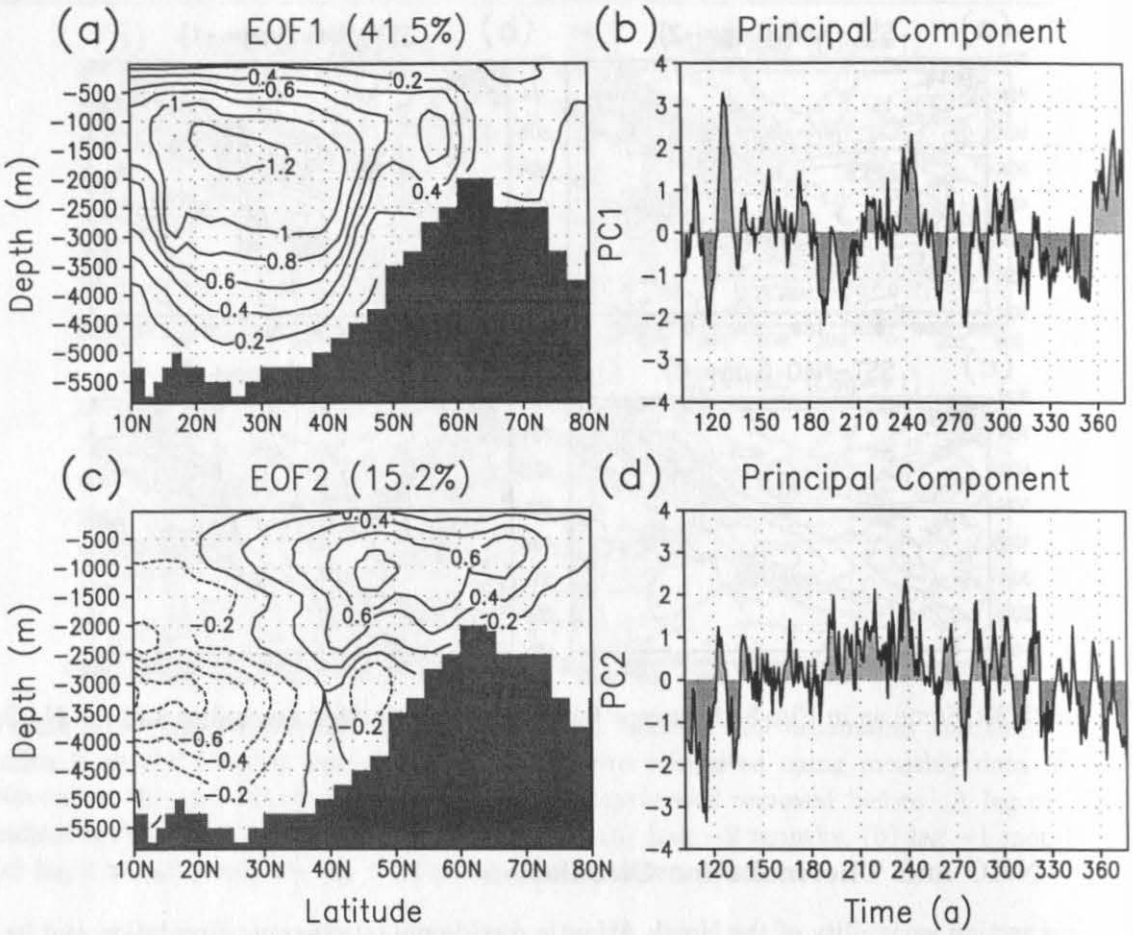

Figure 5.21: First (a) EOF and (b) PC along with the second (c) EOF and (d) PC of anomalous annual-mean North Atlantic meridional stream function from the coupled model. Contour interval is 0.2 Sv in (a) and (c). PCs are normalized to unit variance. Linear trends were removed prior to the analysis. The first (second) EOF explains 41.5% (15.2%) of the total variance. The leading EOFs are well-separated according to the criterion of North et al. (1982).

A prerequisite for a possible forcing of the NAO by the North Atlantic meridional overturning circulation is that oceanic changes leave their imprint on the sea surface. Modelled North Atlantic SST and surface drift anomalies during wintertime, which are associated with the first PC of the anomalous meridional overturing circulation, are shown in Fig. 5.22. In the coupled model, an enhancement of the North Atlantic overturning circulation is associated with positive SST anomalies in the mid-latitude North Atlantic (40^o–60^oN) locally explaining up to 18% of the SST variance (not shown). Largest SST anomalies are located east of Newfoundland, which can be explained by an anomalous northerly surface flow. Note, that in this region interannual SST variability is also most pronounced (Fig. 5.2c). Summarizing, changes in the North Atlantic overturning leave their imprint on the sea surface via SST anomalies. The same analysis was repeated for North Atlantic SLP anomalies (not shown) instead of SST and sea surface drift anomalies.

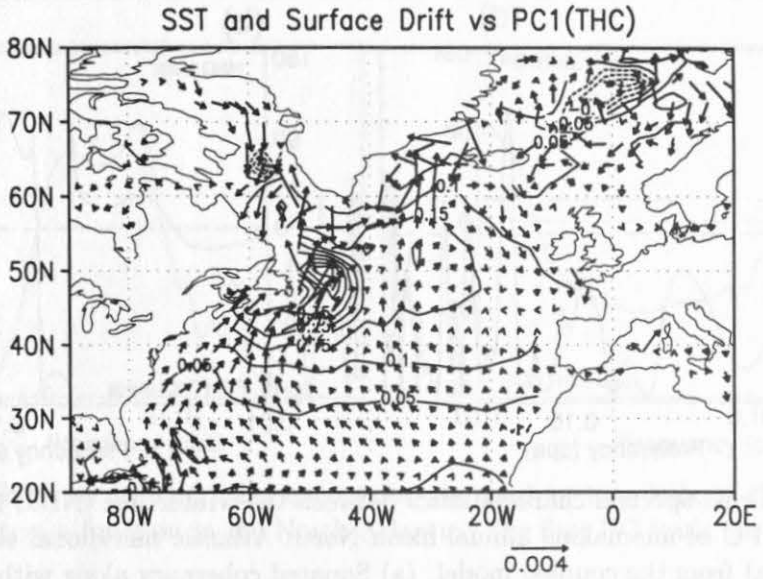

Figure 5.22: Same as in Fig. 5.14a, except for simulated (a) SST and (b) surface drift anomalies (NDJFM) that are associated with the first PC of North Atlantic meridional overturing anomalies. Contour interval is 0.1 K for SST. A reference vector for the surface drift is also given (0.004 m/s).

Associated SLP changes resemble the NAO. However, locally less than 4% of the total SLP variability is explained by this relationship

Variability of the meridional overturing in the high-latitude North Atlantic, as described by the second PC (Fig. 5.21c,d), is also associated with SST and surface drift anomalies (not shown). These anomalies, however, are confined to the northern North Atlantic (north of 60^oN). As for the first PC, no significant atmospheric changes are associated with the second PC (not shown).

The first two PCs show considerable variability on decadal and interdecadal time scales

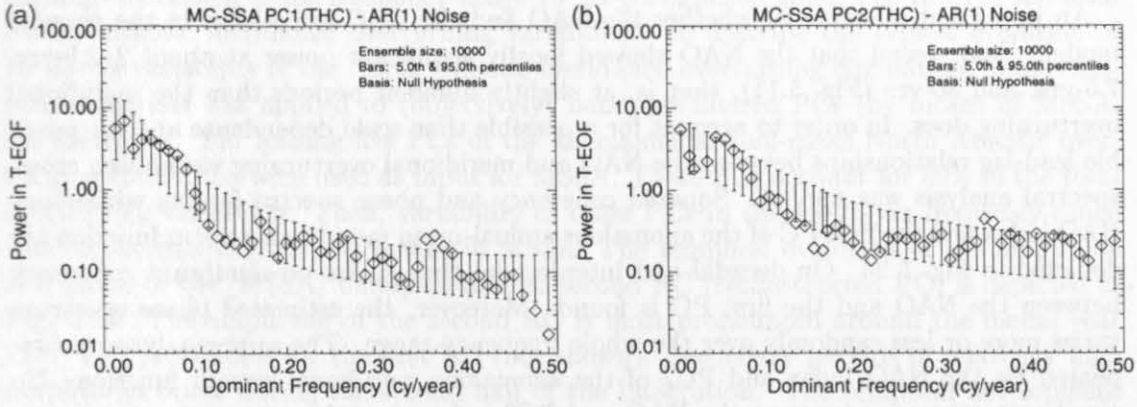

Figure 5.23: Same as in Fig. 5.11, except for the (a) first (Fig. 5.21b) and (b) second (Fig. 5.21d) principal component of the anomalous North Atlantic meridional stream function from the coupled model. A window-length of 50-yrs was used.

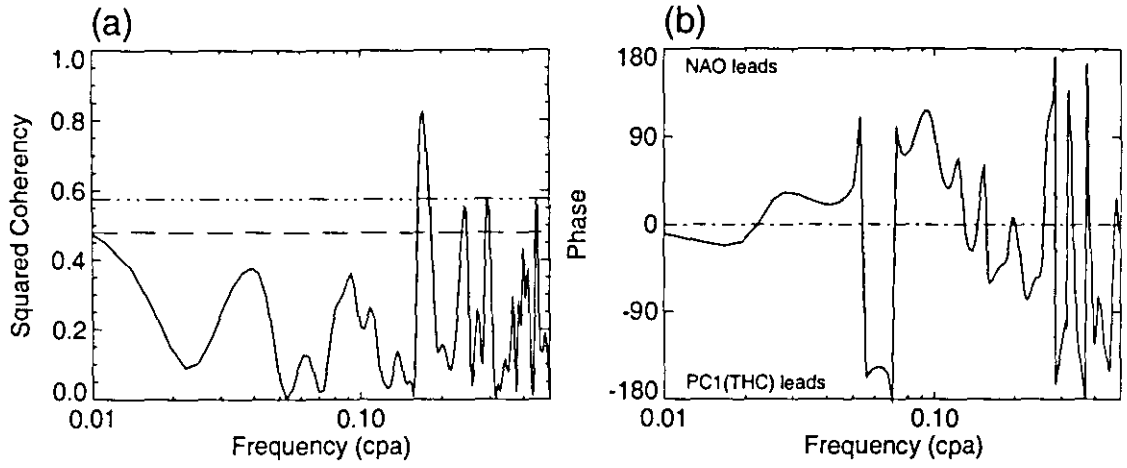

Figure 5.24: Cross-spectral characteristics between the wintertime (NDJFM) NAO index and the first PC of anomalous annual-mean North Atlantic meridional stream function (see Fig. 5.21a) from the coupled model. (a) Squared coherency along with 95% (dashed) and 99% (dash-dotted) confidence levels and (b) phase spectrum. NAO index leads for positive lags. A Tukey-window with a maximum lag of 60-yrs was used for smoothing. Methodological details are given by Jenkins and Watts (1968).

(Fig. 5.21). To test whether there is statistical evidence for the presence of deterministic components in the North Atlantic meridional overturning circulation, Monte Carlo SSA was applied to the first two PCs using a window-width of 50-yrs (Fig. 5.23). For both time series 5 excursions above 95th percentiles occur. The probability for 5 or more excursions (out of 50 possible) to occur just by change is 15% under the global null hypothesis of AR(1) noise. Therefore, variability of the first two PCs is unusual compared to realizations of AR(1) noise at 85% confidence. Both PCs show enhanced power over a relatively broad frequency range from about 10- to 25-yrs. Apart from this frequency-band, locally significant power is evident around 2.5-yrs for both PCs. The second PC shows also significant power on very long time scales (about 300-yrs, compare Fig. 5.21).

An important question is, whether the NAO and the THC are related in the coupled model. First, recall that the NAO showed locally significant power at about 2–2.5-yrs, 7.5-yrs, and 30-yrs (Fig. 5.11), that is, at slightly different periods than the meridional overturning does. In order to account for a possible time scale dependence and for possible lead-lag relationships between the NAO and meridional overturning variability, cross-spectral analysis was applied. Squared coherency and phase spectra for the wintertime NAO index and the first PC of the anomalous annual-mean meridional stream function are depicted in Fig. 5.24. On decadal and interdecadal time scales no significant coherency between the NAO and the first PC is found. Moreover, the estimated phase spectrum varies more or less randomly over the whole frequency-range. The same analysis was repeated for the NAO index and PC2 of the anomalous meridional stream function. No significant coherency between the NAO and PC2 is found; rather, squared coherency is approximately zero on time scales longer than 10-yrs (not shown). Summarizing, in the ECHAM4/OPYC3 model there is no statistical evidence for a significant relationship between the wintertime NAO and the North Atlantic meridional overturning circulation.

As noted above, the first two PCs of the anomalous annual-mean meridional stream-

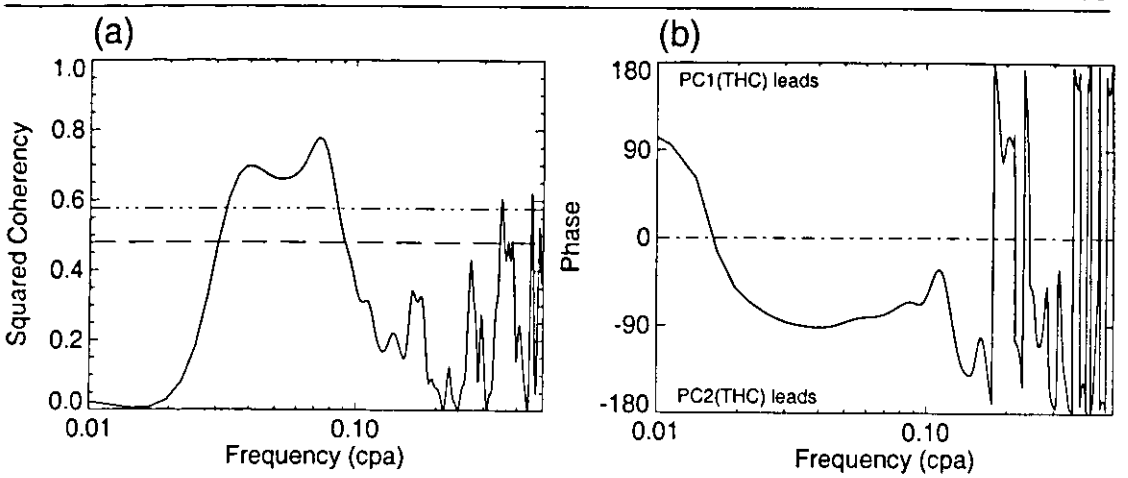

Figure 5.25: Same as in Fig. 5.24, except for the leading two PCs of the anomalous annual-mean stream function in the North Atlantic. The first PC leads for positive lags.

function show enhanced power around 10–25-yrs. Inspection of their temporal evolution (Fig. 5.21b,d) indicates that the second PC leads the first PC by about 90°. This relationship between the first two PCs is quantified in Fig. 5.25 showing their squared coherency and phase spectra. Over the frequency-band from about 15- to 25-yrs significant coherency (at 99% confidence) between the two time series is found. The phase-spectrum reveals that the second PC leads the first PC by about 90°. Note, that this 90° out-of-phase variability is consistent with the orthogonality constraint required for different PCs. Hence, the results from the above analyses suggest that an oscillatory mode (with propagative/advective characteristics) of the North Atlantic meridional streamfunction is present in the coupled model. This mode is most dominant in the frequency-range from 15- to 25-yrs. Moreover, the NAO seems not to be directly involved[27].

Monte Carlo MSSA (see Methods) was applied in order to evaluate the unusualness of this mode. The resulting eigenvalue spectrum (not shown) and its significance is quite similar to those for the first two PCs (Fig. 5.23). Variability of the North Atlantic overturning circulation in the frequency-range 15–25-yrs explains about one third of the total North Atlantic meridional overturning variability. To describe the typical evolution of 15–25-yrs variability of the North Atlantic meridional overturning circulation, phase composite analysis was applied to (objectively) bandpass-filtered PCs (by means of MSSA, see Methods). The leading five PCs of the anomalous annual-mean North Atlantic overturning circulation were used as input for MSSA. These PCs account for 80% of the total overturning variability. Then, variability of these PCs in the 15–25-yrs frequency-range was reconstructed (RCs) by means of MSSA. The temporal evolution of the amplitude and phase of the (MSSA) bandpass-filtered second RC (reconstructed PC) is depicted in Fig. 5.26. The amplitude of the second RC is most pronounced around the model year 120. The same holds for the first RC (not shown). Secondary periods of relatively high amplitudes occur during the second half of the integration. The temporal development of the phase (Fig. 5.26b) is relatively stable during high-amplitude periods, and suggests that the bulk of the variability occurs at periods of about 18-yrs (see also Fig. 5.23b).

The amplitude and phase time series of the second RC, obtained by MSSA, were used

[27]The NAO *could* be necessary to stochastically excite a damped internal oceanic mode.

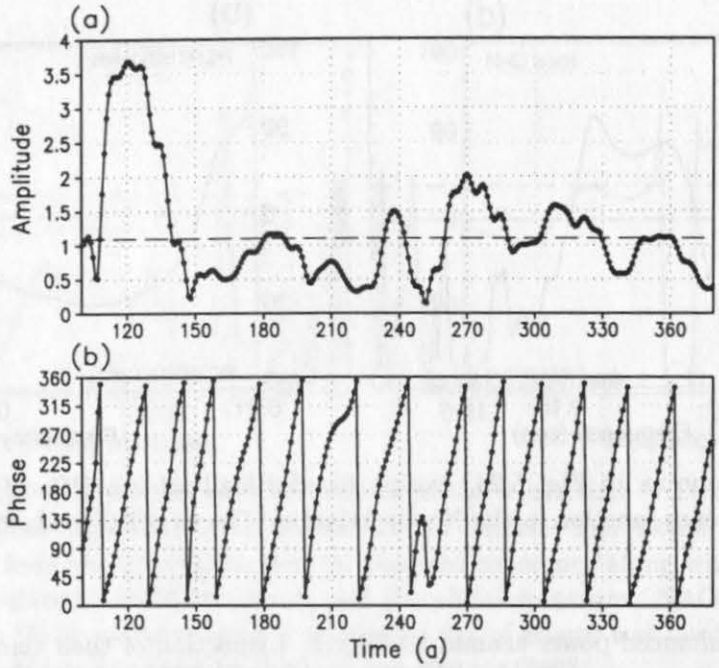

Figure 5.26: (a) Amplitude and (b) phase of the reconstructed second PC (RC) describing variability of the North Atlantic meridional overturning circulation in the frequency-range 15–25-yrs from the coupled model. For the reconstruction of the second RC, all eigenvalues obtained by MSSA in the frequency-range 15–25-yrs were used. See chapter Methods for further details.

to construct phase composites (see Methods) of the anomalous North Atlantic meridional overturning circulation. Only those years with amplitudes exceeding 1.1 (Fig. 5.26a, dashed line) were used for compositing. This threshold was subjectively chosen. However, the conclusions are not sensitive against small changes in this threshold. The "typical" development of the oscillation through the first half of the cycle is depicted in Fig. 5.27. During its mature stage (Fig. 5.27a) the whole North Atlantic meridional overturing is strengthened. Deep water formation takes place in two regions, that is, in the mid-latitude (40^o–50^oN) and high-latitude (70^o–80^oN) North Atlantic. About 2.5-yrs later (Fig. 5.27b) deep water formation in the high-latitude North Atlantic has stopped. The meridional overturning is confined to the North Atlantic ocean south of about 50^oN. About 5-yrs after the meridional overturning circulation was in its mature stage (Fig. 5.27c) a cell of counterclockwise circulation has formed in the northern North Atlantic (35^o–75^oN). This anomalous circulation is presumably associated with anomalously weak convection in the GIN Seas. At this stage the clockwise circulation anomaly has weakened at higher levels in the subtropical North Atlantic. About 2.5-yrs years later (Fig. 5.27d) the meridional overturning circulation is almost reversed compared to the initial anomaly 7.5-yrs earlier. At this stage anomalously less deep water is produced in the high-latitude and mid-latitude North Atlantic. After additional 2.5-yrs the anomalous meridional overturning circulation equals that depicted in Fig. 5.27a, except for opposite signs.

Summarizing, changes in the strength of the anomalous meridional overturning circulation appear to originate in the high-latitude North Atlantic. From there the signal

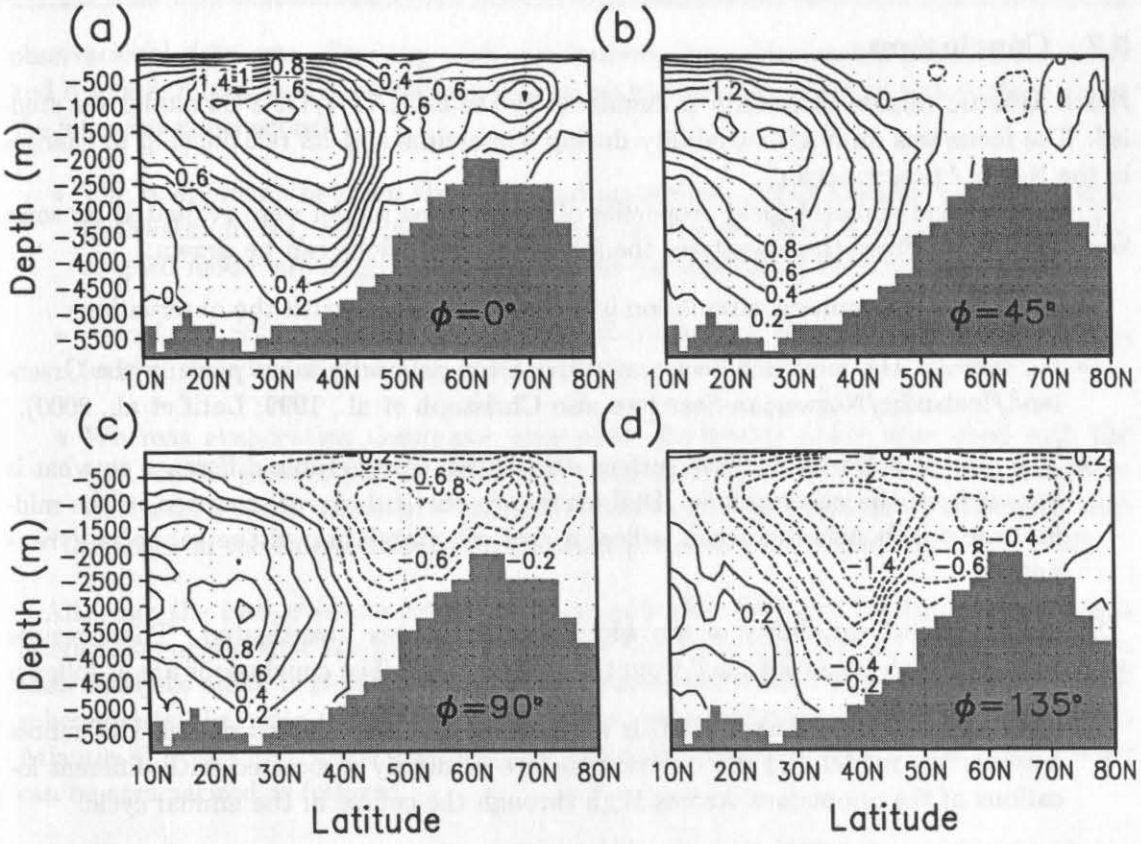

Figure 5.27: Typical evolution of the anomalous North Atlantic meridional overturning circulation (Sv) through the first half of its low-frequency (15–25-yrs) cycle: (a) 0^o–45^o, (b) 45^o–90^o, (c) 90^o–135^o, (d) 135^o–180^o. The temporal difference between (a) and (b) is about 2.5-yrs. Overturning data were composited into different phase-sectors using amplitude and phase information shown in Fig. 5.26. Compositing was only done for those years with amplitudes exceeding 1.1. Anomalies falling into the sector 180^o–225^o were composited into the sector 0^o–45^o using opposite signs. Other sectors were treated similarly. Details are given in chapter Methods.

subsequently spreads southward changing the anomalous North Atlantic overturning circulation after about 7.5–10-yrs. Thus, one might speculate that in this coupled model anomalous convection in the GIN Seas plays a crucial role for the overturing variability in the North Atlantic basin. The picture is complicated, however, by the fact that another center of deep water formations is involved, that is, the mid-latitude North Atlantic. Here, we do not want to go into too much detail[28] about the physics of this mode, since the focus of the present study is on the relationship between the NAO and the THC described above. However, it is worth mentioning that the characteristic time scale of about 15–25-yrs is suggestive for advective processes to be of importance. Moreover, prelimnary analyses indicate that variability of the Arctic sea ice cover is involved.

[28]We also cannot go into too much detail about the physics of these circulation changes. This is because some of the key-parameters (e.g., convective depth and surface density) from the coupled model are currently not available to the author. An in-depth analysis of this mode is part of an ongoing study.

5.7 Conclusions

North Atlantic climate variability as simulated by the ECHAM4/OPYC3 model was studied. The focus was on NAO variability during wintertime and its relationship to changes in the North Atlantic ocean.

First, modelled climatological properties of the coupled model were evaluated for some key-parameters. From these analyses the following conclusions can be drawn:

- The mean atmospheric circulation is in good agreement with the observations.
- On average, the modelled deep water formation primarily takes place in the Greenland/Icelandic/Norwegian Seas (see also Christoph et al., 1999; Latif et al., 2000).
- The modelled North Atlantic surface drift shows considerable difference to what is known from the observations. Differences are particularly pronounced in the mid-latitude North Atlantic ocean, where a cyclonic circulation of the subpolar gyre is missing.

Second, modelled variability of the wintertime NAO was investigated. These results were compared with those obtained from the observations. The conclusions are as follows:

- Seasonality of the observed NAO is well-captured by the coupled model. Differences between the model and the observations are primarily associated with different locations of the anomalous Azores High through the course of the annual cycle.
- EOF analysis of normalized anomalous annual cycles of the modelled NAO reveals intraseasonal coherence from November through March, suggesting some month-to-month memory of the NAO (about 10–15%).
- The modelled NAO shows teleconnections with the North Pacific (Aleutian Low), a characteristic, which is reminiscent of the Arctic Oscillation.
- The estimated probability density function of the modelled wintertime NAO (ND-JFM) is negatively skewed. Hence, high NAO winters tend to be less extreme than low NAO winters. Moreover, intraseasonal variance is more than two time smaller for high NAO winters compared low NAO winters.
- The spectrum of the modelled wintertime NAO index is approximately white. Locally significant excursions above the 92.5% confidence level occur around 2–2.5-yrs, 7.5-yrs, and 30-yrs (see also Christoph et al., 1999). Without *a priori* expectations about the appearence of these peaks the simulated NAO index is unusual compared to realizations of AR(1) noise at 77% confidence.
- Wavelet analysis applied to the modelled wintertime NAO index reveals that changes in the "redness" of the NAO's spectral characteristics are not part of the model's natural variability.
- No significant winter-to-winter persistence of the NAO is found in the coupled model. This is consistent with the white background spectrum of the modelled NAO.

Third, the relationship between the simulated NAO and North Atlantic air-sea interaction was studied. Results from these analyses were compared with those obtained from

observational data sets. Starting with the *instantaneous* relationship between the NAO and North Atlantic air-sea interaction during wintertime the results of this study support the following conclusions:

- The relationship between the NAO and anomalous North Atlantic net heat fluxes, freshwater fluxes, and momentum fluxes at the sea surface as simulated by the coupled model are in good agreement with corresponding observational estimates.

- Associated SST anomalies in the coupled model can primarily be explained by a local surface flux forcing through the NAO.

- Whereas evaporation dominates anomalous freshwater fluxes associated with the NAO in the western part of the North Atlantic, precipitation anomalies dominate in the eastern North Atlantic. Precipitation anomalies are presumably associated with changes in the North Atlantic storm track (see also Hurrell and van Loon, 1997).

Although the instantaneous relationship between the NAO and North Atlantic air-sea interaction suggest that the bulk of air-sea flux variability is governed by the NAO, from these analyses alone it is difficult to decide whether an oceanic feedback onto the atmosphere exists. In order to address this question, lag-correlation analyses between North Atlantic SLP and SST fields from the coupled model were performed. The main results can be summarized as follows:

- Canonical correlation analysis (CCA) reveals that the NAO is associated with the dominant (instantanous) coupled mode of interannual North Atlantic SLP-SST variability (NDJFM). CCA, applied to SLP and SST anomalies for the winter months from November through March yields essentially the same reults.

- Lag-correlation analyses of the canonical correlation coefficients show that the coupling between the NAO and the canonical SST pattern is primarily one-way: Changes of the NAO force SST anomalies, but there is no pronounced forcing of the NAO by these SST anomalies.

Finally, variability of the North Atlantic meridional overturning circulation and its link to the NAO was studied using the coupled model. The results support the following conclusions:

- Natural variability of the modelled North Atlantic meridional overturning circulation amounts to about 5% of the long-term mean value.

- An enhancement of the North Atlantic meridional overturning circulation is associated with SST anomalies in the mid-latitude North Atlantic.

- Cross-spectral analysis reveals that in this model an anomalous basin-wide enhancement of the overturning circulation is not associated with significant changes of the NAO. This holds for different time scales and time lags.

- There is evidence for an oscillatory mode of the overturning circulation in the frequency-range 15–25-yrs. The physics of this mode, however, remain unclear.

5.8 Discussion

North Atlantic climate variability as simulated by the ECHAM4/OPYC3 model is investigated. The focus is on simulated characteristics of the North Atlantic Oscillation and its interaction with the North Atlantic ocean.

From the results presented in this chapter there is little indication for a two-way interaction between the modelled NAO and the North Atlantic ocean. Rather, the results support the notion that, in the ECHAM4/OPYC3 model, wintertime variability of the NAO is primarily governed by internal atmospheric dynamics (see also Christoph et al., 1999). Locally, the NAO generates North Atlantic SST anomalies through associated changes in the surface net heat fluxes and momentum fluxes (mixing). There is little statistical evidence that these SST anomalies feed back onto the atmosphere. This view is consistent with other modelling (e.g., Delworth, 1996; Christoph et al., 1999) and observational (e.g., Zorita et al., 1992) studies. On the other hand, Rodwell et al. (1999) show that about 50% of the observed low-frequency NAO variability (>6.5-yrs) can be explained by the modelled NAO, averaged over five ensemble integrations of the atmospheric general circulation model HadAM2, if observed SST and sea ice fields for the period 1947–1997 are prescribed as lower boundary conditions. The lag-correlation analysis between the NAO and North Atlantic SST anomalies described in this chapter are conceptionally similar to the experiments performed by Rodwell et al. (1999). Notice, however, that the lag-correlation analyses presented in this study focus on the high-frequency part of the spectrum. Two months after a high NAO winter month, for instance, on average pronounced SST anomalies are located in the North Atlantic (Fig. 5.20a), which resemble the SST pattern that influenced the NAO in the HadAM2 model (Rodwell et al., 1999). In the ECHAM4/OPYC3 model and the observations (Zorita et al., 1992), however, there is no average response of the monthly NAO to such a SST forcing (Fig. 5.19a). Missing winter-to-winter persistence of the simulated NAO along with rather weak statistical evidence (77% confidence) against the red noise null hypothesis yield additional evidence against a noteworthy external forcing of the winter NAO in the ECHAM4/OPYC3 model. Note, however, that SST anomalies in the tropical Pacific are negatively correlated ($r = -0.3$) with the wintertime NAO in the coupled model suggesting a weak (10% of the variance) forcing from outside the North Atlantic region.

No pronounced link between the NAO and the North Atlantic meridional overturning circulation was found in the ECHAM4/OPYC3 model (except for a barotropic oceanic response). This finding holds for different time scales and different time lags. Note, that such a link was found in different CGCMs (Delworth and Greatbatch, 2000; Timmermann et al., 1998) and in the OGCM experiment with a realistic forcing by the NAO over the period 1865–1997 (see chapter 4). Christoph et al. (1999) speculate that a missing link in the ECHAM4/OPYC3 model results from the NAO's capability to influence the thermohaline circulation by two inversely operating mechanisms: A high NAO, for example, (i) forces the advection of denser water into the sinking region south of Greenland, and (ii) reduces the near surface density in the GIN Seas locally through an excess of precipitation over evaporation. It remains unclear, however, how strong these mechanisms change the near-surface density and, thus, vertical stratification in the respective regions. Since the response of the surface heat, freshwater, and momentum fluxes to a forcing by the NAO is realistically simulated in the ECHAM4/OPYC3 (Fig. 5.14), the cause for a missing link between the NAO and North Atlantic THC should be associated with the

ocean component of the coupled model.

From the results of this study there is some indication for the existence of an internal mode of North Atlantic overturning variability with preferred time scales of about 15–25-yrs. This mode explains almost 30% of the total North Atlantic meridional overturning variability. The physics that are involved in this mode along with the relative contribution of the NAO in forcing density anomalies in the sinking regions will be addressed in a forthcoming study[29].

When considering North Atlantic climate variability in the ECHAM4/OPYC3 model it has to be kept in mind that the simulated mean North Atlantc circulation shows considerable differences compared to what is known from the observations. These differences are most pronounced in the subpolar North Atlantic where the net surface heat flux forcing by the NAO is also most pronounced. Thus, it cannot be excluded that differences in the mean state of the modelled ocean have profound impacts onto its variability. Nevertheless, variability of the NAO seems to be well simulated by the coupled model.

[29] For the analyses performed in this study only subset of the OPYC3 data was available.

6 Link Between NAO and Arctic Sea Ice Export

6.1 Introduction

Sea ice volume flux out of the Arctic through Fram Strait represents a major source of freshwater for the subpolar North Atlantic (Aagaard and Carmack, 1989). Since melting sea ice of Arctic origin releases freshwater in high latitudes where the density of sea water is sensitive to salinity perturbations, temporal changes of the ice volume flux through Fram Strait may be of importance for the oceanic circulation in subpolar regions.

Recent observational studies indicate a high positive correlation between the NAO and Arctic sea ice export through Fram Strait during the last two decades. Using a 18-year record of passive microwave satellite data, Kwok and Rothrock (1999) found a positive correlation ($r = 0.66$) between the NAO and ice area flux through Fram Strait during wintertime (DJFM). This finding is in agreement with the results by Dickson et al. (2000) who report about a positive correlation between the NAO index and parameterized[30] ice volume flux through Fram Strait during wintertime ($r = 0.77$ from 1976 to 1996). Note, that these estimates are based on fixed values for the ice thickness in Fram Strait. Summarizing, the results by Kwok and Rothrock (1999) and Dickson et al. (2000) support the following conclusion (CLIVAR, 1998):

> *... the NAO appears to exert a significant control on the export of ice and freshwater from the Arctic to the open Atlantic, which with other more localised effects further south, are thought to promote significant changes in the "headwaters" of the global thermohaline circulation.*

Using a sea ice model integration with a realistic atmospheric forcing over the last four decades, Hilmer et al. (1998) (HHL98, hereafter) showed that the atmosphere is the primary driver of ice volume flux variability through Fram Strait: Annual-mean sea level pressure (SLP) anomalies in the Barents and Kara Seas region are associated with meridional wind anomalies near Fram Strait giving rise to ice volume flux anomalies. Since this anomalous SLP pattern shows little resemblence with the NAO pattern, the observational results by Kwok and Rothrock (1999) and Dickson et al. (2000) seem controverse to the modelling results by HHL98.

Subsequently, the link between the NAO and the ice volume flux through Fram Strait is revisited. For this purpose a realistic hindcast simulation of the Arctic sea ice cover over the last four decades is investigated[31] along with century-scale integrations of a coupled general circulation model under present-day climate conditions and increasing greenhouse gas concentrations. The analyses focus on the winter season (DJFM) when interannual variability of the NAO and Arctic sea ice export is most pronounced.

6.2 Data

The Kiel Sea Ice Simulation System (KISS), an optimized dynamic-thermodynamic sea ice model with viscous-plastic rheology (Harder et al., 1998; Hilmer et al., 1998, and references therein), is used in this study. The model domain spans the entire Arctic extending southward to about $55^{o}N$ in the North Atlantic region (see HHL98, their Fig. 1). The horizontal

[30] SLP gradient along Fram Strait times a fixed value for ice thickness in Fram Strait.

[31] The results from these analyses are based on collaboration with Michael Hilmer (see Hilmer and Jung, 2000).

resolution is $1^o \times 1^o$. The thickness of sea ice and snow along with the ice concentration are prognostic variables. Sea ice drift components are determined diagnostically. The sea ice model is forced with daily fields of near-surface (2 m) air temperature and near-surface (10 m) wind fields over the last four decades (1958–1997). Both forcing fields were derived from the National Center for Environmental Predicition/National Center for Atmospheric Research (NCEP/NCAR) reanalysis (Kalnay et al., 1996). All other forcing fields were prescribed as climatological annual cycles. Thus, simulated sea ice variability is solely forced by atmospheric variability. Details about this integration are given by HHL98.

SLP fields from the NCEP/NCAR reanalysis (1958–1997) and from an updated version of historical analyses for the period 1899–1997 (Trenberth and Paolino, 1980) are used to investigate the link between the NAO index, the modelled ice volume flux through Fram Strait, and the atmospheric circulation. Here, the NAO index is defined as the difference between normalized SLP time series from the Azores and Iceland (Rogers, 1984).

To study the long-term characteristics of the relationship between the NAO and the ice volume flux through Fram Strait along with possible changes under enhanced greenhouse gas concentrations, two century-scale integrations of the coupled general circulation model ECHAM4/OPYC3 are used. The first integration is a control experiment (300-yrs) under present-day conditions (Roeckner et al., 1996; Christoph et al., 1999). The second integration is from a transient experiment under increasing greenhouse gas concentrations for the period 1860–2099 (Roeckner et al., 1999; Ulbrich and Christoph, 1999; Paeth et al., 1999). The anthropogenic greenhouse gas forcing is prescribed using observations for the period 1860–1990. Thereafter, the IPCC scenario IS92a is used (Houghton et al., 1996). The effects from ozone and sulfate aerosols are not taken into account. The atmospheric component ECHAM4 is the fourth generation of a hierarchy of models that was developed at the MPI Hamburg from the former European Center for Medium Range Weather Forecast (ECMWF) model (Roeckner et al., 1992, 1996). ECHAM4 has a horizontal resolution of T42 (approx. 2.8^o by 2.8^o) and 19 hybrid levels in the vertical. OPYC3 is a three-component model including an isopycnial interior ocean, a mixed-layer component, and a dynamic-thermodynamic sea ice model that represents internal stresses by a viscous-plastic rheology (Oberhuber, 1993b,a). In contrast to KISS, zonal and meridional ice flux components are formulated as prognostics variables. An annual mean flux correction scheme has been applied. Further details are given by Roeckner et al. (1996).

The ice volume flux through Fram Strait (IVF) is calculated for a zonal (coupled model) and an almost zonal (KISS) section, respectively, connecting the northern tip of Greenland with the northern tip of Spitzbergen according to (see, e.g., Harder et al., 1998):

$$IVF = \int_{\Gamma} v(r)h(r)dr, \tag{6.1}$$

where r denotes the position along the section Γ, $v(r)$ is the ice drift perpendicular to this section, and $h(r)$ is the ice thickness along Γ. Furthermore, the southward drift speed through Fram Strait (SDS, hereafter) and the ice thickness in Fram Strait (h, hereafter) are determined by averaging over all grid points along Γ.

6.3 Observed NAO and Modelled Sea Ice

Winter time series of the modelled sea ice export through Fram Strait as well as SDS and h in Fram Strait are depicted in Fig. 6.1 together with the observed NAO index. Visual

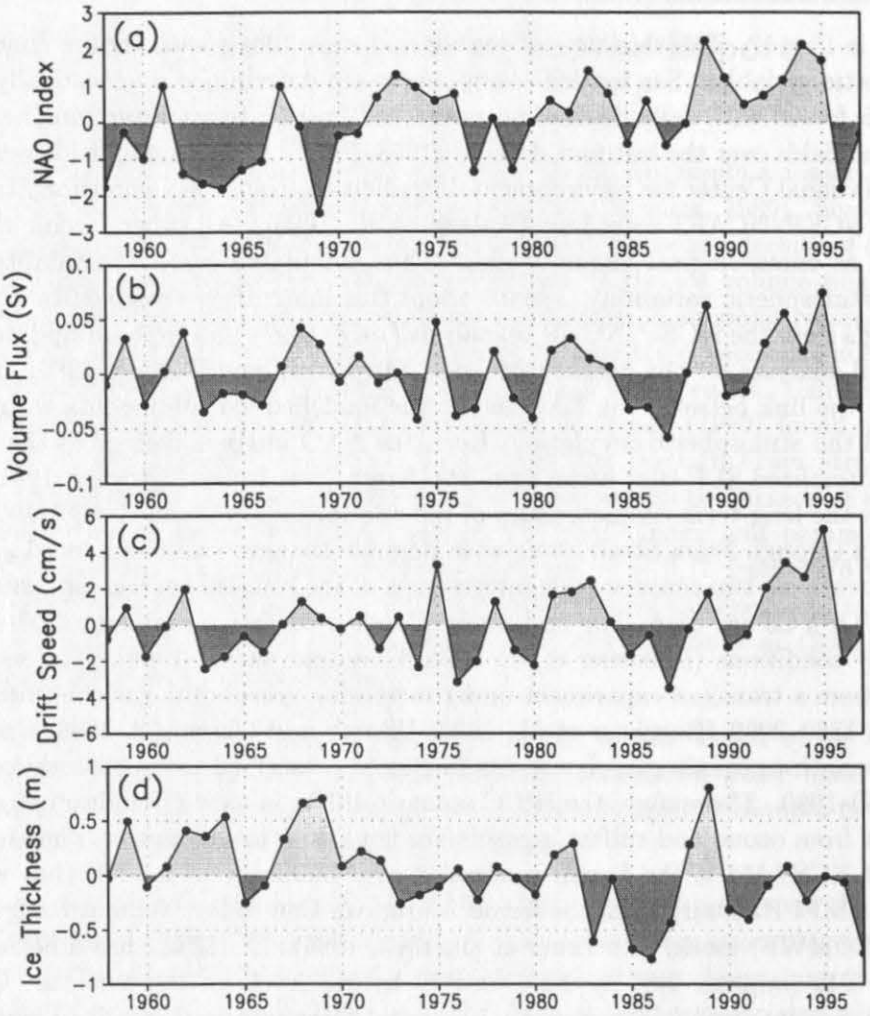

Figure 6.1: Winter time series (DJFM) of the observed NAO index and anomalies of simulated sea ice quantities in Fram Strait (KISS) for the period 1958–1997: (a) observed NAO index and modelled (b) ice volume export (Sv), (c) sea ice drift speed (cm/s), (d) sea ice thickness (m).

inspection of the modelled sea ice time series suggests that primarily SDS contributes to variability of the ice volume flux through Fram Strait. This relationship is quantified in Tab. 6.1 summarzing the results from a correlation analysis. Whereas SDS explains more than 80% of the variance ($r^2 \cdot 100$) of the ice volume flux through Fram Strait, the contribution from interannual variability of h is much less pronounced (25%). No significant correlation between SDS and h is found. Note, that these results are stable with respect to different subperiods. Moreover, Fig. 6.1 reveals the different character of years with high ice exports through Fram Strait. In the mean, SDS dominates the ice volume flux variability but there exist exceptions like in 1968 and 1969. The simulated *ice area* flux through Fram Strait (not shown, see Hilmer and Jung, 2000, their Fig. 1) is in very good agreement ($r = 0.88$) with satellite-based estimates from Kwok and Rothrock (1999) during the overlapping period 1978–1996.

In agreement with observational estimates (Kwok and Rothrock, 1999; Dickson et al., 2000), the observed NAO index is significantly positive correlated with the simulated ice volume flux through Fram Strait ($r = 0.7$) during the winters 1978–1997 (P2, hereafter). The moderate correlation between the two time series for the whole period ($r = 0.4$, 1958–1997) can be explained by a missing link ($r = 0.1$) during the period 1958–1977 (P1, hereafter)(Fig. 6.1 and Tab. 6.1). Primarily changes in the correlation between the NAO index and SDS are responsible for these changes (Tab. 6.1). Since SDS variability is primarily governed by atmospheric variability (wind forcing), one might speculate that atmospheric changes from P1 to P2 were involved.

So far, the whole time series was separated into P1 and P2 to allow for a direct comparison between sea ice estimates from the model integration (this study) and those obtained from observational data sets (Kwok and Rothrock, 1999; Dickson et al., 2000), the latter which are confined to the last two decades (P2). To shed further light onto the time-dependent characteristics of the link between the NAO and Arctic sea ice export, wavelet co-spectra were estimated (Fig. 6.2). Wavelet co-spectra allow to analyze the time-dependency of *in-phase* and *out-of-phase* covariability between two time series in a data-adaptive manner (see Methods). In-phase variability between the NAO index and Arctic sea ice export through Fram Strait increased markedly after the late 1970s (Fig. 6.2). The same analysis was repeated using Paul wavelets (not shown), which allow for a higher (lower) resolution in the time (frequency) domain compared to Morlet wavelets (Torrence and Compo, 1998). Since the gross features of the local wavelet co-spectra are not very sensitive with respect to the choice of the mother-wavelet and, therefore, side effects, the results from the wavelet analysis yield additional support that the separation of the whole time series into P1 and P2 is a good compromise between the length of the time series and the detection of the signal (increased in-phase variability).

Anomalous SLP patterns that are associated with (i) anomalous ice volume exports through Fram Strait ("Fram pattern", hereafter) for the period 1958–1997 and (ii) NAO winters for the two subperiods P1 and P2 are shown in Fig. 6.3. The Fram pattern (Fig. 6.3c) is characterized by anomalously low SLP in the Barents Sea leading to anomalous southerly winds near Fram Strait and, therefore, to a high ice volume export. The gross features of this pattern are very similar to those obtained from *annual-mean* data (Hilmer et al., 1998, their Fig. 5). During P1 the primary center of the NAO's northern cell was located near the southern tip of Greenland (Fig. 6.3a). No anomalous southerly wind component was present near Fram Strait that may have affected SDS and, thus, the

Table 6.1: Linear correlations for winter averages (DJFM) of the observed NAO index and the simulated ice volume flux (IVF) through Fram Strait, southward drift speed (SDS) and ice thickness (h) in Fram Strait (KISS) for different periods (1958–1977/1978–1997/1958–1997). Non-zero correlations at the 95% confidence level are bold (two-sided t-test taking serial correlation into account).

	IVF	SDS	h
NAO	0.06/**0.70**/**0.40**	0.12/**0.72**/**0.49**	-0.10/0.24/-0.16
SDS	**0.95**/**0.93**/**0.93**	**1.0**/**1.0**/**1.0**	0.27/0.37/0.21
h	**0.52**/**0.64**/**0.52**	0.27/0.37/0.21	**1.0**/**1.0**/**1.0**

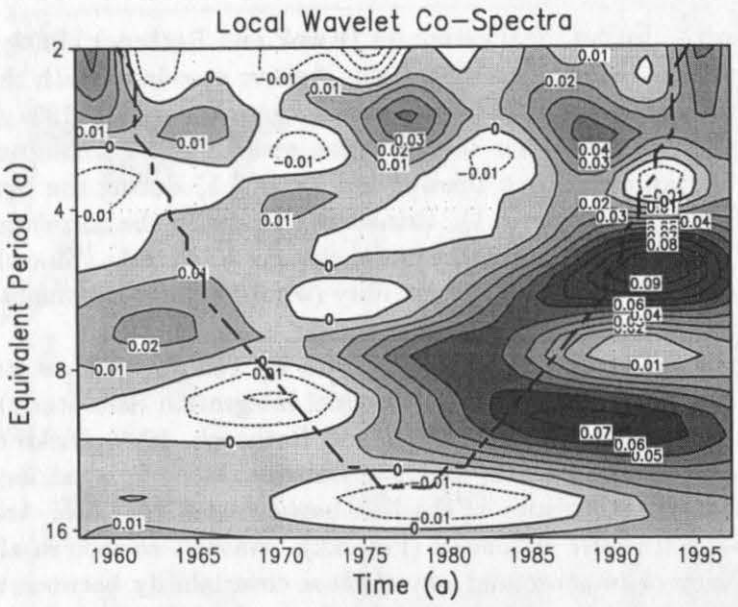

Figure 6.2: Local wavelet co-spectra (Sv) for winter averages (DJFM) of the observed NAO index and simulated ice export through Fram Strait (KISS). The wavelet co-spectra are based on Morlet wavelets calculated as decribed in Torrence and Compo (1998). The co-spectra give the local strength of in-phase (0^o, positive values) and out-of-phase (180^o, negative values) variability between the two time series in the plane of equivalent period ($\approx$ period) versus time. Estimates within the cone of influence (dashed) are influenced by side-effects.

ice volume export. Interannual NAO variability intensified in the Scandinavian region and over the Iberian Peninsula during P2, whereas SLP anomalies decreased further westward (Fig. 6.3b). This eastward shift of the NAO-related SLP variability led to pronounced anomalous meridional wind components between Greenland and Spitzbergen during P2 and, therefore, to in-phase variability between the NAO index and ice volume flux through Fram Strait on interannual time scales (Fig. 6.2, Tab. 6.1). The eastward displacement of the NAO's centers of interannual variability from P1 to P2 is not an artifact due to sampling problems over the Arctic. Rather, largest differences between the SLP patterns occur close to Scandinavia and Greenland (Fig. 6.3d), that is, over relatively well-sampled areas.

The eastward displacement of interannual NAO variability was also accompanied by changes in meridional wind components near Davis Strait and Denmark Strait (Fig. 6.3) and, thus, corresponding anomalous ice volume exports: The time-dependence of the link between the NAO and ice export through Denmark Strait ($r = 0.01$ for P1 and $r = 0.69$ for P2) is similar to those for the ice volume export through Fram Strait. In contrast, the correlation between the NAO and ice export through Davis Strait was higher during P1 ($r = 0.63$) compared to P2 ($r = 0.13$).

The results from the regression analyses show that the NAO's centers of interannual variability have moved towards the east during the last two decades. Since the NAO index is defined at fixed locations, it is natural to ask whether secular changes of interannual atmospheric variability during the last four decades are most efficiently described using

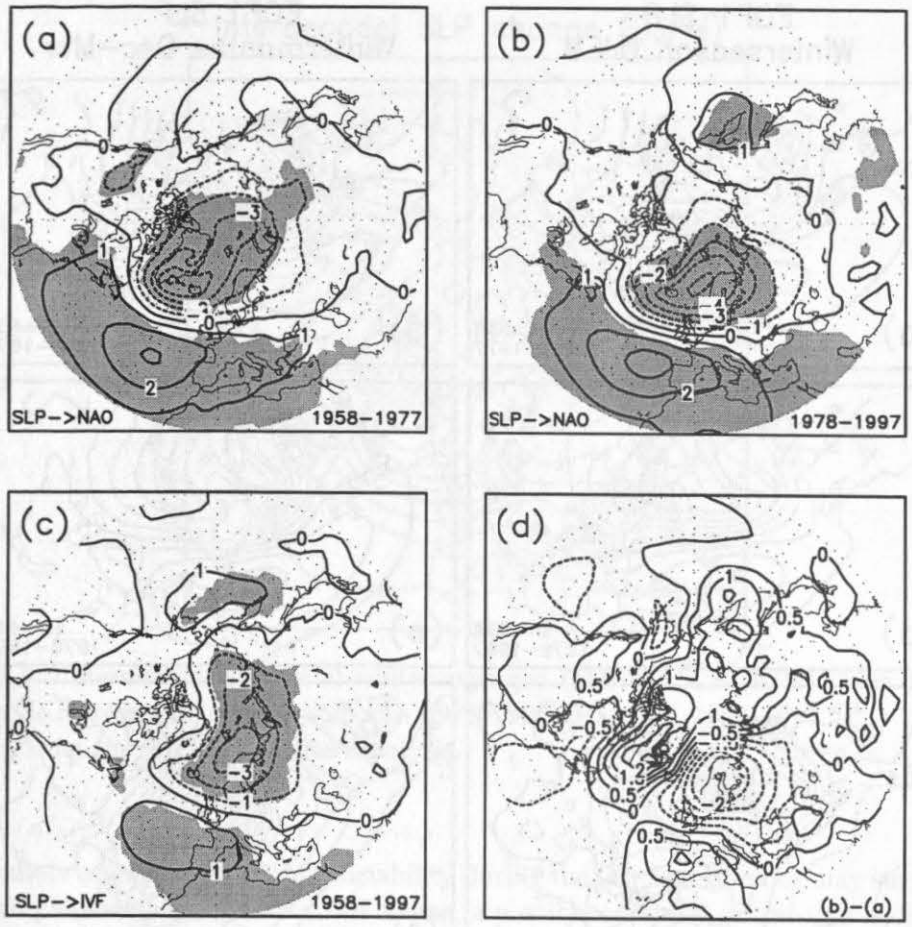

Figure 6.3: SLP anomalies (hPa) associated with the NAO index during (a) 1958–1977 and (b) 1978–1997 and wintertime (DJFM). (c), same as in (a) and (b), except for the modelled ice volume flux through Fram Strait over the full period 1958–1997. Anomalous SLP fields were regressed onto the normalized time series. Statistically significant slope parameters (95% confidence level) are shaded. Contour interval is 1 hPa. (d), difference of the NAO-related anomalous SLP fields, (b) minus (a), between the periods 1978–1997 and 1958–1977. Contour interval is 0.5 hPa. Linear trends were removed prior to the analyses. Since the standard deviations of the NAO indices for P1 and P2 are equal, the patterns in (a) and (b) can be directly compared.

the NAO index. To answer this question, EOF analysis was applied to anomalous monthly (December through March) and winter-averaged (DJFM) SLP fields for the periods P1 and P2. The gross features of the recent shift of interannual NAO variability (Fig. 6.3) are well-captured by the dominant EOFs (Fig. 6.4). The EOF patterns for winter-averaged data, however, are somewhat less biased towards the NAO's centers of variability (Iceland and the Azores) than the regression patterns are. Note, that the first EOF of winter-averaged SLP anomalies for P2 resembles the Fram pattern (Fig. 6.3c and Fig. 6.4b). For monthly data the agreement with the results from the regression analyses is relatively good, especially in high-latitudes and east of about 30^oW. This similarity suggests that

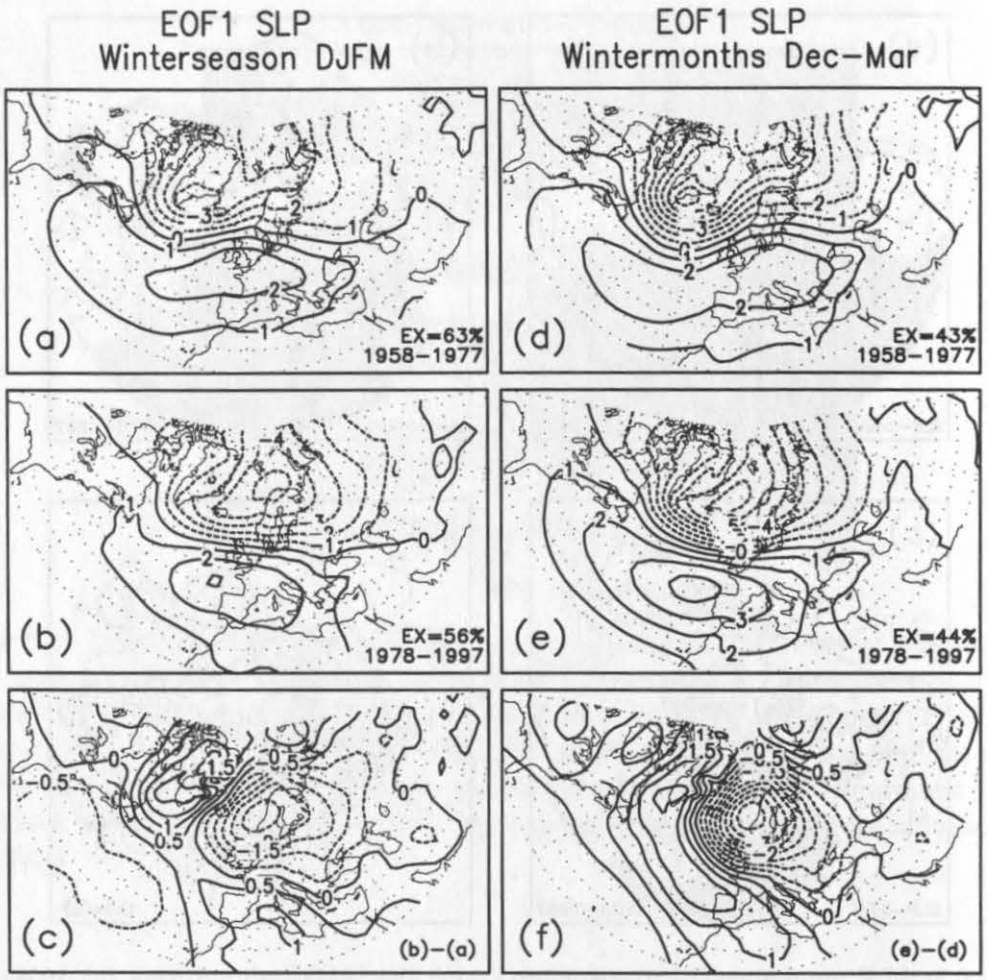

Figure 6.4: Leading EOFs (hPa) of winter-averaged (DJFM) SLP anomalies during (a) 1958–1977 (P1), (b) 1978–1997 (P2), and (c) the difference (b) minus (a). (d)–(f) are the same as (a)–(c), except for monthly anomalies during wintertime (December–March). Prior to the EOF analyses linear trends were removed at each grid point. EX (%) denotes the percentage of explained variance. The leading EOFs are well separated from subsequent modes according to the criterion of North et al. (1982). NCEP/NCAR reanalysis data were used.

the recent shift is also evident on intraseasonal time scales.

The late 1970s, separating P1 from P2, are marked by the change of the NAO from its interdecadal low (P1) towards its interdecadal high (P2) state (e.g., Hurrell, 1995; Jung and Ruprecht, 1999, and Fig. 3.7). This *interdecadal* SLP change can be inferred from Fig. 6.5 showing the difference between epoch-averaged SLP for P2 and P1 during wintertime. SLP near Iceland (the Azores) decreased (increased) by about 4 hPa (2 hPa) from P1 towards P2. Notice, that this interdecadal change of the NAO is not accompanied by anomalous meridional wind components near Fram Strait. This may explain why the positive trend of SDS is relatively small compared to those of the NAO index (Fig. 6.1). The origin of the trend in h is described elsewhere (Hilmer and Lemke, 2000).

The cooccurrence of the *interdecadal* increase of the NAO and the eastward displacement

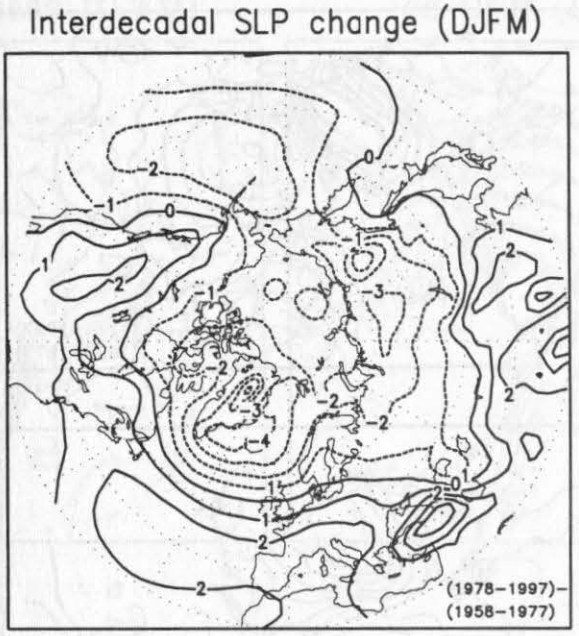

Figure 6.5: Interdecadal change of winter-averaged (DJFM) SLP (hPa). The difference between SLP averaged over the epochs 1978–1997 (P2) and 1958–1997 (P1) is shown. Data are from the NCEP/NCAR reanalysis.

of the centers of *interannual* NAO variability during the last four decades may suggests the that both phenomena are related. Of course, a possible causality of this link is difficult to test from observational time series alone, especially due to their shortness. What can be done, however, is to gather evidence for and against this hypothesis. The first two decades of the 20th century (about 1905–1925, P3, hereafter) represent another period when the NAO resided preferentially in its positive phase (e.g., Hurrell, 1995; Jung and Ruprecht, 1999, and Fig. 3.7). Thus, SLP anomalies were regressed onto the normalized NAO index for the periods P1, P2 and P3 using an updated version of historical SLP analyses (Trenberth and Paolino, 1980). The difference of the regression patterns between P2 and P1 as well as P3 and P1, both representing epoch differences between interdecadal high and low states of the NAO, are shown in Fig. 6.6. First, the secular change of the longitudinal position of interannual NAO variability from P1 towards P2 is obviously not an artifact that is associated with the NCEP/NCAR reanalysis system, because the shift is also evident from SLP *analyses* (compare Figs. 6.3d and 6.6a). Differences in the longitudinal position of the NAO's centers of interannual variability between P3 and P1 (Fig. 6.6b) are more difficult to assess. There is correspondence[32] between the patterns in Fig. 6.6a,b in the western part of the North Atlantic basin (west of about 30^oW). On the other hand, SLP anomalies are quite different further eastward. Overall, the pattern in Fig. 6.6b resembles those for a negative NAO. This might be partly due to the time-dependence of the number of measurements that enter monthly SLP means. It is well-known that the slope of a regression model depends on the variance that is explained by the regression model and

[32]If the longitudinal position of interannual NAO variability is governed by interdecadal changes of the NAO, then a perfect agreement between the patterns in Fig. 6.6a,b would be expected, except for different magnitudes.

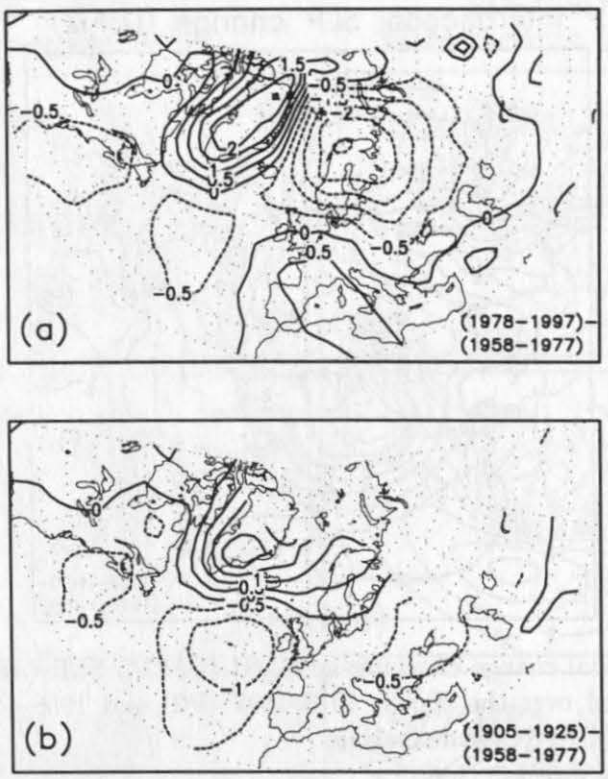

Figure 6.6: (a), same as in Fig. 6.3d, except for updated SLP analyses from Trenberth and Paolino (1980). (b), same as in (a), except for the epoch difference 1905–1925 (P3) minus 1958–1977 (P1). Notice, that in (b) no values are drawn north of 75^oN due to missing data. To allow a direct comparison between P1 and P3, the pattern for P3 is expressed in standard deviations of the NAO index during P1.

the noise component of the predictor as well as the predictant. Moreover, the parameters of the regression model were estimated from relatively short segments (20-yrs) and are subject to sampling variability. Summarizing, since the observational record suffers from its shortness and the time-dependence of the number of observations, it is difficult to make confident statements about a possible interaction between interdecadal and interannual variability of the NAO using observations. Nevertheless, there seems to be little evidence that the centers of interannual NAO variability were located further eastward during the period 1905–1925 compared to 1958–1977.

6.4 The Link as Simulated by a Coupled Climate Model

Using observations and a realistic integration of a state-of-the-art sea ice model, evidence was presented that the link between the NAO and Arctic sea ice export through Fram Strait on interannual time scales underwent interdecadal changes during the last four decades. Although there is some indication that the link between the NAO and ice volume flux through Fram Strait during the last two decades is rather unusual, this conclusion suffers from the shortness of the observational record and the time-dependent sampling. To circumvent these problems, subsequently, century-scale CGCM integrations are analyzed.

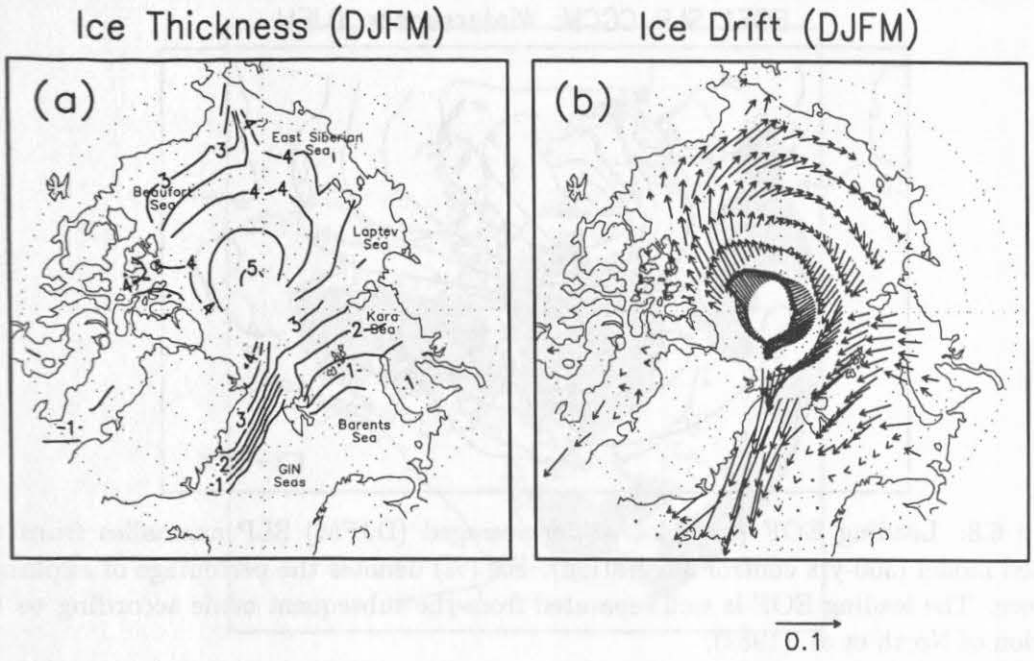

Figure 6.7: Long-term mean of winter-averaged (DJFM): (a) Ice thickness (m), and (b) ice drift (m/s) over the Arctic as simulated by the coupled model (280-yrs). Contour interval in (a) is 0.5 m. In (b), every second vector in longitudinal direction was omitted. A reference vector for the ice drift (0.1 cm/s) is given.

Of course, this advantage cannot be obtained without model-specific uncertainties. Since the secular changes described above occurred in recent years and the trajectory of the observed climate system may be subject to a possible anthropogenic forcing, the analyses will be performed for two experiments: A control integration under present-day conditions and a transient scenario experiment under increasing greenhouse gas concentrations.

6.4.1 Present-Day Climate

The link between the NAO and ice export through Fram Strait is further investigated using a century-scale integration of the coupled ECHAM4/OPYC3 model under present-day conditions. Before such an analysis is carried out, it is neccessary, however, to compare climatological properties of some of the key-parameters (atmosphere and sea ice) as simulated by the CGCM with observations and the results from the realistic hindcast simulation (KISS). A description of simulated characteristics of the atmosphere over the North Atlantic region is given in chapter 5.

Long-term averages of the Arctic ice thickness and ice drift during wintertime (DJFM) as simulated by the CGCM are shown in Fig. 6.7. The gross structures and magnitudes are in good agreement with estimates from the realistic hindcast simulation of KISS (not shown, M. Hilmer, personal communication). In the CGCM, both, the maxima of ice thickness and the center of the anticyclonic Beaufort Gyre are somewhat biased towards the North Pole in comparison to KISS.

Long-term averages and standard deviations for winter-averaged data of the ice volume flux through Fram Strait as well as SDS and h in Fram Strait as simulated by the CGCM

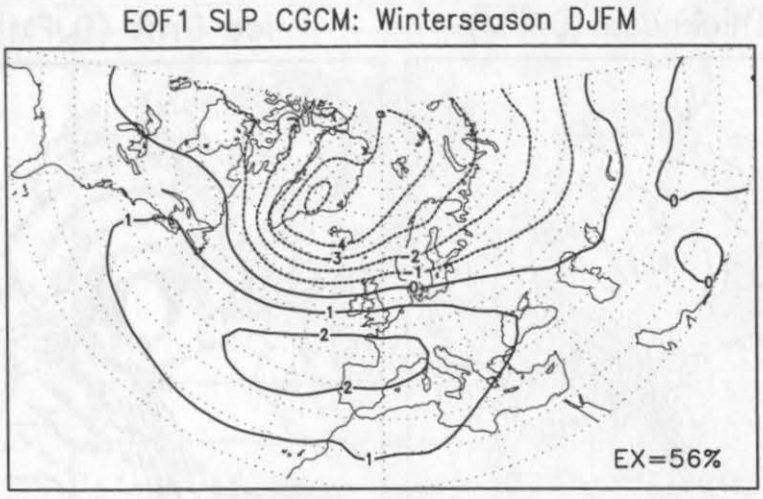

Figure 6.8: Leading EOF (hPa) of winter-averaged (DJFM) SLP anomalies from the coupled model (300-yrs control integration). EX (%) denotes the percentage of explained variance. The leading EOF is well separated from the subsequent mode according to the criterion of North et al. (1982).

and KISS are summarized in Tab. 6.2. Simulated average ice volume fluxes and SDSs are in relatively good agreement. The simulated h, however, is considerably lower for the CGCM compared to KISS. Note, that this difference might be a rather conservative estimate, since h as simulated by KISS shows a significant decrease during the course of the integration (Fig. 6.1). This negative trend of h, which comes in parallel with the decrease of Arctic sea ice volume, is presumably due to the recent warming over the Arctic (Hilmer and Lemke, 2000, and references therein). Furthermore, a direct comparison of h from the models suffers from relatively large ice thickness gradients near Fram Strait (Fig. 6.7a). Thus, slight changes in the definition of the Fram Strait section may results in large differences of h. Similar arguments hold for the ice drift, especially north of Fram Strait. In the CGCM interannual variability of sea ice quantities in Fram Strait are more pronounced than in KISS. This holds particularly for h (Tab. 6.2). The standard deviation-to-average ratio for the ice volume export amounts to 40% for the CGCM and to 28% for KISS.

Table 6.2: Mean and standard deviation (Stdev) for winter averages (DJFM) of the ice volume flux (IVF) through Fram Strait as well as southward drift speed (SDS) and ice thickness (h) in Fram Strait as simulated by the coupled model (280-yrs) and KISS (1958–1997) for winter averaged data (DJFM).

	ECHAM4/OPYC3			KISS		
	IVF (Sv)	SDS (cm/s)	h (m)	IVF (Sv)	SDS (cm/s)	h (m)
Average	0.121	7.05	2.25	0.116	7.39	3.60
Stdev	0.048	2.23	0.53	0.033	1.96	0.38

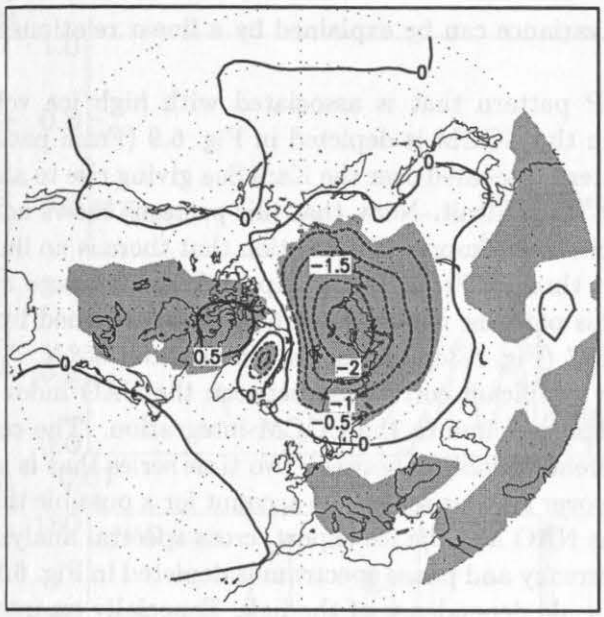

Figure 6.9: Same as in Fig. 6.3c, except for the control simulation of the coupled model (280-yrs). Contour interval is 0.5 hPa.

The first EOF of North Atlantic SLP anomalies during wintertime from the CGCM integration is depicted in Fig. 6.8. This EOF explains 56% of the total SLP variance and resembles closely the observed NAO pattern during the period 1958–1977 (Figs. 6.3a and 6.4a) with centers of action northeast of Iceland and the Iberian Peninsula. Hence, the long-term characteristics of the NAO as simulated by the CGCM yield additional support for the hypothesis that the location of the NAO's centers of interannual variability during the last two decades is rather unusual. The temporal correlation between the first principal component of North Atlantic (normalized) SLP anomalies and the NAO index[33] is ($r = 0.87$) $r = 0.84$. Moreover, the regression of North Atlantic SLP anomalies onto the normalized NAO index yields a pattern (see Fig. 5.9) that closely resembles the first EOF of North Atlantic SLP anomalies. Thus, following the methodology in previous sections, subsequent analyses are based on the NAO index. Similar conclusions are obtained, however, if the first principal component is used instead of the NAO index.

The NAO pattern as simulated by the CGCM shows no pronounced meridional wind components near Fram Strait. Therefore, it can be expected that the NAO index and the ice export through Fram Strait are not significantly correlated. Correlations between the NAO index and different sea ice quantities in Fram Strait as simulated by the CGCM are summarized in Tab. 6.3. The NAO is neither significantly linked with the ice volume export through Fram Strait ($r = 0.0$) nor with SDS ($r = 0.0$) and h ($r = -0.1$) in Fram Strait. Notice, that as for KISS (Tab. 6.1) primarily SDS contributes to the ice volume flux (Tab. 6.3). However, the relative contribution from h to the ice volume flux is larger in the CGCM compared to KISS. Although SDS and h are significantly correlated (r=0.23),

[33]The NAO index is defined as the difference between normalized SLP time series near the Iberian Peninsula ($10°$–$15°W$ and $40°$–$42.5°N$) and Iceland ($17.5°$–$20°W$ and $65°$–$67.5°N$). Further details are given in chapter 5.

only about 5% of the variance can be explained by a linear relationship between the two time series.

The anomalous SLP pattern that is associated with high ice volume export events through Fram Strait in the CGCM is depicted in Fig. 6.9 (Fram pattern). The center of action of the Fram pattern is located over the Kara Sea giving rise to anomalous meridional wind components near Fram Strait. Note, that this patterns shows no projection onto the NAO's centers of action, which supports the notion that there is no link between the NAO and ice volume export through Fram Strait. Apart from the more northerly position of the anomalous low, this patterns closely resembles those obtained from the observations for the period 1958–1997 (Fig. 6.3c), at least north of about 65^oN.

As shown above, no significant correlation between the NAO index and the ice volume flux through Fram Strait is found in the CGCM integration. The correlation coefficient describes (linear) coherent variability between two time series that is in-phase and characteristic for the average over all time scales. To account for a possible time scale dependence of the link between the NAO and the ice export, cross-spectral analysis was applied. The estimated squared coherency and phase spectrum is depicted in Fig. 6.10. Obviously, there is no systematic time scale dependence of the link. Especially on interannual time scales no significant coherency is found, apart from a few excursions at the high-frequency end. Moreover, the phase spectrum appears to fluctuate more or less randomly and there is no evidence for noteworthy in-phase variability. Hence, the results from the cross-spectral analysis confirm that in the CGCM integration there is no significant in-phase variability between the NAO index and the ice export volume export from interannual to interdecadal time scales.

Once the long-term characteristics of the link between the NAO and Arctic ice export as simulated by the CGCM are described, subsequently, its time-dependence is investigated. The cross-correlation function (19-yr running window) for the NAO index and the ice export time series is shown in Fig. 6.11 along with the lowpass-filtered (19-yr running mean) NAO index. Out of the 262 overlapping chunks (19-yrs length) the highest cross-correlation does not exceed $r = 0.5$. Note, that a correlation of $r = 0.7$ was found during the period 1978–1997 for the realistic hindcast simulation using KISS (Tab. 6.1) and that the percentage of variance explained by a linear relationship is quadratic in the correlation coefficient. The long-term average of the cross-correlation function amounts to about zero and its standard deviation amounts to 0.25. Thus, provided that the CGCM performs realistically in simulating natural variability of the NAO and Arctic sea ice, the relatively high correlation between the NAO and the ice volume flux through Fram Strait as observed

Table 6.3: Linear cross-correlations for winter averages (DJFM) of the NAO index, ice volume flux through Fram Strait, as well as the southward drift speed (SDS) and ice thickness (h) in Fram Strait from the couled model (280-yrs). Nonzero correlations at the 95% confidence level are bold (t-test).

	Ice Volume Flux	SDS	h
NAO	0.00	0.00	-0.10
SDS	**0.84**	**1.00**	**0.23**
h	**0.67**	**0.23**	**1.00**

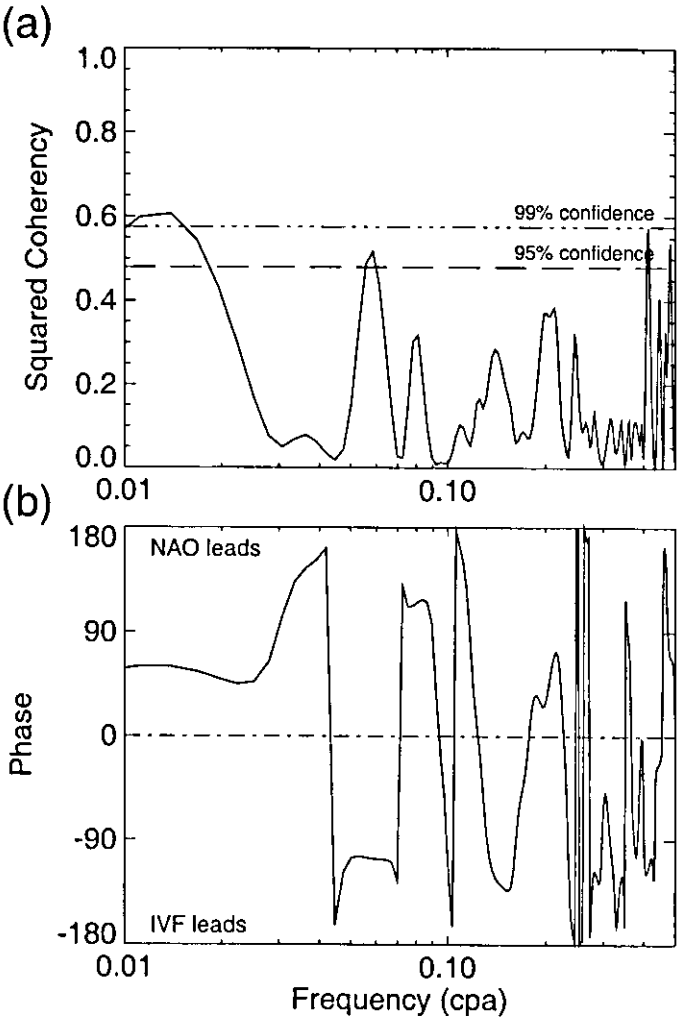

Figure 6.10: (a) Squared coherency and (b) phase spectrum for winter averages (DJFM) of the NAO index and ice volume flux (IVF) through Fram Strait from the coupled model (280-yrs). The NAO leads for positive phases. A Tukey-window with a maximum lag of 60-yrs was used for smoothing (12.4 degrees of freedom). 95% (dashed) and 99% (dash-dotted) confidence levels for non-zero coherency are displayed in (a).

during the last two decades appears to be rather unusual.

A Monte Carlo experiment was performed in order to investigate how the cross-correlation coefficient is distributed under the null hypothesis that the NAO index and the ice volume export through Fram Strait as simulated by the CGCM are realizations of independent first-order auto-regressive (AR(1)) processes. The AR(1) parameters were estimated from the time series (280-yrs) following the procedure outlined by Allen and Smith (1996). Then, 10000 realizations of the null hypothesis, each having a length of 19-yrs, were generated. The 2.5th and 97.5th percentiles of the estimated cross-correlation coefficients are given by -0.45 and 0.47, respectively. Seven excursions of the cross-correlation function above the 97.5th percentile occur in Fig. 6.11. Note, however, that on average $0.025 \cdot 262 = 6.6$ excursions are expected to occur just by change — even for *independent*

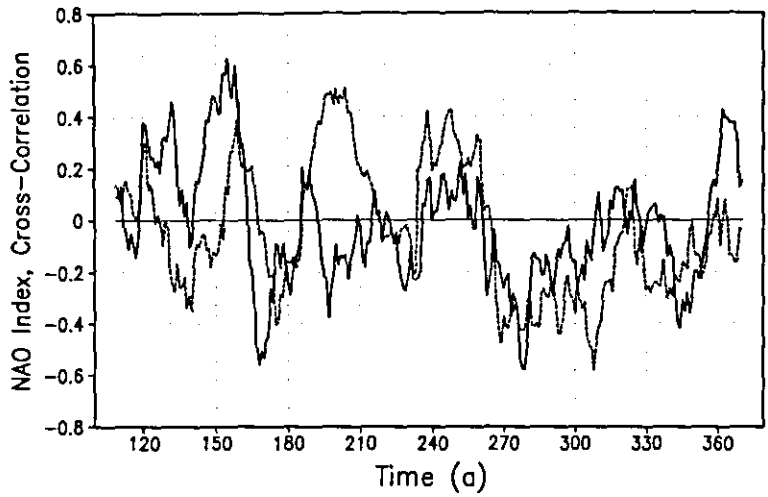

Figure 6.11: Interdecadal NAO variability (19-yr running mean, solid) along with the cross-correlation function for the NAO index and ice volume export through Fram Strait (19-yr running window, dotted) between winter averages (DJFM) from the coupled model (280-yrs control integration).

estimates. The standard deviation of the ensemble of cross-correlations amounts to 0.24 which is in close agreement with the estimate obtained from the data (0.25, see above).

Moreover, the correlation between low-frequency variability of the NAO and the cross-correlation function is rather weak (r=0.24). An additional Monte Carlo experiment was performed to assess the unusualness of this correlation taking into account the strong serial correlation (lag-1 correlation>0.9) of the time series in Fig. 6.11: The 2.5th and 97.5th percentiles are $r_{2.5} = -0.78$ and $r_{97.5} = 0.78$, respectively. Hence, from the statistical analyses presented above it can be concluded that in the control integration of the CGCM there is neither a significant linear relationship between the the NAO and the ice volume export through Fram Strait nor do interdecadal changes of the NAO exert a significant control on the coherence between the NAO and the ice export on interannual time scales.

6.4.2 Increasing Greenhouse Gases

Recently, Ulbrich and Christoph (1999) (UC99, hereafter) reported that the NAO's northern center of action (Icelandic Low) shows a systematic eastward shift from a position close to the east coast of Greenland in the control run to the Norwegian Sea under enhanced greenhouse gas forcing ($\geq 3W/m^2$) in the ECHAM4/OPYC3 model. Moreover, UC99 show that the position of the NAO is stable during the course of the control integration. This appears to be in agreement with the results presented in the previous paragraph, because otherwise persistent periods of significant interannual coherence between the NAO and the ice volume flux through Fram Strait should have been found. Subsequently, it is investigated whether the eastward shift under enhanced greenhouse gases (UC99) resembles the observed shift during the last two decades. This analysis may be seen as an extension to the study by UC99, because here the influence from secular changes of *mean* SLP are considered separately from secular changes of SLP *variability*.

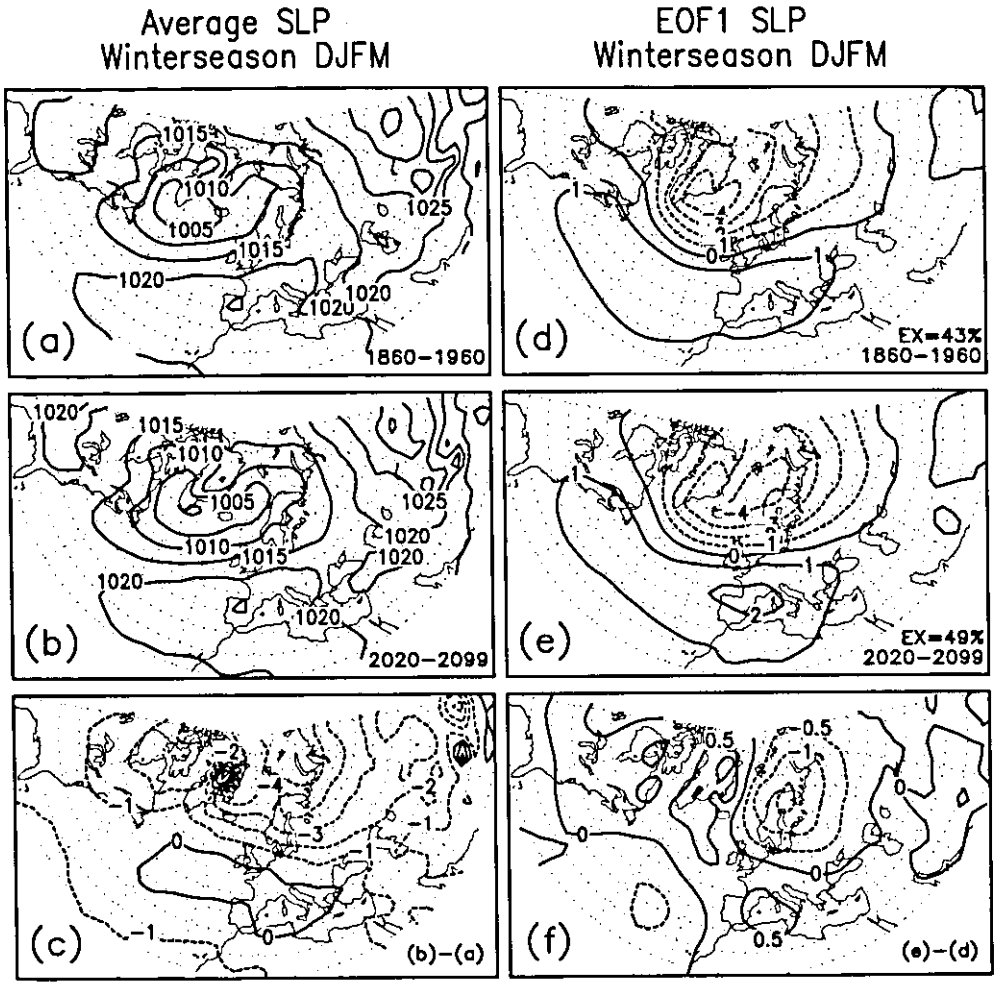

Figure 6.12: Average SLP (hPa) for (a) 1860–1960 and (b) 2020–2099 along with their (c) difference (b) minus (a) for winter averages (DJFM) from the coupled model. (d)–(f), Same as (a)–(c) except for the first EOFs of SLP anomalies SLP. Prior to the EOF analyses linear trends were removed at each grid point. EX (%) denotes the percentage of explained field variance. The first EOFs are well separated from subsequent modes according to the criterion of North et al. (1982).

In the scenario integration of the ECHAM4/OPYC3 model anthropogenically forced atmospheric changes follow closely the greenhouse gas forcing and exceed the band of natural variability around the year 2020 (UC99). Thus, a possible impact of enhanced greenhouse gas concentrations is studied by comparing the period 2020–2099 with the period 1860–1960 (Fig. 6.12). As shown by UC99 (their Fig. 9), in this CGCM increasing greenhouse gases are accompanied by a reduction of SLP in high-latitudes (Fig. 6.12a–c). Strongest changes occur over the Barents and Kara Seas and no changes are evident near the Azores. Therefore, in this model increasing greenhouse gas concentrations lead to rather weak secular changes of the NAO (see also, UC99; Paeth et al., 1999). Note, that observed secular SLP changes in the North Atlantic region project strongly onto the NAO (Fig. 6.5).

Following UC99, EOF analysis was applied to anomalous SLP fields in the North Atlantic region for the periods 1860–1960 and 2020–2099 (Fig. 6.12d–f). In contrast to UC98, however, prior to the decomposition linear trends were removed for each period to focus on greenhouse gas forced changes of interannual to decadal SLP variability. The linear SLP trend pattern (not shown) resembles the SLP difference between the periods 2020–2099 and 1860–1960 (Fig. 6.12c). During the period 1860–1960 (weak forcing) the first EOF is quite similar to those for the control run (compare Figs. 6.12a and 6.8). In agreement with the results by UC99 (with linear trend), the centers of NAO variability were located further eastward during the period 2020–2099 (strong forcing) compared to 1860–1960. The difference pattern (Fig. 6.12f) shows an astonishing resemblence with that obtained from the observations (Figs. 6.3d and 6.4c,f), apart from smaller magnitudes for the CGCM. Thus, it can be expected that in the ECHAM4/OPYC3 model the NAO and Arctic sea ice export through Fram Strait[34] show coherent variability on interannual to decadal time scales under increasing greenhouse gas concentrations. In the control run there is no link between the NAO and Arctic sea ice export through Fram Strait.

6.5 Conclusions

The link between the NAO and Arctic sea ice export through Fram Strait was investigated using data from different sources. The focus was on the winter season (DJFM).

First, observations (reanalyses) were analyzed along with a realistic hindcast simulation of the Artic sea ice cover using a state-of-the-art sea ice model that was driven with daily varying fields of near-surface wind and temperature over the period 1958–1997. The conclusions are as follows:

- In agreement with previous observational studies (Kwok and Rothrock, 1999; Dickson et al., 2000) it is shown that high (low) NAO winters were accompanied by enhanced (decreased) Arctic ice volume exports through Fram Strait during the last two decades (1978–1997). The corresponding correlation coefficient amounts to $r = 0.70$.

- During the period 1958–1977 a significant link between the NAO and Arctic sea ice export through Fram Strait was missing ($r = 0.06$).

- Differences between the periods 1958–1977 ($r = 0.06$) and 1978–1997 ($r = 0.70$) can be traced back to the more easterly location of the NAO's centers of interannual variability during the last two decades. Only during the latter period interannual NAO variability was accompanied by meridional wind anomalies near Fram Strait giving rise to anomalous meridional drift speeds and, therefore, ice volume exports through Fram Strait.

- The recent eastward shift in the position of the NAO's centers of interannual variability came in parallel with the relatively strong increase of the NAO during the last three decades.

- Although the observational time series suffer from their shortness, evidence is presented that the location of the NAO's centers of interannual variability during the last two decades is rather unusual.

[34] Unfortunately, sea ice data were not available for the scenario run.

Moreover, it was shown (see also the Appendix) that the eastward shift of the NAO's centers of interannual variability during the last two decades left its imprint also on other parameters:

- Secular changes in the link between the NAO and the ice volume export through Denmark Strait (Davis Strait) are similar (opposite) to those between the NAO and the ice volume export through Fram Strait.
- The more easterly position of the centers of interannual NAO variability led to an enhanced (reduced) near-surface temperature response to interannual variability of the NAO over parts of central Europe (northeastern and southeastern United States) (see Appendix, Fig. A.1).
- Similarly, the association between anomalous turbulent heat fluxes and the NAO was reduced over the western part of the North Atlantic basin during the last two decades (see Appendix, Fig. A.2).

Furthermore, the link between the NAO and Arctic sea ice export through Fram Strait was investigated using a century-scale integration of a CGCM (ECHAM4/OPYC3) under present-day conditions. The following conclusions can be drawn:

- The long-term mean characteristics of Arctic sea ice as simulated by the CGCM are in relatively good agreement with the results from the realistic hindcast simulation.
- There is no significant instantaneous link between the NAO and sea ice volume export through Fram Strait from interannual to interdecadal time scales.
- The NAO's centers of action are in close agreement with the observed ones during the period 1958–1977.
- Changes in the ice volume export through Fram Strait are associated with SLP anomalies over the Kara Sea.
- There is no indication that the link between the NAO and the ice volume flux on interannual time scales is governed by low-frequency changes of the NAO.

Finally, based on previous work by Ulbrich and Christoph (1999), it is shown that

- the shift of the centers of interannual to decadal NAO variability under enhanced greenhouse gas concentrations (about $\geq 3W/m^2$, i.e., year 2020) in the scenario integration of the ECHAM4/OPYC3 model is quite similar to the observed one.

6.6 Discussion

As outlined in the initial implementation plan for the Climate Variability and Predictability (CLIVAR, 1998) programme, it was expected that the NAO exerts a significant control on the export of ice from the Arctic through Fram Strait into the North Atlantic. As mentioned in the Introduction this notion is supported by recent observational studies (Kwok and Rothrock, 1999; Dickson et al., 2000) that are based on data from the last two decades. While the results from this study confirm the findings by Kwok and Rothrock (1999) and Dickson et al. (2000) for the overlapping period (1978–1997), it is also shown that during

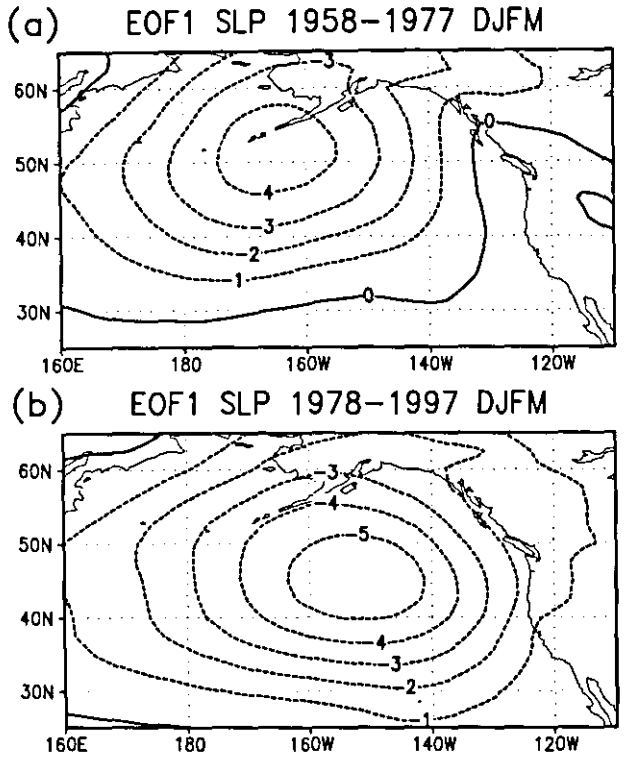

Figure 6.13: Same as in Fig. 6.4a and b, except for North Pacific SLP anomalies. The first EOF explains (a) 43% and (b) 61% of the total field variance.

the previous two decades (1958–1977) a link between the NAO and Arctic sea ice export through Fram Strait was missing. Thus, the results from this study highlight the problem to draw conclusions from relatively short time series of a climate system that varies on a broad range of frequencies.

From the analysis of historical SLP analyses during the 20th century and a century-scale integration of a CGCM under present-day conditions it is proposed that a missing link between the NAO and Arctic sea ice export is a long-term property of the North Atlantic climate system. In this context interannual NAO variability was rather unusual during the last two decades.

Due to the outstanding role of the NAO for the North Atlantic region its shift had profound impacts on other parameters that are of climatological importance. In the Appendix it is shown that the shift was accompanied by considerable changes in the near-surface temperature (Fig. A.1) and turbulent surface heat flux response (Fig. A.2) to a forcing by the NAO. In the Labrador Sea region, for example, turbulent surface heat flux anomalies during high and low NAO winters were reduced during the last two decades compared to the period 1958–1977. It may be expected, therefore, that the shift left its imprints also in the oceanic response to an interannual NAO forcing via associated changes in Labrador Sea convection. More generally, studies that are intended to estimate the response of regional climates to large-scale North Atlantic climate variability have to take into account the recent shift, especially if long-term characteristics are estimated from recent observational time series.

It was shown that the change in the position of the NAO's centers of interannual variability occurred around the late 1970s, that is, during a time when the change of the NAO from its persistent low phase during the 1960s to its persistent high phase during the late 1980s and early 1990s was most pronounced (e.g., Hurrell, 1995, 1996). It is worth mentioning, that considerable changes took also place in the Pacific basin around the late 1970s. SLP in the northern North Pacific, for example, decreased markedly after 1976 (Trenberth and Hurrell, 1994) as can be inferred from Fig. 6.5. Note, that the *combined* effect of the intensified Aleutian low and of the persistent high phase of the NAO during the last two decades explains the bulk of the Northern Hemispheric warming in recent years (Hurrell, 1996). Moreover, there is observational evidence that a "regime shift" in El Niño/Southern Oscillation (ENSO) variability took place in 1977 (e.g., Monahan and Crisis Points Group, 1999), which is associated with differences in the evolution of ENSO events before and after 1977. Thus, it is natural to ask whether the deepening of the Aleutian low after 1976 was also accompanied by a shift of its centers of interannual variability. In an exploratory analysis the first EOF of anomalous North Pacific SLP was separately estimated for the periods 1958–1977 (P1) and 1978–1997 (P2) (Fig. 6.13). During P2 interannual SLP was much more pronounced (up to $-3\ hPa$) in the southeastern part of the North Pacific basin compared to P1. Thus, the eastward shift of interannual NAO variability seems to have its counterpart in the North Pacific region too.

The causes for the recent secular increase of the NAO during wintertime, which is part of one interdecadal swing starting around the beginning of the 20th century, have attracted considerable scientific interest. The paleoclimatic reconstruction of the NAO from snow accumulation over western Greenland (Appenzeller et al., 1998b) for the past 350 years may support the hypothesis that the recent increase of the NAO is rather unusual. The results from different CGCM integrations under increasing greenhouse gas concentrations, however, yield a somewhat controverse picture how the atmosphere (NAO) in the North Atlantic region may respond to an anthropogenic forcing. There is agreement between different CGCM integrations that SLP over the Arctic decreases in parallel with an increasing greenhouse gas forcing (Shindell et al., 1999; Fyfe et al., 1999, UC99). However, the degree to which simulated SLP trends resemble the NAO is quite different. A relatively strong positive trend of the NAO under an increasing greenhouse gas forcing is described by Shindell et al. (1999); the studies by Paeth et al. (1999) and UC99 suggest that the NAO index, defined at fixed locations, is not an optimal measure to describe this trend; and Fyfe et al. (1999) found no projection of the simulated trend onto the NAO's centers of action. Similarly, there is considerable scatter among different CGCM integrations how NAO *variability* will change under increasing greenhouse gas concentrations (UC99; Fyfe et al., 1999; Paeth et al., 1999; Monahan et al., 2000). The observed eastward shift of interannual NAO variability during the last two decades that came in parallel with the secular increase of the NAO is very similar to what happens in the ECHAM4/OPYC3 model under increasing greenhouse gas concentrations. However, due to the spread of possible future changes among different CGCM integrations, considerable uncertainties remain how the atmosphere over the North Atlantic region responds to an increasing greenhouse gas forcing.

7 Final Discussion and Outlook

Twenty years from now you'll be more disappointed by the things you didn't do, than by the ones you did do. So throw off the bowlines. Sail away from the safe harbor. Catch the trade winds in your sails. Explore. Dream. Discover.

Mark Twain

In this study climate variablity in the North Atlantic region is investigated with special emphasis on variability of the NAO and its interaction with the North Atlantic ocean as well as the Arctic sea ice export through Fram Strait.

The results of this study suggest that *interdecadal* NAO variability during the 20th century (chapter 3) was associated with considerable changes in (i) the circulation of the North Atlantic ocean (chapter 4) and (ii) the link between the NAO and Arctic sea ice export through Fram Strait on interannual time scales (chapter 6). From a statistical point of view NAO variability on interannual and quasi-decadal time scales is consistent with what is expected from realizations of "white noise" (chapter 3).

It is important, thus, to unravel the mechanism(s) that gave rise to interdecadal NAO variability during the 20th century. The modelled response of the North Atlantic ocean to a surface flux forcing that was solely based on the observed NAO (chapter 4) provides evidence that on interdecadal time scales oceanic changes lag behind the NAO by about 90^o (Fig. 4.10). Since an atmospheric response to an oceanic forcing should be expected to occur *instantaneously*, the modelled phase-relationship between the NAO and the North Atlantic ocean on interdecadal time scales does not support the presence of a two-way coupled mode of (interdecadal) variability, as found for instance, by Timmermann et al. (1998) in a century-scale integration of the ECHAM3/LSG model[35]. Although the agreement between the observed and modelled evolution of interdecadal North Atlantic SST anomalies during the 20th century (Fig. 4.4) suggest that this simulation performed realistically, our confidence in this integration could be further enhanced by comparing modelled subsurface data with observations, at least where possible.

Since the results of this study provide little evidence for the presence of two-way air-sea interaction in the North Atlantic region on interdecadal time scales, other possible mechanisms have to be taken into account in order to explain interdecadal NAO variability during the 20th century. It cannot be ruled out that the recent positive trend of the NAO is forced by increased greenhouse gas concentrations. This notion is supported, for instance, by

- the strong projection of the NAO onto the recent Northern Hemisphere warming[36] (Hurrell, 1996),

[35] In this model the NAO and the North Atlantic THC are approximately in phase on interdecadal time scales (Axel Timmermann, personal communication).

[36] The increasing frequency of El Niño events in recent years also contributed to this warming (Hurrell, 1996). Notice, that Timmermann et al. (1999) found a warming of tropical Pacific SST under increasing greenhouse gas concentrations in the ECHAM4/OPYC3 model.

- increasing interdecadal NAO variability throughout the 20th century (Fig. 3.10) (see also Hurrell and van Loon, 1997),

- relatively weak interdecadal NAO variability before the mid-19th century (about 1650–1850) century as suggested by Greenland ice core data (Appenzeller et al., 1998b),

- decreasing SLP over the high-latitude Northern Hemisphere under increasing greenhouse gas concentrations in different CGCM experiments (e.g., Ulbrich and Christoph, 1999; Shindell et al., 1999; Fyfe et al., 1999; Paeth et al., 1999), although some uncertainties about the centers of the strongest secular changes remain.

- the similarity of the eastward shift of the NAO's centers of interannual variability as observed during the last two decades (Fig. 6.3d) and simulated under an enhanced greenhouse gas forcing (about 2020) by the ECHAM4/OPYC3 model (Fig. 6.12f) (see also Ulbrich and Christoph, 1999, their Fig. 6).

When discussing secular changes of the NAO under increasing greenhouse gas concentrations using state-of-the-art CGCMs, it has to be kept in mind, however, that the mechanisms giving rise to natural interdecadal climate variability in the North Atlantic region differ from model to model. These differences introduce considerable uncertainties in the context of modelled feedbacks.

Throughout this study interannual to interdecadal NAO variability was studied using winter-averaged data. As demonstrated by Madden and Jones (1999) the analysis of winter-averaged data is associated with considerable aliasing: *"In the case of one sample per year (e.g., time series of Januaries or Winter Seasons), the aliased variance at resolved frequencies is an increadible 92% and 75% for 30 and 90 days averages"*. Thus, care has to be taken when interpreting the results, since a considerable amount of "interannual" variability may result from intraseasonal sampling variability. The aliasing problem may be expressed in more physical terms: Atmospheric climate variability can be understood in terms of changes in the occupation statistics of *intraseasonal* large-scale circulation patterns (e.g., Palmer, 1993, 1999; Corti et al., 1999). Hence, in order to improve our understanding about interannual to interdecadal NAO variability, it is important to understand the nature of intraseasonal variability (so-called weather regimes).

There is a growing body of evidence that low-frequency intraseasonal variability of the extratropical atmosphere is governed by nonlinear dynamics (e.g., Kimoto and Ghil, 1993a,b; Corti et al., 1999; Smyth et al., 1999). If the extratropical atmosphere is treated as a nonlinear dynamical system, then the interpretation of a possible external forcing of the atmosphere is influenced (Palmer, 1993, 1999): An external forcing may primarily appear as a change in the frequency of occurrence of fixed natural modes of atmospheric variability, rather than as a change in their location. The observed eastward shift of the NAO's centers of interannual variability around the late 1970s may be seen as evidence against Palmer's nonlinear paradigm. On the other hand, it cannot be ruled-out that this shift resulted from changes in the occupation statistic of more than one natural mode of variability. Thus, it is of importance to study this shift from the point of view of intraseasonal variability. Since a similar shift is observed in ECHAM4/OPYC3 model under increased greenhouse gas concentrations, this model integration provides a valueable data source to further study the nature of this shift.

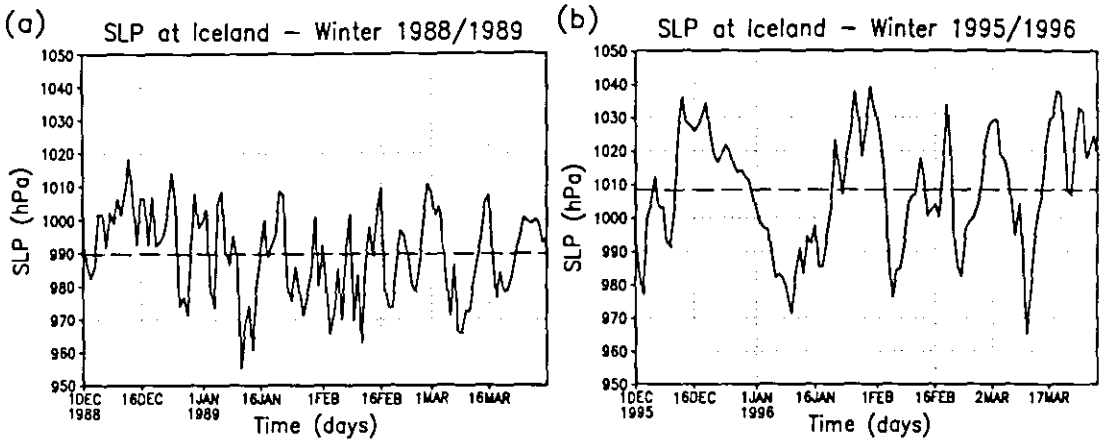

Figure 7.1: Daily SLP at Iceland (solid in hPa) during the (a) high NAO winter 1988/1989 and the (b) low NAO winter 1995/1996. Winter averaged SLP (December through March) is given as dashed line.

It is worth mentioning that this shift may well be in agreement with Palmer's nonlinear paradigm taking into account the possibility for bifurcations of the extratropical atmosphere under an external forcing. Modelling evidence has been presented by Molteni and Corti (1998) that the extratropical atmosphere over the North Pacific resides in the neighbourhood of a bifurcation point[37]. The results by Molteni and Corti (1998) suggest that in this model changes in the tropical forcing can bring the atmosphere beyond a bifurcation point. This bifurcation becomes evident from differences in the intraseasonal variance between winters with strong and weak projections onto the Pacific/North American pattern (PNA pattern). Similar differences are associated with high and low NAO winters in the North Atlantic region (Fig. 3.5a and Fig. 5.10b). To further illustrate this difference, Fig. 7.1 shows daily SLP time series from Iceland during the high and low NAO winters 1988/1989 and 1995/1996, respectively. (Compare Fig. 6.1 for the choice of these years.) Obviously, SLP at Iceland was relatively persistent during the high NAO winter 1988/1989, whereas considerable variability at the low-frequency end of the intraseasonal SLP spectrum took place at Iceland during the low NAO winter 1995/1996. These differences may be of importance when considering the physics, predictability, and impacts of intraseasonal atmospheric variability.

From the results of this study and their dicussion in the context of other recent publications (see above) — in my view — the following items deserve special focus in future studies in order to improve our understanding about natural variability and possible anthropogenically induced changes of the North Atlantic climate system:

- **Further assessment how the North Atlantic ocean responds to a forcing by the NAO, especially on interdecadal time scales. A thorough understanding of this response is a prerequisite to realistically model low-frequency changes of the coupled North Atlantic climate system.**

- **Future studies on extratropical climate variability should be based on a**

[37]Note, that an eastward shift of the dominant mode of atmospheric variability around the late 1970s is also evident in the North Pacific basin (Fig. 6.13).

broader range of frequencies taking into account atmospheric variability from days to decades (compare Fig. 1.1).

A Shift of NAO and Impact on North Atlantic Climate

In chapter 6 (Link Between NAO and Arctic Ice Export) it is shown that the longitudinal position of the NAO's centers of interannual variability underwent secular changes during the last forty years. These atmospheric changes left their imprint on the variability of the ice volume export through Fram Strait, Denmark Strait and Davis Strait. Here, it is shown that this shift affected also the near-surface temperature and turbulent surface heat flux (latent and sensible heat fluxes) response to an interannual forcing by the NAO. Near-surface temperature is a key-parameter for social and economical affairs; and turbulent surface heat fluxes play a crucial role for air-sea interaction (see chapter 4), especially during the winter season.

It is well-known that high and low NAO winters are accompanied by large-scale near-surface temperature anomalies over the neighbouring continents (e.g., Hurrell, 1995; Hurrell and van Loon, 1997). In the long-term context (1864–1994) high NAO winters, for example, are accompanied by anomalously high near-surface temperatures over northern Europe, northern Russia and the southeastern U.S.; at the same time the northwestern part of the North Atlantic region and regions south of the Mediterranean face anomalously

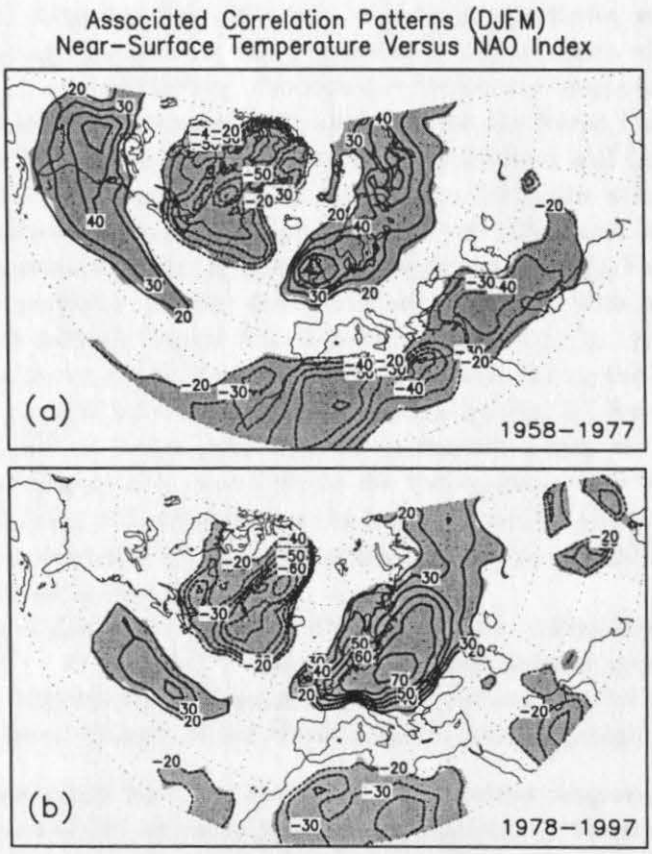

Figure A.1: Local correlations ($r^2 \cdot 100 \cdot \mathrm{sgn}(r)$ in %) between winter-averaged (DJFM) near-surface ($2m$) air temperature anomalies and the observed NAO index for the period (a) 1958–1977, and (b) 1978–1997. The sign of the correlation enters via $\mathrm{sgn}(r) = r/|r|$. The contour interval is 10% for magnitudes $\geq 20\%$ (shaded).

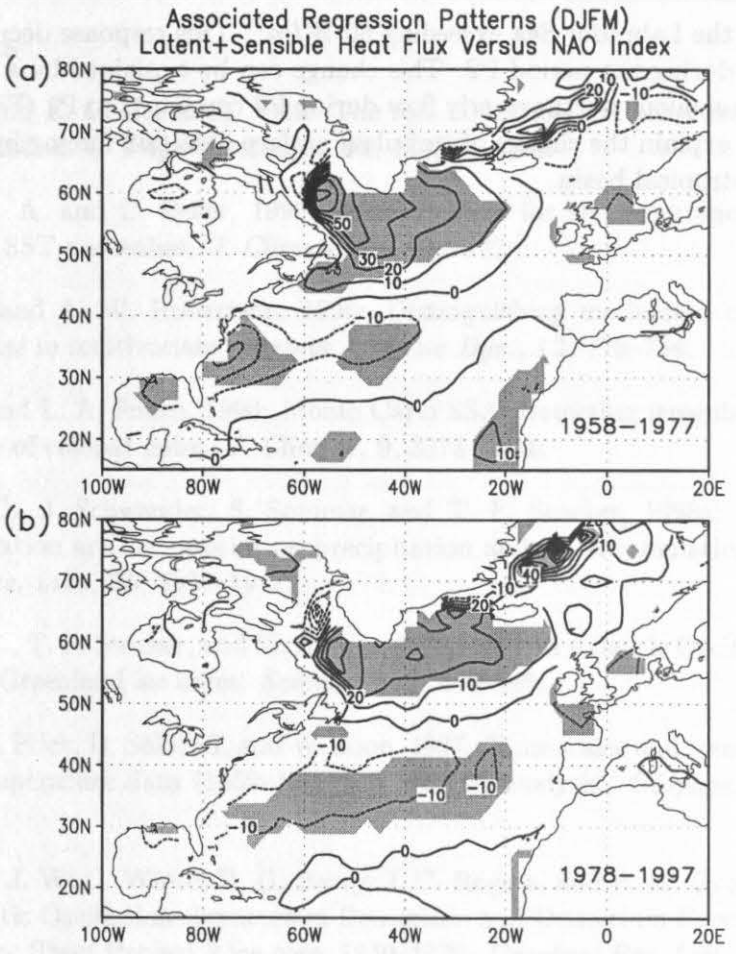

Figure A.2: (a) and (b), as in Fig. 6.3a and Fig. 6.3b, except for turbulent surface heat flux anomalies (W/m^2). Contour interval is 10 W/m^2. Positive flux anomalies are directed from the ocean to the atmosphere.

cold conditions (see Hurrell and van Loon, 1997, their Fig. 6). This long-term near-surface temperature response to a forcing by the NAO becomes evident for the period P1 (1958–1977) (Fig. A.1a); considerable deviations from this response pattern, however, are evident for the period P2 (1978–1997) (Fig. A.1b). During P2 the NAO exerted no significant influence on near-surface temperature anomalies over the southeastern U.S.. The percentage of near-surface temperature variance explained by the NAO over eastern Europe (Poland, Belarussia, eastern Russia) increased considerably compared to P1. These differences can be explained by an increase (decrease) of the NAO-related zonal (meridional) flow over Europe (southeastern U.S.) from P1 towards P2 (Figs. 6.3d and A.1). Similar arguments hold for the near-surface temperature response change over eastern parts of Canada.

Secular changes of the interannual turbulent surface heat flux response to a forcing by the NAO are most pronounced over the eastern part of the North Atlantic basin (Fig. A.2), that is, in regions where the temperature (humidity) contrast between land and ocean is most pronounced. During P1 high NAO winters (one standard deviation above normal), for example, were accompanied by anomalous turbulent surface heat flux anomalies out

of the ocean in the Labrador Sea exceeding 60 W/m^2. This response decreased by about a factor of two during the period P2. This change can be explained by a decrease of the NAO-related anomalous northwesterly flow during P2 compared to P1 (Fig. 6.3). Similar arguments may explain the change of turbulent surface heat flux forcing by the NAO over the western subtropical basin.

References

Aagaard, K. and E. C. Carmack, 1989: The role of sea ice and other fresh water in the Arctic circulation. *J. Phys. Oceanogr.*, **94**, 14485–14498.

Alexander, M. A. and C. Deser, 1995: A mechanism for the recurrence of wintertime midlatitude SST anomalies. *J. Climate*, **25**, 122–137.

Allen, M. R. and A. W. Robertson, 1996: Distinguishing modulated oscillations from coloured noise in multivariate datasets. *Climate Dyn.*, **12**, 775–784.

Allen, M. R. and L. A. Smith, 1996: Monte Carlo SSA: Detecting irregular oscillations in the presence of colored noise. *J. Climate*, **9**, 3373–3404.

Appenzeller, C., J. Schwander, S. Sommer, and T. F. Stocker, 1998a: The North Atlantic Oscillation and its imprint on precipitation and ice accumulation in Greenland. *Geophys. Res. Lett.*, **25**, 1939–1942.

Appenzeller, C., T. F. Stocker, and M. Anklin, 1998b: North Atlantic Oscillation dynamics recorded in Greenland ice cores. *Science*, **282**, 446–449.

Baliunas, S., P. Frick, D. Solokoff, and W. Soon, 1997: Time scales and trends in the central England temperature data (1659–1990): A wavelet analysis. *Geophys. Res. Lett.*, **24**, 1351–1354.

Barlow, L. K., J. W. C. White, R. G. Barry, J. C. Rogers, and P. M. Grootes, 1993: The North Atlantic Oscillation signature in Deuterium and Deuterium Excess signals in the Greenland Ice Sheet Project 2 ice core, 1840–1970. *Geophys. Res. Lett.*, **20**, 2901–2904.

Barnett, T. P., 1985: Variations in near-global sea level pressure. *J. Atmos. Sci.*, **42**, 478–501.

Barnett, T. P. and R. Preisendorfer, 1987: Origins and levels of monthly and seasonal forecast skill for United States surface air temperatures determined by Canonical Correlation Analysis. *Mon. Wea. Rev*, **115**, 1825–1850.

Barnier, B., L. Siefridt, and P. Marchesiello, 1995: Thermal forcing for a global ocean circulation model using a three year climatology of ECMWF analysis. *J. Mar. Sys.*, **6**, 363–380.

Barnston, A. G. and R. E. Livezey, 1987: Classification, seasonality and persistence of low-frequency atmospheric circulation patterns. *Mon. Wea. Rev*, **115**, 1083–1126.

Bjerknes, J., 1964: Atlantic air sea interaction. *Adv. Geophys.*, **10**, 1–82.

Bresch, D. N., 1998: *Coupled Flow and SST Patterns of the North Atlantic*. Ph.D. thesis, Swiss Federal Institute of Technology (ETH), Zürich.

Bretherton, C. S. and D. S. Battisti, 2000: An interpretation of the results from atmospheric general circulation models forced by the time history of the observed sea surface temperature distribution. *Geophys. Res. Lett.*, **27**, 767–770.

Bretherton, C. S., C. Smith, and J. W. Wallace, 1992: An intercomparison of methods for finding coupled patterns in climate data. *J. Climate*, **5**, 541–560.

Broomhead, D. S. and G. King, 1986: Extracting qualitative dynamics from experimental data. *Physica D*, **20**, 217–236.

Cayan, D. R., 1992a: Latent and sensible heat flux anomalies over the northern oceans: Driving the sea surface temperature. *J. Phys. Oceanogr.*, **22**, 859–881.

Cayan, D. R., 1992b: Latent and sensible heat flux anomalies over the northern oceans: The connection to monthly atmospheric circulation. *J. Climate*, **5**, 354–369.

Christoph, M., U. Ulbrich, J. M. Oberhuber, and E. Roeckner, 1999: The role of ocean dynamics for low-frequency fluctuations of the NAO in a coupled ocean-atmosphere GCM. *J. Climate*. Submitted.

CLIVAR, 1998: CLIVAR Initial Implementation Plan. WMO/TD No. 869. World Climate Research Program Report No. 103.

Cook, E. R., R. D. D'Arrigo, and K. R. Briffa, 1998: A reconstruction of the North Atlantic Oscillation using tree-ring chronologies from North America and Europe. *The Holocene*, **8**, 9–17.

Corti, S., F. Molteni, and T. N. Palmer, 1999: Signature of recent climate change in the frequency of natural atmospheric circulation regimes. *Nature*, **398**, 799–802.

Curry, R. G., M. S. McCartney, and T. M. Joyce, 1998: Oceanic transport of subpolar climate signals to mid-depth subtropical waters. *Nature*, **391**, 575–577.

Defant, A., 1924: Die Schwankungen der atmosphärischen Zirkulation über dem Nordatlantischen Ozean im 25-jährigen Zeitraum 1881–1905. *Geografiska Annaler*, **6**, 13–41.

Delworth, T. L., 1996: North Atlantic interannual variability in a coupled ocean-atmosphere model. *J. Climate*, **9**, 2356–2375.

Delworth, T. L. and R. J. Greatbatch, 2000: Multidecadal thermohaline circulation variability driven by atmospheric surface flux forcing. *J. Climate*. In press.

Delworth, T. L., S. Manabe, and R. J. Stouffer, 1993: Interdecadal variations of the thermohaline circulation in a coupled ocean-atmosphere model. *J. Climate*, **6**, 1993–2011.

Delworth, T. L., S. Manabe, and R. J. Stouffer, 1997: Multidecadal climate variability in the Greenland Sea and surrounding regions: A coupled model simulation. *Geophys. Res. Lett.*, **24**, 257–261.

Deser, C., 2000: On the teleconnectivity of the "Arctic Oscillation". *Geophys. Res. Lett.*, **27**, 779–782.

Deser, C. and M. L. Blackmon, 1993: Surface climate variability over the North Atlantic ocean during winter: 1900–1989. *J. Climate*, **6**, 1743–1753.

Dickson, R., J. Lazier, J. Meincke, P. Rhines, and J. Swift, 1996: Long-term coordinated changes in the convective activity of the North Atlantic. *Prog. Oceanogr.*, **38**, 241–295.

Dickson, R. R., J. Meincke, M. S.-A., and A. J. Lee, 1988: The "Great Salinity Anomaly" in the northern North Atlantic 1968–1982. *Prog. Oceanogr.*, **20**, 103–151.

Dickson, R. R., T. J. Osborn, J. W. Hurrell, J. Mencke, J. Blindheim, B. Adlandsvik, T. Vinje, G. Alekseev, and W. Maslowski, 2000: The Arctic ocean response to the North Atlantic Oscillation. *J. Climate*. In press.

Eden, C., 1999: *Interannual to interdecadal variability in the North Atlantic ocean*. Ph.D. thesis, Christian-Albrechts-Unversität Kiel, Institut für Meereskunde Kiel.

Eden, C. and J. Willebrand, 2000: Mechanisms of interannual to decadal variability of the North Atlantic circulation. *J. Climate*. Submitted.

Fang, Z. and J. M. Wallace, 1994: Arctic sea ice variability on a timescale of weeks and its relation to atmospheric forcing. *J. Climate*, **7**, 1897–1914.

FLAME group, 1999: FLAME — a Family of linked Atlantic model experiments. Technical report, AWI Bremerhaven, Bremerhaven, Germany.

Frankignoul, C., 1985: Sea surface temperature anomalies, planetary waves, and air-sea feedback in the middle latitudes. *Rev. Geophys.*, **23**, 357–390.

Fyfe, J. C., G. J. Boer, and G. M. Flato, 1999: The Arctic and Antarctic Oscillations and their projected changes under global warming. *Geophys. Res. Lett.*, **26**, 1601–1604.

Ghil, M. and C. Taricco, 1997: Advanced spectral analysis methods. In: G. Cini Castagnoli and A. Provenzale, eds., *Past and Present Variability of the Solar-Terrestrial System: Measurement, Data Analysis and Theoretical Models*, pp. 137–159. Societa Italiana di Fisica, Bologna, & IOS Press, Amsterdam.

Ghil, M. and P. Yiou, 1996: Spectral Methods: What they can and cannot do for climatic time series. In: D. Anderson and J. Willebrand, eds., *Decadal Climate Variability: Dynamics and Predictability*, pp. 446–482. Elsevier.

Grötzner, A., M. Latif, and T. P. Barnett, 1998: A decadal climate cycle in the North Atlantic ocean as simulated by the ECHO coupled GCM. *J. Climate*, **11**, 831–847.

Grötzner, A., M. Latif, A. Timmermann, and R. Voss, 1999: Interannual to decadal predictability in a coupled ocean-atmosphere general circulation model. *J. Climate*, **12**, 2607–2624.

Gulev, S. K., T. Jung, and E. Ruprecht, 2000a: Interannual and seasonal variability in the intensity of synoptic-scale processes in the North Atlantic from the NCEP/NCAR reanalysis data. *J. Climate*. Submitted.

Gulev, S. K., T. Jung, and E. Ruprecht, 2000b: Intercomparison of the ocean-atmosphere heat fluxes from voluntary observing ship data and NCEP/NCAR reanalysis in the North Atlantic. *J. Hydromet.*. Submitted.

Häkkinen, S., 1999: Variability of the simulated meridional heat transport in the North Atlantic for the period 1951–1993. *J. Geophys. Res.*, **104**, 10991–11007.

Halliwell, G. R., 1998: Simulation of North Atlantic decadal/multidecadal winter SST anomalies driven by basin-scale atmospheric circulation anomalies. *J. Phys. Oceanogr.*, **28**, 5–21.

Haney, R. L., 1971: Surface thermal boundary conditions for ocean circulation models. *J. Phys. Oceanogr.*, **1**, 79–93.

Hann, J., 1890: Zur Witterungsgeschichte von Nord-Grönland, Westküste. *Meteor. Z.*, **7**, 109–115.

Harder, M., P. Lemke, and M. Hilmer, 1998: Simulation of sea ice transport through Fram Strait: Natural variability and sensitivity to forcing. *J. Geophys. Res.*, **103**, 5595–5606.

Hasselmann, K., 1976: Stochastic climate models. *Tellus*, **27**, 473–484.

Higuchi, K., J. Huang, and A. Shabbar, 1999: A wavelet characterization of the North Atlantic Oscillation variation and its relationship to North Atlantic sea surface temperatures. *Int. J. Climatol.*, **19**, 1119–1129.

Hilmer, M., M. Harder, and P. Lemke, 1998: Sea ice transport: A highly variable link between Arctic and North Atlantic. *Geophys. Res. Lett.*, **25**, 3359–3362.

Hilmer, M. and T. Jung, 2000: Evidence for a recent change in the link between the North Atlantic Oscillation and Arctic sea ice export. *Geophys. Res. Lett.*, **27**, 989–992.

Hilmer, M. and P. Lemke, 2000: On the decrease of Arctic sea ice volume. *Geophys. Res. Lett.*. Submitted.

Hoerling, M. P., A. Kumar, and M. Zhong, 1997: El Niño, La Niña, and the nonlinearity of their teleconnections. *J. Climate*, **10**, 1769–1786.

Houghton, J. T., L. G. Meira Filho, B. A. Callander, N. Harris, A. Kattenberg, and K. Maskell, eds., 1996: *Climate Change 1995: The Science of Climate Change*. Cambridge Univ. Press.

Hurrell, J. W., 1995: Decadal trends in the North Atlantic Oscillation: Regional temperatures and precipitation. *Science*, **269**, 676–679.

Hurrell, J. W., 1996: Influence of variations in extratropical wintertime teleconnections on Northern Hemisphere temperature. *Geophys. Res. Lett.*, **23**, 665–668.

Hurrell, J. W. and H. van Loon, 1997: Decadal variations in climate associated with the North Atlantic Oscillation. *Clim. Change*, **36**, 301–326.

James, I. N. and P. M. James, 1989: Ultra-low frequency variability in a simple atmospheric circulation model. *Nature*, **342**, 53–55.

Jenkins, G. M. and D. G. Watts, 1968: *Spectral analysis and its application*. Holden-Day. 525 pp.

Jones, P. D., T. Jonsson, and D. Wheeler, 1997: Extension to the North Atlantic Oscillation using early instrumental pressure observations from Gibraltar and south-west Iceland. *Int. J. Climatol.*, **17**, 1433–1450.

Jung, T. and E. Ruprecht, 1999: On the nature of the North Atlantic Oscillation and its interdecadal variability. In: *10th Symposium on Global Change Studies in Dallas*, pp. 143–146. American Meteorological Society. AMS-Preprint Volume.

Jung, T., E. Ruprecht, and M. Hilmer, 1998: Dekadische Klimavariabilität im Nordatlantik. *Ann. Meteor.*, **37**(2), 497–498.

Kalnay, E., M. Kanamitsu, R. Kistler, W. Collins, D. Deaven, L. Gandin, M. Iredell, S. Saha, G. White, J. Woollen, Y. Zhu, M. Chelliah, W. Ebiszusaki, W. Higgins, J. Janowiak, K. Mo, C. Ropelewski, J. Wang, A. Leetmaa, R. Reynolds, R. Jenne, and D. Joseph, 1996: The NCEP/NCAR 40-year reanalysis project. *Bull. Amer. Meteor. Soc.*, **77**, 437–471.

Kimoto, M. and M. Ghil, 1993a: Multiple flow regimes in the Northern Hemisphere winter. Part I: Methodology and hemispheric regimes. *J. Atmos. Sci.*, **50**, 2625–2643.

Kimoto, M. and M. Ghil, 1993b: Multiple flow regimes in the Northern Hemisphere winter. Part II: Sectorial regimes and preferred transitions. *J. Atmos. Sci.*, **50**, 2645–2673.

Kumar, P. and E. Foufoula-Georgiou, 1997: Wavelet analysis for geophysical applications. *Rev. Geophys.*, **35**, 385–412.

Kushnir, Y., 1994: Interdecadal variations in North Atlantic surface temperature and associated atmospheric conditions. *J. Climate*, **7**, 141–157.

Kushnir, Y. and I. M. Held, 1996: Equilibrium atmospheric response to North Atlantic SST anomalies. *J. Climate*, **9**, 1208–1220.

Kushnir, Y., R. Seager, M. Visbeck, N. Naik, and J. Miller, 1999: Modeling Atlantic ocean SST variability 1958–1998. In: *8th Conference on Climate Variations in Denver*, pp. 172–175. American Meteorological Society. AMS-Preprint Volume.

Kwok, R. and D. A. Rothrock, 1999: Variability of Fram Strait ice flux and North Atlantic Oscillation. *J. Geophys. Res.*, **104**, 5177–5189.

Latif, M., 1997: Dynamics of interdecadal variability in coupled ocean-atmosphere models. *J. Climate*, **11**, 602–624.

Latif, M. and T. P. Barnett, 1994: Causes of decadal climate variability over the North Pacific and North America. *Science*, **266**, 634–637.

Latif, M., E. Roeckner, U. Mikolajewicz, and R. Voss, 2000: Tropical stabilisation of the thermohaline circulation in a greenhouse warming simulation. *J. Climate*. Submitted.

Lau, K. M. and H. Weng, 1995: Climate signal detection using wavelet transform: How to make a time series sing? *Bull. Amer. Meteor. Soc.*, **76**, 2391–2402.

Limpasuvan, V. and D. L. Hartmann, 1999: Eddies and the annular modes of climate variability. *Geophys. Res. Lett.*, **26**, 3133–3136.

Livezey, R. E. and W. Y. Chen, 1983: Statistical field significance and its determination by Monte Carlo techniques. *Mon. Wea. Rev*, **111**, 46–59.

Mächel, H., A. Kapala, and H. Flohn, 1998: Behaviour of the centres of action above the Atlantic since 1881. Part 1: Characteristics of seasonal and interannual variability. *Int. J. Climatol.*, **18**, 1–22.

Madden, R. A. and R. H. Jones, 1999: Aliasing in the spectrum of time-averaged data. In: *8th Conference on Climate Variations in Denver*, pp. 229–231. American Meteorological Society. AMS-Preprint Volume.

Manabe, S. and R. J. Stouffer, 1999: The role of the thermohaline circulation in climate. *Tellus*, **51A–B**, 91–109.

Mechl, G. A. and H. van Loon, 1979: The seesaw in winter temperatures between Greenland and Northern Europe. Part 3: Teleconnections with lower latitudes. *Mon. Wea. Rev*, **107**, 1095–1106.

Mitchell, J. M., 1976: An overview of climatic variability and its causal mechanisms. *Quaternary Res.*, **6**, 481–493.

Molteni, F. and S. Corti, 1998: Long-term fluctuations in the statistical properties of low-frequency variability: Dynamical origin and predictability. *Quart. J. Roy. Meteor. Soc.*, **124**, 495–526.

Monahan, A. H. and Crisis Points Group, 1999: Nonlinear principal component analysis by neural networks: Tropical Indo-Pacific sea surface temperature and sea level pressure. *J. Climate*. Submitted.

Monahan, A. H., J. C. Fyfe, and G. M. Flato, 2000: A regime view of Northern Hemisphere atmospheric variability and change under global warming. *Geophys. Res. Lett.*, **27**, 1139–1142.

Moron, V., R. Vautard, and M. Ghil, 1998: Trends, interdecadal and interannual oscillation in global sea-surface temperatures. *Climate Dyn.*, **14**, 545–569.

Nakamura, H. and J. M. Wallace, 1991: Skewness of low-frequency fluctuations in the tropospheric circulation during Northern Hemispheric winter. *J. Atmos. Sci.*, **48**, 1441–1448.

Namias, J. and R. M. Born, 1970: Temporal coherence in North Pacific sea-surface temperature patterns. *J. Geophys. Res.*, **75**, 5952–5955.

North, G. R., T. L. Bell, and R. F. Cahalan, 1982: Sampling errors in the estimation of Empirical Orthogonal Functions. *Mon. Wea. Rev*, **110**, 699–706.

Oberhuber, J. M., 1993a: The OPYC ocean general circulation model. Technicial Report 7, Deutsches Klimarechenzentrum GmbH, Hamburg, Germany.

Oberhuber, J. M., 1993b: Simulation of the Atlantic circulation with a coupled sea ice - mixed layer - isopycnial general circulation model. Part I: Model description. *J. Phys. Oceanogr.*, **22**, 808–829.

Oberhuber, J. M., 1993c: Simulation of the Atlantic circulation with a coupled sea ice - mixed layer - isopycnial general circulation model. Part II: Model experiment. *J. Phys. Oceanogr.*, **22**, 808–829.

Osborn, T. J., K. R. Briffa, S. F. B. Tett, P. D. Jones, and R. M. Trigo, 1999: Evaluation of the North Atlantic Oscillation as simulated by a coupled climate model. *Climate Dyn.*, **15**, 685–702.

Pacanowski, R. C., 1995: MOM 2 Documentation, User's Guide and Reference Manual. Technical report, GFDL Ocean Group, GFDL, Princeton, USA.

Paeth, H., A. Hense, R. Glowienka-Hense, R. Voss, and U. Cubasch, 1999: The North Atlantic Oscillation as an indicator for greenhouse-gas induced climate change. *Climate Dyn.*. Submitted.

Palmer, T. N., 1993: Extended-range atmospheric prediction and the Lorenz model. *Bull. Amer. Meteor. Soc.*, **74**, 49–65.

Palmer, T. N., 1999: A nonlinear dynamical perspective on climate prediction. *J. Climate*, **12**, 575–591.

Palmer, T. N. and Z. Sun, 1985: A modelling and observational study of the relationship between sea surface temperature in the north-west Atlantic and the atmospheric general circulation. *Quart. J. R. Met. Soc.*, **111**, 947–975.

Peixoto, J. P. and A. H. Oort, 1992: *Physics of Climate*. American Institute of Physics, New York.

Plaut, G., M. Ghil, and R. Vautard, 1995: Interannual and interdecadal variability in 335 years of central England temperatures. *Science*, **268**, 710–713.

Plaut, G. and R. Vautard, 1994: Spells of low-frequency oscillations and weather regimes in the Northern Hemisphere. *J. Atmos. Sci.*, **51**, 210–236.

Rajagopalan, B., Y. Kushnir, and M. Tourre, 1998: Observed decadal midlatitude and tropical Atlantic climate variability. *Geophys. Res. Lett.*, **25**, 3967–3970.

Rayner, N. A., E. B. Horton, D. E. Parker, F. C. K., and H. R. B., 1996: Version 2.2 of the global sea-ice and sea surface temperature data set, 1903–1994. Technicial Note 74, Hadley Center, London Road, Bracknell, Berkshire RG 12 2SY.

Richman, M. B., 1986: Rotation of principal components. *J. Climatol.*, **6**, 293–335.

Rodwell, M., D. P. Rowell, and C. K. Folland, 1999: Oceanic forcing of the wintertime North Atlantic Oscillation and European climate. *Nature*, **398**, 320–323.

Roeckner, E., K. Arpe, L. Bengtsson, S. Brinkop, L. Dümenil, M. Esch, E. Kirk, F. Lunkeit, M. Ponater, B. Rockel, R. Sausen, U. Schlese, S. Schubert, and M. Windelband, 1992: Simulation of the present-day climate with the ECHAM model: Impact of model physics and resolution. MPI-Report 93, Max-Planck-Institut für Meteorologie, Hamburg, Germany.

Roeckner, E., L. Bengtsson, J. Feichter, J. Lelieveld, and H. Rhode, 1999: Transient climate change simulations with a coupled atmosphere-ocean GCM including the tropospheric sulfur cycle. *J. Climate*, **12**(10), 3004–3032.

Roeckner, E., J. M. Oberhuber, A. Bacher, M. Christoph, and I. Kirchner, 1996: ENSO variability and atmospheric response in a global coupled atmosphere-ocean GCM. *Climate Dyn.*, **12**, 737–754.

Rogers, J. C., 1984: The association between the North Atlantic Oscillation and the Southern Oscillation in the Northern Hemisphere. *Mon. Wea. Rev*, **112**, 1999–2015.

Rogers, J. C., 1990: Patterns of low-frequency monthly sea level pressure variability (1899–1986) and associated wave cyclone frequencies. *J. Climate*, **3**, 1364–1379.

Rogers, J. C. and H. van Loon, 1979: The seesaw in winter temperatures between Greenland and northern Europe. Part 2: Some oceanic and atmospheric effects in middle and high latitudes. *Mon. Wea. Rev*, **107**, 509–519.

Shindell, D. T., R. L. Miller, G. A. Schmidt, and L. Pandolfo, 1999: Simulation of recent northern winter climate trends by greenhouse-gas forcing. *Nature*, **399**, 452–455.

Silverman, B. W., 1986: *Density Estimation for Statistics and Data Analysis*. Chapman & Hall/CRC.

Smith, T. M., R. W. Reynolds, R. E. Livezey, and D. C. Stokes, 1996: Reconstruction of historical sea surface temperatures using empirical orthogonal functions. *J. Climate*, **9**, 1403–1420.

Smyth, T. M., K. Ide, and M. Ghil, 1999: Multiple regimes in Northern Hemisphere height fields via mixture model clustering. *J. Atmos. Sci.*, **56**, 3704–3723.

Sutton, R. T. and M. R. Allen, 1997: Decadal predictability of North Atlantic sea surface temperature and climate. *Nature*, **388**, 563–567.

Thompson, D. W. J. and J. M. Wallace, 1998: The Arctic Oscillation signature in the wintertime geopotential height and temperature fields. *Geophys. Res. Lett.*, **25**, 1297–1300.

Timmermann, A., M. Latif, R. Voss, and A. Grötzner, 1998: Northern Hemispheric interdecadal variability: A coupled air-sea mode. *J. Climate*, **11**, 1906–1931.

Timmermann, A., J. Oberhuber, A. Bacher, M. Esch, M. Latif, and E. Roeckner, 1999: ENSO response to greenhouse warming. *Nature*, **398**, 694–696.

Torrence, C. and G. P. Compo, 1998: A practical guide to wavelet analysis. *Bull. Amer. Meteor. Soc.*, **79**, 61–78.

Trenberth, K. E., 1983: What are the seasons? *Bull. Amer. Meteor. Soc.*, **64**, 1276–1282.

Trenberth, K. E. and J. W. Hurrell, 1994: Decadal atmosphere-ocean variations in the Pacific. *Climate Dyn.*, **9**, 303–319.

Trenberth, K. E. and D. A. Paolino, 1980: The Northern Hemisphere sea-level-pressure data set: Trends, errors and discontinuities. *Mon. Wea. Rev*, **108**, 855–872.

Ulbrich, U. and M. Christoph, 1999: A shift of the NAO and increasing storm track activity over Europe due to anthropogenic greenhouse gas forcing. *Climate Dyn.*, **15**, 551–559.

van Loon, H. and J. C. Rogers, 1978: The seesaw in winter temperatures between Greenland and Northern Europe. Part I: General description. *Mon. Wea. Rev*, **106**, 296–310.

Vautard, R., 1995: Patterns in Time: SSA and MSSA. In: H. von Storch and A. Navarra, eds., *Analysis of Climate Variability: Application of Statistical Techniques*, pp. 259–279. Springer Verlag.

Vautard, R. and M. Ghil, 1989: Singular spectrum analysis in nonlinear dynamics with application to paleoclimatic time series. *Physica D*, **35**, 395–424.

Vautard, R., Y. Yiou, and M. Ghil, 1992: Singular spectrum analysis: A toolkit for short, noisy and chaotic time series. *Physica D*, **58**, 95–126.

von Storch, H., 1995: Spatial patterns: EOFs and CCA. In: H. von Storch and A. Navarra, eds., *Analysis of Climate Variability: Application of Statistical Techniques*, pp. 227–257. Springer Verlag.

von Storch, H., T. Bruns, I. Fischer-Bruns, and K. F. Hasselmann, 1988: Principal oscillation pattern analysis of the 30- to 60-day oscillation in a general circulation model equatorial troposphere. *J. Geophys. Res.*, **93**, 11022–11036.

von Storch, H. and F. W. Zwiers, 1999: *Statistical Analysis in Climate Research*. Cambridge University Press. 484 pp.

Walker, G. T., 1924: Correlation in seasonal variation of weather, IX. *Mem. Indian. Meteor. Dep.*, **24**(9), 275–332.

Wallace, J. M. and D. S. Gutzler, 1981: Teleconnections in the geopotential height field during the Northern Hemisphere winter. *Mon. Wea. Rev*, **109**, 784–812.

Wang, B. and Y. Wang, 1996: Temporal structure of the Southern Oscillation as revealed by waveform and wavelet analysis. *J. Climate*, **9**, 1586–1598.

White, G. H., 1980: Skewness, kurtosis and extreme values of Northern Hemisphere geopotential heights. *Mon. Wea. Rev*, **108**, 1446–1455.

Wohlleben, T. M. H. and A. J. Weaver, 1995: Interdecadal climate variability in the subpolar North Atlantic. *Climate Dyn.*, **11**, 459-467.

Xie, S. P. and Y. Tanimoto, 1998: A pan-Atlantic decadal climate oscillation. *Geophys. Res. Lett.*, **25**, 2185–2188.

Zorita, E., V. Kharin, and H. von Storch, 1992: The atmospheric circulation and sea surface temperature in the North Atlantic area in winter: Their interaction and relevance for Iberian Precipitation. *J. Climate*, **5**, 1097–1108.

Zwiers, F. W. and H. Storch, 1995: Taking serial correlation into account in tests of the mean. *J. Climate*, **8**, 336-351.

Aknowledgements

I am very greatful to Prof. Dr. Eberhard Ruprecht for supervising this thesis, and for continously supporting my scientific interests from the very beginning.

It is a pleasure to acknowledge Michael Hilmer, Dr. Carsten Eden, and Dr. Sergey Gulev for very fruitful discussions and collaborations — the imprints, which are evident throughout the whole manuscript.

It was a pleasure to graduate in parallel with Renate Hagedorn, who kept company in many scientific and private affairs during numerous unconventional working hours. I am greatful to my family and my friends for staying in contact with a "workaholic".

My colleagues of the Department of Meteorology provided a stimulating atmosphere. The work of Kai Grunau and Dr. Jürgen Kielmann in maintaing high computer standards at the IfM is very much acknowledged. Oliver Timm, Torben Kahl, and Sandy Ubl provided valueable technicial support.

Dr. P. D. Jones kindly provided SLP time series from the Azores, Gibraltar, and Iceland. Data from the control run of the ECHAM4/OPYC3 model were provided by Drs. E. Roeckner, M. Esch, and J. M. Oberhuber. Thanks go to Dr. U. Ulbrich for making available to me sea level pressure data from the scenario run of the coupled ECHAM4/OPYC3 model. NCEP/NCAR reanalysis data were provided through the NOAA Climate Diagnostic Center. The ocean general circulation model was kindly provided through the FLAME group.

The German Research Foundation provided financial support in the framework of the Sonderforschungsbereich 460 "Dynamics of Thermohaline Circulation Variability".

BERICHTE AUS DEM INSTITUT FÜR MEERESKUNDE
Verzeichnis der veröffentlichten Arbeiten

(Auskünfte über die vorangegangenen Veröffentlichungen erteilt die Bibliothek)

250 (1994)	SAYIN, E.	Modelling Water and Salt Exchange through the Belt and Sound
251 (1994)	MEYERHÖFER, M.	Plankton-Pigmente und deren Abbauprodukte als Biomarker zur Beschreibung und Abschätzung der Phytoplankton-Sukzession und -Sedimentation im Nordatlantik
252 (1994)	THETMEYER, H.	Respiration von *Gobiusculus flavescens* und *Pomatoschistus minutus* bei spontaner Schwimmaktivität
253 (1994)	QUACK, B.	Leichtflüchtige Halogenkohlenwasserstoffe in der marinen Atmosphäre: Bestand, Herkunft und Massenbilanzen über Nord- und Ostsee
254 (1994)	REUSCH, T.B.H.	Factors structuring the *Mytilus*- and *Zostera*-community in the Western Baltic: an experimental approach (Strukturbestimmende Faktoren für die *Mytilus*- und *Zostera*-Gemeinschaft der westlichen Ostsee: ein experimenteller Ansatz)
255 (1994)	KOEVE, W.	New Production of Phytoplankton in the tropical and subarctic North Atlantic
256 (1994)	OSCHLIES, A.	Assimilation of Satellite Altimeter Data into an Eddy-Resolving Primitive Equation Model of the North Atlantic Ocean
257 (1994)	DÖSCHER, R.	Die thermohaline Zirkulation in einem numerischen Modell des Nordatlantischen Ozenans: quasistationäre Zustände und Adaptationsprozesse
258 (1994)	KRAUSS, W.	Sonderforschungsbereich 133 "Warmwassersphäre des Atlantiks" — Eine Dokumentation —
259 (1994)	NEHRING, ST.	Dinoflagellaten-Dauercysten in deutschen Küstengewässern: Vorkommen, Verbreitung und Bedeutung als Rekrutierungspotential
260 (1994)	HOLFORT, J.	Großräumige Zirkulation und meridionale Transporte im Südatlantik
261 (1994)	KÖSTER, F.W.	Der Einfluß von Bruträubern auf die Sterblichkeit früher Jugendstadien des Dorsches *(Gadus morhua)* und der Sprotte *(Sprattus sprattus)* in der zentralen Ostsee
262 (1994)	AUF DEM VENNE, H.	Zur Verbreitung und ökologischen Bedeutung planktischer Ciliaten in zwei verschiedenen Meeresgebieten: Grönlandsee und Ostsee
263 (1995)	DETMER, A.	Verbreitung, Abundanz und Bedeutung von autotrophem Pico- und Nanoplankton in polaren, temperierten und subtropischen Regionen
264 (1995)	HUMBORG, CH.	Untersuchungen zum Verbleib der Nährstoff-Frachten der Donau
265 (1995)	DIAZ, H.F. ISEMER, H.-J.	Proceedings of the International COADS Winds Workshop, Kiel, Germany, May 31 — June 2, 1994 (In Verbindung mit National Oceanic and Atmospheric Administration NOAA)
266 (1995)	WIELAND, K.	Einfluß der Hydrographie auf die Vertikalverteilung und Sterblichkeit der Eier des Ostseedorsches *(Gadus morhua callarias)* im Bornholmbecken, südliche zentrale Ostsee

267 (1995)	FUHRHOP, R.	Fehleranalyse passiver Mikrowellenmessungen des Special Sensor Microwave / Imager
268 (1995)	PULFRICH, A.	Reproduction and Recruitment in Schleswig-Holstein Wadden Sea Edible Mussel *(Mytilus edulis L.)* Populations
269 (1995)	HEISE, S.	Der Einfluß von Umweltfaktoren auf die Bildung von exopolymerer Substanz (EP) durch ein marines Bakterium
270 (1995)	SENOCAK, T.	Schwermetalluntersuchung an Fischen der deutschen Ostseeküste (Kliesche *Limanda limanda;* Flunder *Platichthys flesus;* Hering *Clupea harengus* und Dorsch *Gadus morhua*)
271 (1995)	SCHORIES, D.	Populationsökologie und Massenentwicklung von *Enteromorpha* spp. (Chlorophyta) im Sylter Wattenmeer
272 (1995)	KÖRTZINGER, A.	Anthropogenes CO_2 im Nordatlantik Methodische Entwicklungen und Messungen zur Quantifizierung des anthropogenen CO_2-Signals
273 (1995)	DAHMEN, K.	Vertikalverteilung und produktionsbiologische Bedeutung des Mesozooplanktons im Bornholm-Becken (Südliche Ostsee)
274 (1995)	SCHRADER, M.	Ein Dreiskalenmodell zur Berechnung der Reflektivität der Ozeanoberfläche im Mikrobwellenfrequenzbereich
275 (1995)	PALM, H.W.	Untersuchungen zur Systematik von Rüsselbandwürmern (Cestoda: Trypanorhyncha) aus atlantischen Fischen
276 (1995)	PIKER, L.	Dynamik der Sulfatatmung und ihre Bedeutung für die Kohlenstoff-Mineralisierung in Ostsee-Sedimenten
277 (1995)	BLANZ, TH.	Dokumentation und Massenbilanz des Chlorbiphenyl-Eintrags der Oder in die Südpommersche Bucht
278 (1995)	GROSSKLAUS, M.	Niederschlagsmessung auf dem Ozean von fahrenden Schiffen
279 (1995)	NEUGUM, A.	Systematische Einflüsse auf die Bestimmung der Schubspannung mit der "Dissipationsmethode" auf See
280 (1995)	PFANNKUCHE, O. HOPPE, H.-G. THIEL, H. WEIKERT, H.	BIO-C-FLUX — Biologischer Kohlenstoffluß in der bodennahen Wasserschicht des küstenfernen Ozeans Schlußbericht für den Förderzeitraum 1.1.1990-31.12.1994
281 (1995)	ZANGENBERG, N.	Die Zirkulation des Oberflächen- und des Tiefenwassers im Südlichen Brasilianischen Becken
282 (1995)	HEVIA, M.	Ein Simulationsmodell zum Einfluß intensiver Lachszucht auf die Umwelt und Auswirkungen standortbedingter Umweltparameter auf das Wachstum des atlantischen Lachses *(Salmo salar L.)* an der Küste Chiles
283 (1996)	LUNDGREEN, U.	Aminosäuren im Nordatlantik: Partikelzusammensetzung und Remineralisierung

284 (1996)	MEIER, H.E.M.	Ein regionales Modell der westlichen Ostsee mit offenen Randbedingungen und Datenassimilation
285 (1996)	THUROW, F.	Estimation of the total fish biomass in the Baltic Sea during the 20th centry
286 (1996)	EFTHIMIOU,S.	Performance of juvenile and ongrowing common Dentex (Dentex dentex, L. 1758, Sparidae) in relation to nutrition under culture
287 (1997)	STUTZER, S.	Modellierung der mittleren Zirkulation im Südatlantik
288 (1997)	SIEDLER, G. ZENK, W.	Untersuchungen zu den tiefen Wassermassen und planktologische Beobachtungen im tropischen Westpazifik während der SONNE-Fahrt Nr. 113 (TROPAC)
289 (1997)	JAHN, A.	Ökophysiologische Untersuchungen an *Macoma balthica* (Bivalvia) und *Cyprideis torosa* (Ostracoda) über Anpassungen an den Umweltfaktor Schwefelwasserstoff
290 (1997)	SANDERS, D.	Alkenone in sedimentierenden Partikeln im Nordostatlantik: Regionale und saisonale Variabilität
291 (1997)	BRUHN, R.	Chlorierte Schadstoffe in Schweinswalen *(Phocoena phocoena)*: Verteilung, Akkumulation und Metabolismus in Abhängigkeit von der Struktur
292 (1997)	SEILERT, H.E.W.	Freilanduntersuchungen zur Verteilung der Miesmuschel *Mytilus edulis L.* in einem zweifach geschichteten Ästuar
293 (1997)	KAREZ, R.	Factors causing the zonation of three *Fucus* species (Phaeophyta) in the intertidal zone of Helgoland (German Bight, North Sea) Testing the validity of Keddy's 'competitive hierarchy model'
294 (1997)	DYNAMO GROUP	DYNAMO – Dynamics of North Atlantic Models: Simulation and assimilation with high resolution models
295 (1997)	DONNER, G.	Beziehungen zwischen Struktur und Funktion bakterieller Gemeinschaften in Mikrokosmos- und Freiwasser-Chemoklinen
296 (1997)	WIRYAWAN, B.	Mesozooplankton dynamics in the northern Adriatic Sea and the influence of eutrophication by the river Po
297 (1997)	FUHRHOP, R. SIMMER, C. SCHRADER, M. HEYGSTER, G. JOHNSEN, K.-P. SCHLÜSSEL, P.	Study of Remote Sensing of the atmosphere and surface ice
298 (1997)	BROWN, A.W.	Mikroorganismen als mögliche Indikatoren zur Beurteilung des Wasser- und Sedimentzustandes im Bereich küstennaher Zuchtanlagen für die Regenbogenforelle *(Oncorhynchus mykiss)*
299 (1997)	WIEDEMEYER, W.	Analysis of the benthic food web of a mangrove ecosystem at noreastern Brazil

300 (1998)	ENGEL, A.	Bildung, Zusammensetzung und Sinkgeschwindigkeiten mariner Aggregate
301 (1998)	BIASTOCH, A.	Zirkulation und Dynamik in der Agulhas-Region anhand eines numerischen Modells
101 (1982)	SIEDLER, G.	SI-Einheiten in der Ozeanographie
		SI Units in Oceanography
(1988)		2. revidierte Auflage
(1998)		3. revidierte Auflage
302 (1998)	KNOLL, M. MÜLLER, T.J. SIEDLER, G.	ESTOC/CANIGO cruises with FS POSEIDON: cruises 202/1, 212, 233, 237/3
303 (1998)	LOTZE, H.K.	Population dynamics and species interactions in macroalgal blooms: abiotic versus biotic control at different life-cycle stages
304 (1998)	FÜG, C.	Validierung des hydrologischen Zyklus des BALTEX-Gebietes im Regionalmodell REMO mit Mikrowellenbeobachtungen vom Satelliten aus
305 (1999)	RICK, S.	The spring bloom in the German Bight: Effects of high inorganic N:P ratios on the phytoplankton development
306 (1999)	KRIEST, I.	The influence of phytoplankton aggregation on sedimentation - A model study
307 (1999)	PALM, H.W. KLIMPEL, S. BUCHER, CH.	Checklist of metazoan fish parasites of German coastal waters
308 (1999)	HILLEBRAND, H.	Effect of biotic interactions on the structure of microphytobenthos
309 (1999)	SELLMER, C.	Phytoplanktologische Studien im westlichen Arabischen Meer zur Zeit des SW-Monsuns - Ein Beitrag zum Verständnis des regionalen Kohlenstoffkreislaufs -
310 (1999)	KÖHL, A.	An adjoint method for the assimilation of statistical characteristics into eddy-resolving ocean models
311 (1999)	EDEN, C.	Interannual to interdecadal variability in the North Atlantic Ocean
312 (1999)	ROHLF, N.	Verhaltensänderungen der Larven des Ostseedorsches (*Gadus morphua callarias)* während der Dottersackphase
313 (2000)	MÜLLER, A.	Mg/Ca- und Sr/Ca-Verhältnisse in biogenem Carbonat planktischer Foraminiferen und benthischer Ostracoden
314 (2000)	HAGEDORN, R.	Ein gekoppeltes Atmosphäre-Ozean-Modell für das Ostsee-Einzugsgebiet
315 (2000)	JUNG, T.	The North Atlantic Oscillation: Variability and Interactions with the North Atlantic Ocean and Arctic Sea Ice